AD-A071 376 BRITISH COLUMBIA UNIV VANCOUVER INST OF OCEANOGRAPHY F/G 8/3
HEATED ANEMOMETRY AND THERMOMETRY IN WATER.(U)
MAY 79 R G LUECK N00014-76-C-0446

UNCLASSIFIED NL

1 OF 2
AD A071376

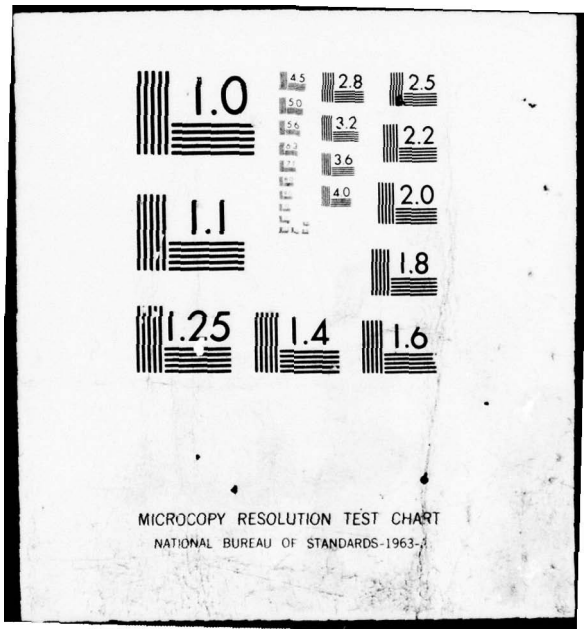
1.0
1.1
1.25
1.4
1.6
1.8
2.0
2.2
2.5
2.8
3.2
3.6
4.0
4.5
5.0
5.6
MICROCOPY RESOLUTION TEST CHART
NATIONAL BUREAU OF STANDARDS-1963-A

LEVEL II

12

OCEANOGRAPHY

THE UNIVERSITY OF BRITISH COLUMBIA

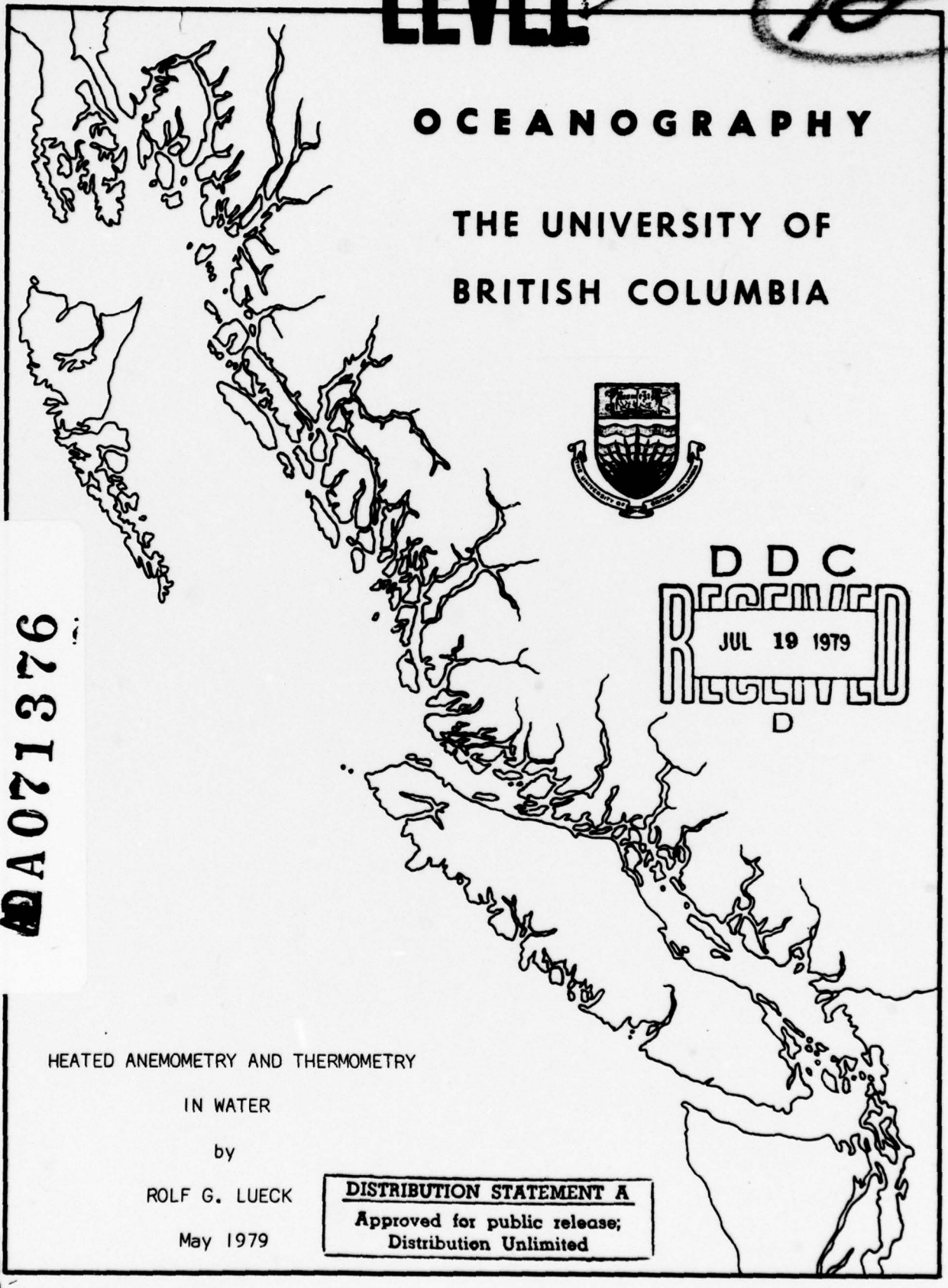

HEATED ANEMOMETRY AND THERMOMETRY IN WATER

by

ROLF G. LUECK

May 1979

Unclassified

SECURITY CLASSIFICATION OF THIS PAGE (When Data Entered)

REPORT DOCUMENTATION PAGE	READ INSTRUCTIONS BEFORE COMPLETING FORM
1. REPORT NUMBER -- / 2. GOVT ACCESSION NO.	3. RECIPIENT'S CATALOG NUMBER
4. TITLE (and Subtitle) HEATED ANEMOMETRY AND THERMOMETRY IN WATER (6)	5. TYPE OF REPORT & PERIOD COVERED Ph.D. Thesis
	6. PERFORMING ORG. REPORT NUMBER --
7. AUTHOR(s) (10) Rolf E. Lueck (GeRo)	8. CONTRACT OR GRANT NUMBER(s) (15) N00014-76-C-0446 NR 083 207
9. PERFORMING ORGANIZATION NAME AND ADDRESS Inst. Department of Oceanography, University of British Columbia, Vancouver, B.C., Canada. V6T 1W5 063770	10. PROGRAM ELEMENT, PROJECT, TASK AREA & WORK UNIT NUMBERS —
11. CONTROLLING OFFICE NAME AND ADDRESS Office of Naval Research, Code 480, NSTL STATION, Mississippi 39529. (11)	12. REPORT DATE May 1979 / 13. NUMBER OF PAGES 157
14. MONITORING AGENCY NAME & ADDRESS (if different from Controlling Office) (12) 169 p.	15. SECURITY CLASS. (of this report) - UNCLASSIFIED / 15a. DECLASSIFICATION/DOWNGRADING SCHEDULE --

16. DISTRIBUTION STATEMENT (of this Report)

Unlimited

DISTRIBUTION STATEMENT A
Approved for public release; Distribution Unlimited

17. DISTRIBUTION STATEMENT (of the abstract entered in Block 20, if different from Report)

(9) Doctoral thesis,

18. SUPPLEMENTARY NOTES

--

19. KEY WORDS (Continue on reverse side if necessary and identify by block number)

Heated Anemometry, Thermometry, Water, Turbulence

20. ABSTRACT (Continue on reverse side if necessary and identify by block number)

The characteristics of several types of heated sensors used for measuring oceanic turbulence have been examined. The author measured the steady heat flux from glass coated ellipsoidal microbead thermistors, computed numerically the unsteady heat flux from an ideal constant temperature flat plate, and analyzed the steady flow calibration data of a paralene-c coated plate thermistor as well as the steady and unsteady calibration data of two conical constant temperature hot film

DD FORM 1 JAN 73 1473 EDITION OF 1 NOV 65 IS OBSOLETE S/N 0102 LF 014 6601

Unclassified 063770

SECURITY CLASSIFICATION OF THIS PAGE (When Data Entered)

CONT

anemometers. In order to understand the behaviour of probes alone, thermal models of these sensors have been developed. The models incorporate a Nusselt number governed steady heat flux from the wetted surface and the thermal effects of a surface coating and a supportive substrate. Derived functional relationships between the steady heat flux and the flow rate agree favourably with the available calibration data. The quasi-steady sensitivity of these probes when used as anemometers or thermometers as well as their signal contamination by temperature or velocity are calculated using the functional heat flux relationships. The substrate and the coating reduce the sensitivity to temperature and to speed as well as the ratio of speed-to-temperature sensitivity.

The response of sensors is not governed by the Nusselt number when the boundary layer is unsteady. The unsteady response of a sensor to velocity oscillations is governed by its unsteady viscous boundary layer and may increase with increasing frequency over some frequency ranges. The response bandwidth is wider for velocity than for temperature. The ratio of unsteady temperature-to-velocity sensitivity is highest at zero frequency. Frequency response calibration methods must realistically simulate the sensor's unsteady viscous boundary layer.

LEVEL II

12

HEATED ANEMOMETRY AND THERMOMETRY IN WATER

by

ROLF GERO LUECK

B.A.Sc., University of British Columbia, 1973

A THESIS SUBMITTED IN PARTIAL FULFILLMENT OF

THE REQUIREMENTS FOR THE DEGREE OF

DOCTOR OF PHILOSOPHY

in the

DEPARTMENT OF PHYSICS

and the

INSTITUTE OF OCEANOGRAPHY

We accept this thesis as conforming

to the required standard

Thomas Osborn .....

.....

R.W. Burling .....

THE UNIVERSITY OF BRITISH COLUMBIA

1979

Abstract

The characteristics of several types of heated sensors used for measuring oceanic turbulence have been examined. The author measured the steady heat flux from glass coated ellipsoidal microbead thermistors, computed numerically the unsteady heat flux from an ideal constant temperature flat plate, and analyzed the steady flow calibration data of a paralene-c coated plate thermistor as well as the steady and unsteady calibration data of two conical constant temperature hot film anemometers. In order to understand the behaviour of probes alone, thermal models of these sensors have been developed. The models incorporate a Nusselt number governed steady heat flux from the wetted surface and the thermal effects of a surface coating and a supportive substrate. Derived functional relationships between the steady heat flux and the flow rate agree favourably with the available calibration data. The quasi-steady sensitivity of these probes when used as anemometers or thermometers as well as their signal contamination by temperature or velocity are calculated using the functional heat flux relationships. The substrate and the coating reduce the sensitivity to temperature and to speed as well as the ratio of speed-to-temperature sensitivity.

The response of sensors is not governed by the Nusselt number when the boundary layer is unsteady. The unsteady response of a sensor to velocity oscillations is governed by its unsteady viscous boundary layer and may increase with increasing frequency over some frequency ranges. The response bandwidth is wider for velocity than for temperature. The ratio of unsteady temperature-to-velocity sensitivity is highest at zero frequency. Frequency response calibrations methods

Table of Contents

List of Tables

List of Figures

Appendix A

Acknowledgements

Professor T.R. Osborn has provided encouragement, guidance and support throughout my graduate studies. I would also like to express appreciation to the following:

- Dr. A. Gargett, Dr. P. Nasmyth and Mr. G. Chase of the Ocean Mixing Group at the Institute of Ocean Sciences, Patricia Bay and Mr. D. Evans, formerly of the Defense Research Establishment, Pacific, for providing the hot film calibration data and needed information.
- Dr. E. Lange of the Scripps Institute of Oceanography for providing his thermistor calibration data.
- Professors P.H. LeBlond and L. Mysak for their comments and discussions.
- Ms. P. Lust for her diligent typing of this manuscript.

The National Research Council of Canada has supported me personally for four years of my Graduate Studies at U.B.C.

1. Introduction

This thesis discusses some salient features of heated anemometry and thermometry in water with emphasis on oceanic applications. The discussion separates the hydrodynamic characteristics of probes from their associated electronics. Many pertinent features of a probe's behaviour can now be deduced unobscured by the characteristics of the probe's electronics. The three appendices in this thesis are manuscripts that have been submitted to refereed journals and deal with three different but related aspects of the subject of thermometry and heated anemometry. This thesis inter-relates and summarizes the contents of the three manuscripts.

2. Background

The direct observation of turbulence is important to oceanography. Observations of the mixing of momentum, salinity and temperature between water masses could clarify the details of frontal dynamics (Gargett, 1978) and the role of turbulence in general circulations. The measurement of turbulence on scales small enough to resolve the dissipation spectrum is presently the only practical way to estimate the vertical Reynolds shear stress in open ocean shear flows (Crawford and Osborn, 1978). The correlation of orthogonal velocity fluctuations in river estuaries could yield the internal stress, an important but so far unmeasured term in the balance of forces.

An understanding of the hydrodynamics of the employed sensors is crucial to the successful interpretation of turbulence data. Invariably a sensor must be mounted on a platform such as a towed body (Gargett, 1978; Grant, Stewart and Moilliet, 1962), a self propelled vehicle (Grant, Moilliet and Vogel, 1968), a free falling package (Osborn, 1978), a tethered falling package (Mamorino and Caldwell, 1978) or a platform attached to the bottom or the shore. The motions of the platform are also important for data interpretation but are beyond the scope of this thesis.

A diagrammatic summary of turbulence sensors that have been used for oceanic measurements is shown in Figure 1. A summary of salinity sensors has been given by Gregg and Pederson (1978). Cylindrical film and wire sensors, absent from Figure 1, have so far only seen use in laboratories (Tan-atichat, Nagib and Pluister, 1973 and Gust, 1976).

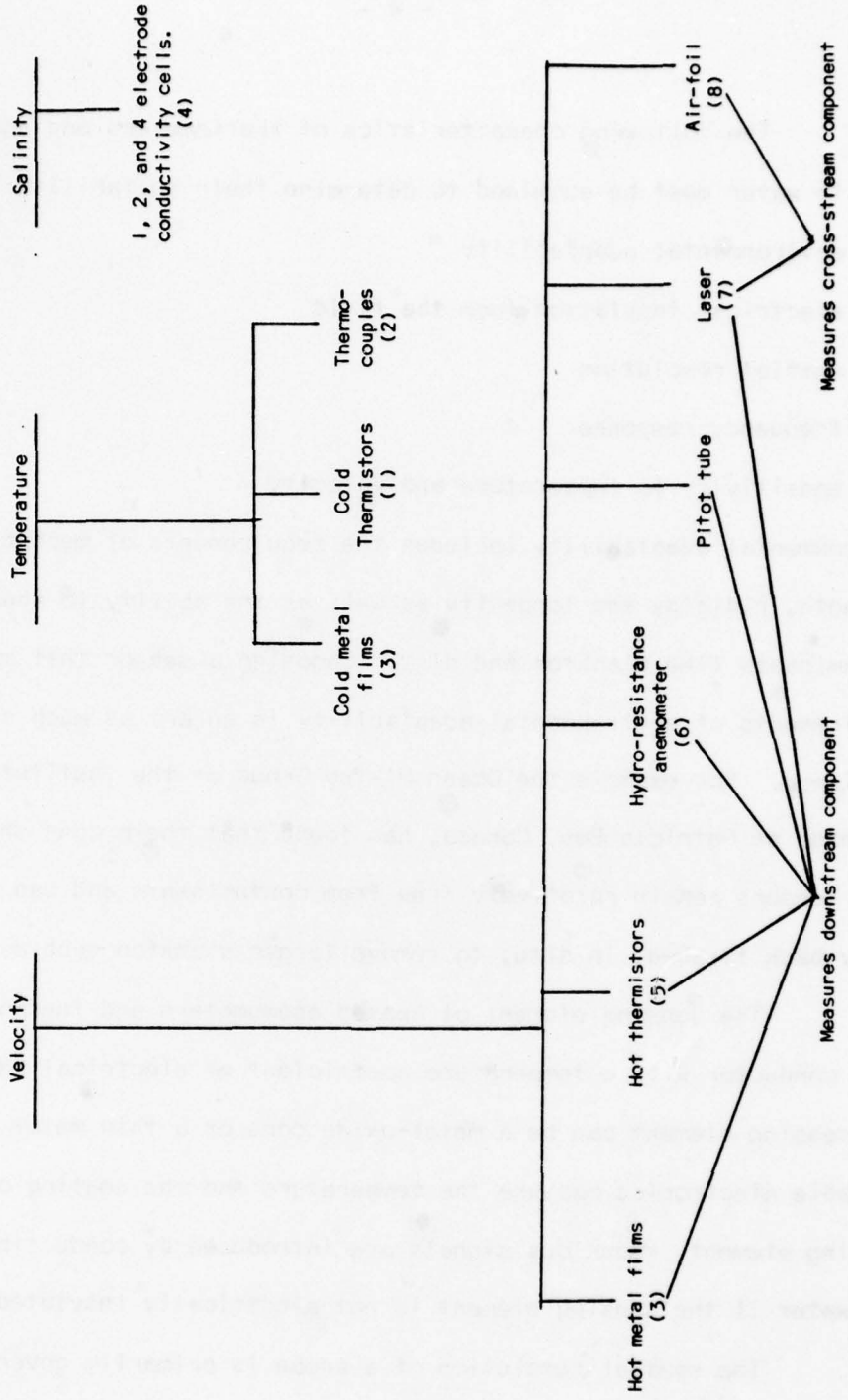

Figure 1. Diagrammatic summary of oceanic turbulence sensors.

(1) Osborn, 1978.
(2) Mamorino and Caldwell, 1978.
(3) Gargett, 1978.
(4) Gregg and Pederson, 1978.
(5) Lange, personal communication.
(6) Belyaev, Gezentsvey, Monin, Ozmidov and Paka, 1975.
(7) John Woods, personal communication.
(8) Crawford and Osborn, 1978.

The following characteristics of thermometers and anemometers used in water must be examined to determine their suitability:

(1) environmental adaptability

(2) electrical insulation from the fluid

(3) spatial resolution

(4) frequency response

(5) sensitivity to temperature and velocity

Environmental adaptability includes the requirements of mechanical strength, ridigidy and longevity as well as the ability to shed contaminants like plankton and dirt. Choosing a sensor that meets the requirements of environmental adaptability is an art as much as it is a science. For example the Ocean Mixing Group of the Institute of Ocean Sciences at Patricia Bay, Canada, has found that their cone shaped hot film sensors remain relatively free from contaminants and can be successfully back flushed, in situ, to remove larger plankton such as jelly-fish.

The sensing element of heated anemometers and thermometers is a conductor with a temperature coefficient of electrical resistance. The sensing element can be a metal-oxide core or a thin metal film. Suitable electronics measure the temperature and the heating of the sensing element. Spurious signals are introduced by conduction through sea water if the sensing element is not electrically insulated.

The spatial resolution of a probe is primarily governed by its size. The turbulence cannot be fully resolved if its spatial scale is comparable to or smaller than the probe. A detailed discussion of the spatial resolution of probes is outside the scope of this thesis. A spatial structure of wavelength λ advected past a probe at speed U has,

for the probe, an apparent frequency U/λ. If U/λ exceeds the frequency resolution of the probe then there is an apparent spatial response limitation caused by frequency response limitations. Frequency response is discussed in Chapter 4.

Determining sensitivity to temperature or velocity is a fundamental problem of thermometry and heated anemometry. Temperature sensors and heated anemometers are simultaneously sensitive to both temperature and velocity. Thermometers have a small amount of internal heating because of the electric current passing through them and consequently have some sensitivity to speed. The level of internal heating that can be tolerated is not clear. Gregg, Meagher, Pederson and Aagaard (1978) write:

> "A third, more obvious, approach [*to increase the sensitivity of thermistors*] would be to increase the current through the thermistors; however, by increasing the power dissipation, this increases the ventilation noise [*sensitivity to speed*]. As neither the velocity spectra nor the coefficients for computing the cooling have been well known, we have followed the conservative position of Cox, et al (1969) in maintaining a low power dissipation, i.e. 4 to 13 μw [10^{-6} *watts*]. With further information it may be possible safely to increase the power."

The contents of the square brackets have been added for clarity. The heat flux from grossly heated sensors responds to variations of the ambient fluid's speed as well as its temperature. Increasing the sensor's temperature increases the ratio of speed-to-temperature sensitivity. Eventually the formation of bubbles and a shortening of the operating life limit the allowable overheat. Gargett (1978) comments on the problems of limited overheat:

" . . . a second problem arises because the hot film is not, in fact, very hot (measurements were taken with an overheat of 20°C, a value chosen as a compromise between velocity sensitivity and film corrosion, both of which increase with increasing overheat), and as such it is sensitive to temperature as well as velocity. A single test of the hot film probe in the plume tank used to calibrate cold film temperature probes [Fabula, 1968] suggests that this temperature sensitivity may be higher than would be expected at the high-frequency end of the velocity dissipation range, high enough to be a significant problem in most regions of the main thermocline, where microscale temperature fluctuations almost always accompany dissipative velocity events. Until this problem receives further attention, the velocity data from our tows in the main thermocline remain suspect."

3. Steady Heat Transfer

Much work has been published on the steady heat transfer from ideal bodies, that is, probes with a constant temperature wetted surface. Real probes have a coating that insulates the sensing element and some have a substrate that conducts heat away from the sensing element. However, the concepts of heat transfer from ideal probes can be fruitfully applied to real probes used for oceanic work to deduce their steady and quasi-steady characteristics.

3.1 Ideal Probes

The rate of heat transfer from a constant temperature wetted surface (an ideal probe) to its fluid environment depends on (Hinze, 1975)

(1) the flow velocity

(2) the temperature difference between the surface and the ambient fluid (over-heat $\Delta\theta$) and

(3) the physical properties of the fluid.

The rate of heat transfer from a given constant temperature wetted surface is characterized by a dimensionless parameter called the Nusselt number (Nu). The dependence of the Nusselt number on other dimensionless groups of importance may be expressed by (Hinze, 1975)

$$Nu = f\left\{R_e, Pr, Gr, \frac{\Delta\theta}{T}, \frac{U^2}{C_p \Delta\theta}, Z, \emptyset\right\} \qquad (1)$$

where

$$R_e = \frac{UL}{\nu}, \quad Pr = \nu/\kappa, \quad Gr = \frac{gL^3\beta\Delta\theta}{\nu^2}$$

$\Delta\theta$= temperature difference between the wetted surface and the ambient fluid (overheat),

L = a relevant dimension of the probe,

κ = thermal diffusivity of the fluid,

ν = kinematic viscosity of the fluid,

ρ = density of the fluid,

C_p = specific heat of the fluid,

β = coefficient of thermal expansion,

g = gravitational acceleration,

U = speed of the fluid,

T = absolute temperature of the fluid,

Z = a parameter group representing the effect of geometry,

ϕ = angle between the flow direction and the axis of the probe (if it has one).

The term $U^2/C_p\Delta\theta$ represents the relative importance of flow induced heating (stagnation remperature, U^2/C_p) which equals $\sim 1/4000$ ^oC for typical fluid speeds of 100 cm/sec. The stagnation temperature is possibly important for thermometry ($\Delta\theta \sim 10^{-3}$ ^oC) but not for anemometry where $\Delta\theta \sim 10^oC$. Collins and Williams (1959) showed that, for wires in air, buoyancy effects (thermal convection) may be neglected whenever

$$G_r < R_e^3$$

If the above condition also holds for water and other shapes then buoyancy effects are small whenever

$$500 \frac{U^3}{\Delta\theta} > 1 \text{ in units of cm/sec and } ^oC$$

a condition that is always well satisfied in oceanic work. The term $\Delta\theta/T$ is important if the overheat is sufficient to change either the Reynolds number or the Prandtl number. For water both the Prandtl

number and the kinematic viscosity depend strongly on temperature (table 1), consequently $\Delta\theta/T$ may be an important dimensionless group. However, the author is unaware of any attempt to relate the Nusselt number to $\Delta\theta/T$ in water. For anemometry in water the Nusselt number can be expressed as

$$Nu = f\{R_e, Pr, \frac{\Delta\theta}{T}, Z, \phi\} \tag{2}$$

and further discussion is limited to

$$Nu = f\{R_e, Pr, Z\} \tag{3}$$

when $Re \gg 1$ and $1 \lesssim Pr \lesssim 10$.

T °C	Kinematic viscosity cm^2/sec	Prandtl Number
0	1.787×10^{-2}	13.44
5	1.514	
10	1.304	9.45
15	1.138	8.13
20	1.004	7.07
25	0.894	
30	0.802	5.49
35	0.725	
40	0.659	4.34
50	0.554	
60	0.474	3.01
70	0.414	
80	0.366	2.25
90	0.327	
100	0.295	1.78

TABLE 1. The kinematic viscosity and Prandtl number of pure water after Batchelor (1976).

The Nusselt number for a sphere and a cylinder is known from observations. The Nusselt number has been derived analytically and empirically for wedges, including a flat plate, and for cones. The

Nusselt number of a constant temperature sphere is (Kramers, 1946)

$$Nu = 2.0 + 1.3\ Pr^{0.15} + 0.66\ Pr^{0.31}\ R_e^{\frac{1}{2}} \tag{4}$$

where the Reynolds number is based on the sphere's diameter. The rate of heat transfer to the fluid is

$$Q = \pi D \lambda_f \Delta\theta Nu \tag{5}$$

where λ_f is the conductivity of the fluid at the sphere's surface and D is the diameter of the sphere. The Nusselt number for two-dimensional flow over a wedge (Falkner-Skan flow) has been tabulated by White (1974) for a wide range of Prandtl numbers and wedge angles. A flat plate is a wedge of zero angle and has a Nusselt number of $0.664\ Pr^{0.341}\ R_e^{\frac{1}{2}}$. The Nusselt number of a two-dimensional stagnation area is $.715\ Pr^{.37}\ R_e^{\frac{1}{2}}$. The rate of heat transfer from both faces of a wedge is

$$Q = b \lambda_f \Delta\theta Nu \tag{6}$$

where b is the width of the wedge across the flow.

There is a transformation due to Mangler (1948), valid for both incompressible and compressible laminar flow, which converts the axi-symmetric boundary layer equations of a cone into the equations of an equivalent two-dimensional wedge flow. The heat flux from any axi-symmetric body can, in principle, be obtained from the heat flux of an equivalent two-dimensional wedge.

Hinze (1975) gives an extensive discussion on the Nusselt number of a cylinder. All findings are not completely in agreement but a relationship, claimed to be satisfactory for many gases and liquids, is (Kramers, 1946)

$$Nu = 0.42\ Pr^{0.20} + 0.57\ Pr^{1/3}\ R_e^{1/2} \tag{7}$$

The heat flux from a cylinder of length b is

$$Q = \pi b \lambda_f \Delta\theta Nu.$$

The quasi-steady sensitivity of the heat flux to speed for an ideal probe is

$$\frac{\partial Q}{\partial U} = \frac{R_e}{U}\frac{\partial Q}{\partial R_e} = \left(\frac{\Delta\theta}{U}\right)\lambda_f \left(\begin{matrix}\pi D \\ \pi b \\ b\end{matrix}\right)\frac{\partial Nu}{\partial R_e} R_e$$

where the factor πb is used for cylinders, πD for spheres and the factor b for wedges and cones. The quasi-steady sensitivity to temperature oscillations of the ambient fluid is

$$\frac{\partial Q}{\partial(\Delta\theta)} = \lambda_f \left(\begin{matrix}\pi D \\ \pi b \\ b\end{matrix}\right) Nu$$

The ratio of the quasi-steady speed-to-temperature sensitivity is

$$\frac{\partial Q/\partial U}{\partial Q/\partial(\Delta\theta)} = \left(\frac{\Delta\theta}{U}\right)\frac{R_e}{Nu}\frac{\partial Nu}{\partial R_e}$$

This ratio is $\Delta\theta/2U$ if $Nu \propto R_e^{\frac{1}{2}}$ which is the case for wedges and cones but is less than $\Delta\theta/2U$ for cylinders and spheres. For very large Reynolds numbers the ratio of the quasi-steady speed-to-temperature sensitivity for cylinders and spheres appraoches $\Delta\theta/2U$ asymptotically. Thus the maximum value of the ratio of quasi-steady speed-to-temperature sensitivity of heated sensors never exceeds $\Delta\theta/2U$.

3.2 Real Probes

In principle, if the Nusselt number of a probe is known and if its temperature and its heat flux can be measured then the fluid's speed can be uniquely determined. Two difficulties with using the Nusselt number of an ideal probe for a real probe are (aside from geometric imperfections):

(1) All probes are electrically and hence thermally insulated from the fluid. The wetted surface is cooler than the electrically heated element and may not be at a constant or uniform temperature even if the heated element is at a constant and uniform temperature,

(2) Cones, wedges and plates may have a substrate that is not completely enveloped by the heated element. If so, there is a heat loss into the substrate. Similarly cylinders and spheres may have a heat loss into their supports.

In principle, the heat flux from any real probe can be calculated by solving the coupled temperature equations of the boundary layer and the solid probe but, in practice, this would entail an inordinate amount of effort. The heat flux from any probe can also be determined empirically but this by itself would shed little light on the parameters governing the heat flux unless there is insight to help interpret the results.

In practice, only the average temperature of the sensing element and the heat flux from it are known. The temperature of the wetted surface is not directly assessable. Thermal models of real probes that incorporate the concept of a Nusselt number governed heat flux from their wetted surfaces and that also include the thermal effects of the coating and the substrate have been developed (appendices B and C). The temperature of the wetted surface is variable but is assumed to be uniform. With these models a theoretical functional relationship between the heat flux and the flow can be derived without any knowledge of the probe's electronics. These relationships take the form

$$\frac{\Delta\theta}{Q} = h(R_e^{\frac{1}{2}}) \tag{8}$$

and agree favourably with the available calibration data of hot film probes (appendix B) and heated thermistors (appendix C).

Regardless of geometry, a constant temperature surface has a heat flux that is either a proportional or a linear function of $U^{\frac{1}{2}}$. Tan-Atichat, et al (1973) found it impossible to fit the heat flux versus $U^{\frac{1}{2}}$ calibration data of their 0.015 cm diameter, glass coated, cylindrical, hot film probe to a linear relationship. They attempted the more general linearization

$$\frac{Q}{\Delta\theta} = A + BU^n \tag{9}$$

and claimed a best fit when A = 0 and n = 0.23. Equation 9 is often fitted to calibration data from hot wires in air but A is never zero and the exponent n appears to be restricted to 0.45 to 0.52. There is no physical model to justify equation 9 when n does not equal $\frac{1}{2}$. The steady calibration data of two conical hot film probes (appendix B) also show that the heat flux is not a proportional function of $U^{\frac{1}{2}}$, as expected from equation 6, or even a linear function of $U^{\frac{1}{2}}$. Similarly, the calibration data of a paralene-c coated plate-shaped thermistor, a paralene-c coated ellipsoidal microbead thermistor and two glass coated microbead thermistors (appendix C) show that the heat flux is not a linear function of $U^{\frac{1}{2}}$. The heat flux relationship does <u>not</u> take the form

$$\frac{\Delta\theta}{Q} = h(R_e^{\frac{1}{2}}) = [A + B R_e^{\frac{1}{2}}]^{-1}$$

(equation 9 with $n=\frac{1}{2}$) because of the thermal effects of the coating and

the substrate. The heat flux relationships are

$$\frac{\Delta\theta}{Q} = A + \frac{B}{R_e^{\frac{1}{2}}}$$

for a coated plate shaped thermistor,

$$\frac{\Delta\theta}{Q} = A + \frac{B}{Nu}$$

for a coated ellipsoidal microbead thermistor and

$$\frac{\Delta\theta}{Q} = C + \frac{B}{A + R_e^{\frac{1}{2}}}$$

for a coated conical film sensor on a substrate. The parameters, A, B and C depend on the probe's geometry, size, coating thickness, the thermal conductivity of the fluid, the coating and the substrate, and the fluid's Prandtl number. The use of a third parameter for the conical probe model reflects the presence of the substrate.

With a knowledge of the function h the quasi-steady sensitivity to speed $\partial Q/\partial U$, the sensitivity to temperature $\partial Q/\partial(\Delta\theta)$ and the ratio of speed-to-temperature sensitivity are readily determined. The coating and the substrate each reduce the quasi-steady sensitivity to speed and to temperature oscillations of the ambient fluid. The substrate and the coating also reduce the ratio of speed-to-temperature sensitivity below its maximum value of $\Delta\theta/2U$. The effect of a finite coating thickness can be very significant in water. At 15 cm/sec a typical glass coating of 0.0028 cm on a 0.017 cm diameter microbead thermistor reduces the speed sensitivity by a factor of 10 and the ratio of speed-to-temperature sensitivity by a factor of 3.2 from its value in the absence of a coating. This effect increases with increasing speed. A typical glass coating of 1 or 2×10^{-4} cm over a thin film probe reduces the temperature of

the wetted surface by approximately 20%. The glass substrate of a hot film probe can carry about 20% of the total heat flux from the film. The effect of the coating and the substrate depends strongly on the relative conductivity of the fluid. There is a strong coating effect but a moderate substrate effect on probes in water whereas in air the coating effect is not very important but the substrate effect is important.

A knowledge of a probe's sensitivity to both speed and temperature is crucial for oceanic work because temperature activity often accompanies velocity activity. Some measurements of the intensity of temperature and velocity turbulence are now available. System noise and the probe's working life are two other important and sensitivity related considerations. An a priori evaluation of a sensor's performance is possible. The expected signal can be used to judge a sensor's signal-to-noise ratio, its signal contamination and its performance relative to other sensors. Because the temperature-heat flux relationship is sensitive to geometry the merits of various coating materials, coating thicknesses, and probe shapes and sizes can be determined from the appropriate function $h(R_e^{\frac{1}{2}})$.

Oceanic microscale temperature gradients can, at some times and in some locations, be small enough to prohibit their resolution with the best present techniques (Gregg, et al, 1978 using thermistors). An increase of the signal-to-noise ratio is therefore important. Increasing a thermistor's current increases its signal-to-noise ratio but also increases its sensitivity to velocity fluctuations. Because the heat flux relationship

$$\frac{\Delta\theta}{Q} = h(R_e^{\frac{1}{2}})$$

is independent of the level of self heating it applies to thermometers as well as anemometers. The limit to which the current through a thermistor used for thermometry can be increased is governed by its relative velocity-to-temperature sensitivity, the relative velocity-to-temperature activity in the fluid being probed and the level of contamination of the temperature signal that one is willing to accept. Circumstances may vary greatly. By using the observed values for the rates of temperature and kinetic energy dissipation in the ocean it is shown in appendix C that temperature measurements made with glass coated microbead thermistors may be contaminated by velocity in the mixed layer and in other regions of high velocity but low temperature activity when the over-heat $\Delta\theta$ is only $\sim 10^{-2}$ ^{o}C. Heated anemometers, such as grossly heated thin film probes and thermistors, are also sensitive to temperature. Several people have suggested warmed thermistors for high frequency thermometry. However, because even low levels of internal heating may cause velocity contamination it is not likely that even moderately heated probes are practical for thermometry in the ocean.

As a final comment to this section, calibration data is often presented in terms of a bridge voltage and an over-heat ratio. This makes calibration comparisons difficult. To determine the heat flux versus flow relationship one then needs some knowledge of the probe's electronics and the temperature-resistance calibration of the probe. Often the needed information is not published. This is acceptable if the only purpose of publication is to demonstrate that a given operational system works but is not acceptable if the purpose is to

demonstrate the fundamental characteristics of a probe. Understanding of probe characteristics might proceed more swiftly if calibration data were published in terms of relevant parameters such as over-heat $\Delta\theta$, heat flux, Reynolds numbers, Prandtl numbers, and sensor dimensions instead of bridge voltages and over-heat ratios.

4. Unsteady Heat Transfer

The Nusselt number is a steady heat transfer concept. The response of sensors is not governed by the Nusselt number when the viscous boundary layer is unsteady. An understanding of the unsteady characteristics of ideal probes can be used advantageously to understand the unsteady behaviour of real probes.

4.1 Ideal Probes

The behaviour of the unsteady viscous boundary layer over a flat plate has been examined by the author (appendix A), Cheng and Elliott (1957), Hill and Stenning (1960), Lighthill (1954), Ostrach (1955), Rott and Rosenzweig (1960) and others. Only Ostrach (1955) and the author have extended their examination to the unsteady heat flux from a plate. Ostrach's results are limited to very low frequencies whereas the author's results apply to all frequencies. Lighthill (1954) examined the unsteady viscous boundary layer and the heat flux over the frontal surface of a cylinder (two-dimensional stagnation flow). The author (appendix B) has examined the unsteady boundary layer and the heat flux over a cone of half angle 15° under axi-symmetric flow.

The boundary layer over a flat plate of length L departs from its quasi-steady behaviour when the frequency parameter $\omega L/U \gtrsim 0.3$ where ω is the angular frequency in radians/second. Any criterion for unsteady behaviour is (necessarily) arbitrary. The frequency parameter chosen is that for which the unsteady surface shear stress on any part of the surface exceeds the quasi-steady stress by more than 20%. The boundary layer over a cone of half angle less than approximately 20°

becomes unsteady when $\omega L/U \gtrsim 0.9$ and becomes unsteady over the front of a cylinder of diameter D when $\omega D/U \geq 5$.

An examination of the unsteady first order perturbation equations of an ideal constant temperature sensor, like the plate discussed in appendix A, is instructive. The equations are

$$i\omega u_1 + u_o \frac{\partial u_1}{\partial x} + v_o \frac{\partial u_1}{\partial y} + u_1 \frac{\partial u_o}{\partial x} + v_1 \frac{\partial u_o}{\partial y} = i\omega U_o + \nu \frac{\partial^2 u_1}{\partial y^2} \qquad (10)$$

$$u_1 = v_1 = 0 \text{ at } y = 0 \text{ and } x > 0$$

$$u_1 = U_o \qquad \text{at } y \to \infty$$

$$i\omega T_1 + u_o \frac{\partial T_1}{\partial x} + v_o \frac{\partial T_1}{\partial y} - \frac{\partial^2 T_1}{\partial y^2} = - u_1 \frac{\partial T_o}{\partial x} - v_1 \frac{\partial T_o}{\partial y} \qquad (11)$$

$$T_1 = 0 \text{ at } y = 0, \infty \text{ and } x > 0$$

and

$$i\omega\theta + u_o \frac{\partial \theta}{\partial x} + v_o \frac{\partial \theta}{\partial y} - \kappa \frac{\partial^2 \theta}{\partial y^2} = 0 \qquad (12)$$

$$\theta = 0 \text{ at } y = 0, \; x > 0$$

$$\theta = 1 \text{ at } y = \infty$$

from equations 5(a), 16 and 17 in appendix A,

where $(u,v) = (u_o, v_o) + \varepsilon e^{i\omega t}(u_1, v_1)$

$$T = T_o + \varepsilon e^{i\omega t} T_1 + \gamma e^{i\omega t}\theta$$

$$U = U_o(1 + \varepsilon e^{i\omega t})$$

is the free stream speed, $T(x,\infty) = \gamma e^{i\omega t}$ is the free stream temperature and the constants γ and ε are small compared to unity. The boundary layer velocity is represented by the steady field (u_o, v_o) and a small perturbation $\varepsilon e^{i\omega t}(u_1, v_1)$ due to a small fluctuation of the main stream $\varepsilon U_o e^{i\omega t}$.

The steady temperature field due to steady streaming and the constant surface temperature is represented by T_o, $\varepsilon e^{i\omega t} T_1$ is the temperature field due to the unsteady velocity perturbation, and $\gamma\theta e^{i\omega t}$ represents the temperature field due to a small independent perturbation of the main stream temperature $\gamma e^{i\omega t}$. Because of the non-homogeneous term $i\omega U_o$ in equation 10, which represents the unsteady pressure gradient in the fluid, the unsteady boundary layer velocity (u_1, v_1) near the plate increases in magnitude and advances in phase from its quasi-steady value. A comparison of equations 11 and 12 makes it quite clear that the anemometric response (T_1) must be quite different from the temperature response (θ). Equation 10 is non-homogeneous but has homogeneous boundary conditions. The heating source that generates the perturbation temperature field T_1 is not at the boundaries but is intrinsically distributed throughout the entire boundary layer and results from the advection of the steady boundary layer temperature gradient $(\partial T_o/\partial x, \partial T_o/\partial y)$ by the unsteady boundary layer velocity (u_1, v_1). This heating source $\underset{\sim}{u}_1 \cdot \nabla T_o$ is a function of Prandtl number, frequency and position. Proper frequency response calibration requires a faithful simulation of the forcing term $(\underset{\sim}{u}_1 \cdot \nabla T_o)$ which can be provided by vibrating the probe longitudinally in a steady flow (Lighthill, 1954). Calibrations in a steady flow made by internally modulating the probe's temperature by, say, an unsteady electric current (Freymuth, 1977, 1978; Ling, 1955; Tan-atichat, 1973; Gust, 1976 and others) can infer only the quasi-steady response because the unsteady boundary layer is absent (details are discussed in appendix A).

The temperature response equation (11) is homogeneous and driven by a non-homogeneity at the boundary $y = \infty$. This heating source is outside of the boundary layer and can only penetrate the boundary layer by steady advection and by diffusion. Independent of the level of heating, the anemometric response bandwidth is wider than the temperature response bandwidth because (1) the heating source $\underset{\sim}{u}_1 \cdot \nabla T_o$ for the anemometric response increases in magnitude whereas the heating source for the temperature response is constant and (2) the heating source for the anemometric response is intrinsic to the boundary layer but the heating source for the temperature response is external to the boundary layer. The -3 dB response bandwidth for a flat plate in the Prandtl number range $0.7 \leq Pr \leq 15$ is

$$\left.\frac{\omega L}{U}\right|_{3\ dB} = \frac{3.7\ (1 + 2\sqrt{Pr})}{(1 + \sqrt{Pr})^2}$$

for the anemometric response and

$$\left.\frac{\omega L}{U}\right|_{3\ dB} = 0.56\ Pr^{-.38}$$

for the temperature response. Wedges and cones should have a wider bandwidth because their boundary layers are thinner. Lighthill (1954) found that the -3 dB bandwidth of the heat flux from the front of a cylinder in response to speed oscillations is approximately $\omega D/U = 5$ at a Prandtl of 0.7 (air). At a Prandtl number of 0.7 the bandwidth of a cylinder is 1.7 times larger than the bandwidth of a plate (if D=L).

The above bandwidths are independent of the level of steady heating but apply strictly only to constant temperature surfaces. For variable temperature probes the thermal inertia of the probe may also be important and further limit the response bandwidth. For either case, constant temperature or variable temperature probes, the anemometric bandwidth must be larger than the temperature response bandwidth because of the boundary layer's behaviour. However, the difference between the two responses will be less pronounced for variable temperature probes and the amount of this difference will depend on the relative importance of the probe's inertia.

4.2 Real Probes

The high frequency heat flux from the two conical probes examined in appendix B differs significantly from its quasi-steady value. The heated film on these probes spans the entire circumference at a position "downstream" from the apex. The film is narrow compared to its distance from the apex. These probes have a frequency response which at first seems surprising; the response rises with increasing frequency. Because of the film's aspect ratio the unsteady heat flux is proportional to the viscous surface stress over the film which increases in magnitude and phase advance with increasing value of the frequency parameter $\Omega = \omega L/3U$. Increasing the relative width of the film by either moving the film towards the apex or by widening the film would tend to diminish the rise of the frequency response. If the entire cone of 15^{o} half-angle were covered by the film then the frequency response should be similar to the response of a flat plate.

Significant departure from quasi-steady behaviour of the heat flux from a wedge shaped sensor in air at frequencies where the boundary layer must still be quasi-steady have been reported by Bellhouse and Schultz (1967). This effect is caused by the substrate. The heat flux into the substrate must, somewhere, pass through the probe's boundary layer to enter the ambient fluid. If the substrate's conductivity is large compared to the fluid's conductivity, the substrate's heat flux is sensitive to the flow because of the boundary layer in its path. The substrate's unsteady heat flux in response to speed oscillations can decrease with increasing frequency because of the substrate's finite thermal diffusivity. If the substrate's conductivity is not large compared to the fluid's conductivity then the heat flux through the substrate is nearly independent of the flow and does not respond to speed modulations. The heat flux through the substrate in response to oscillations of the ambient fluid's temperature on the other hand, must decrease with increasing frequency regardless of the value of the substrate-to-fluid conductivity ratio. Low frequency attenuation of the heat flux in response to speed oscillations is evidently small in water but large in air. The unsteady calibration data of the two conical hot film probes discussed in appendix B show very little low frequency attenuation. Frequency response calibrations in water by Nowell (1974) do not show any low frequency attenuation.

Because the response bandwidth is wider for speed than for temperature and because the substrate may affect a low frequency attenuation of the temperature response but not the speed response (in water), the ratio of temperature-to-velocity sensitivity is highest

at zero frequency. An upper bound for the temperature contamination of a measured velocity spectrum can be calculated with the temperature spectrum and the quasi-steady sensitivity ratio. Conversely, a lower bound for the velocity contamination of the temperature spectrum can be calculated with the quasi-steady value of the sensitivity ratio.

The high frequency response bandwidth of thin film anemometers is given approximately by $\omega L/U \sim 1$ and depends somewhat on the Prandtl number. If one assumes that a probe traverses through a "frozen" turbulence field at a speed U then the largest wave number σ that can be resolved because of frequency response limitations is

$$\sigma \sim \frac{\omega}{U}$$

which implies that $\sigma L \sim 1$. Thus the scale size corresponding to frequency response limitations is also approximately the scale size corresponding to spatial response limitations.

5. Conclusions

This thesis has discussed the steady and unsteady heat transfer from various types of sensors. The salient conclusions are as follows.

5.1 Steady Heat Transfer

(i) The Nusselt number is a steady heat transfer concept and is limited to the frequency range where the boundary layer is quasi-steady A functional relationship for the steady heat transfer from probes with an insulating coating and a substrate can be derived by incorporating the concept of a Nusselt number governed heat flux from the wetted surface.

(ii) The functional relationship for the steady heat flux has been explicitly derived for flake thermistors, microbead thermistors and conical hot film probes. The functional relationship is $\Delta T/Q = h(R_e^{\frac{1}{2}})$ where $h(R_e^{\frac{1}{2}}) \neq (A + BR_e^{\frac{1}{2}})^{-1}$ because of the thermal effects of the coating and the substrate.

(iii) The function $h(R_e^{\frac{1}{2}})$ can be used to calculate the quasi-steady sensitivity of thermometers and anemometers as well as the quasi-steady contamination of thermometers by velocity and anemometers by temperature.

(iv) The coating and the substrate each reduce the quasi-steady sensitivity to speed and temperature oscillations of the ambient fluid as well as the ratio of speed-to-temperature sensitivity. The maximum value of the ratio of speed-to-temperature sensitivity under forced convective heat transfer is $\Delta\theta/2U$.

(v) With some knowledge of $h(R_e^{\frac{1}{2}})$ an a priori evaluation of a

sensor's performance is possible. The expected signal can be used to judge a sensor's signal-to-noise ratio, its level of contamination, and its merits relative to other sensors. Because the function $h(R_e^{\frac{1}{2}})$ is sensitive to geometry the relative value of various coating materials, coating thicknesses and probe configurations can be assessed. The function $h(R_e^{\frac{1}{2}})$ is independent of the probe's electronics. Inter-comparison of published calibration data would be easier if it were presented in terms of relevant non-electrical parameters such as over-heat $\Delta\theta$, Reynolds numbers, and Prandtl numbers rather than bridge voltages and over-heat ratios.

5.2 Unsteady Heat Transfer

(i) The viscous boundary layer over a probe departs from its quasi-steady behaviour when

(1) $\omega L/U > 0.3$ for a flat plate,

(2) $\omega L/U > 0.9$ for cone of half-angle less than approximately 20°, and

(3) $\omega L/U > 5$ for a cylinder

where L is the stream-wise dimension of the probe or the diameter of the cylinder.

(ii) The heating source that generates the unsteady anemometric effect is, to a first order perturbation, the advection of the steady boundary layer temperature gradient by the unsteady boundary layer velocity, namely $\underset{\sim}{u}_1 \cdot \nabla T_o$. This heating source is intrinsically distributed throughout the boundary layer and is a function of frequency, Prandtl number and position.

(iii) Frequency response calibrations must realistically simulate the generation term $\underset{\sim}{u}_1 \cdot \nabla T_o$ when the boundary layer is unsteady; probe vibration does but internal heating does not.

(iv) The response of the heat flux to oscillation of the ambient fluid's temperature is generated by the unsteady temperature boundary condition at the exterior of the boundary layer. Consequently the response bandwidth is larger for speed oscillations than for temperature oscillations. Both bandwidths depend strongly on the Prandtl number. Because both bandwidths are independent of the level of internal heating the above conclusion also holds for nearly unheated temperature sensors.

(v) The heat flux into the substrate is sensitive to the boundary layer if the ratio of substrate-to-fluid conductivity k_s/k_f is large. If k_s/k_f is not large then the heat flux into the substrate is nearly independent of the flow. If $k_s/k_f >> 1$ then the unsteady heat flux into the substrate in response to speed oscillations decreases with increasing frequency. Regardless of the value of k_s/k_f the heat flux into the substrate in response to temperature oscillations of the ambient fluid decreases with increasing frequency.

(vi) The ratio of temperature-to-velocity sensitivity is highest at zero frequency.

(vii) An upper bound for the temperature contamination of a measured velocity spectrum can be calculated with the temperature spectrum and the quasi-steady sensitivity ratio. Conversely, a lower bound for the velocity contamination of the temperature spectrum can be calculated with the quasi-steady value of the sensitivity ratio.

Bibliography

Batchelor, G.K. 1970. An Introduction to Fluid Mechanics. Cambridge University Press, 615 pages.

Bellhouse, B.J. and D.L. Schultz. 1967. The determination of fluctuating velocity in air with heated thin film gauges. Journal of Fluid Mechanics, 29: 289-295.

Belyaev, V.S., A.N. Gezentsvey, A.S. Monin, R.V. Ozmidov and V.T. Paka. 1975. Spectral characteristics of small-scale fluctuations of the hydrophysical fields in the upper layer of the ocean. Journal of Physical Oceanography, 5: 492-498.

Boston, N.E.J. 1970. An investigation of high wave number temperature and velocity spectra in air. Ph.D. Thesis, University of British Columbia.

Cheng, Sin-I and D. Elliott. 1957. The unsteady laminar boundary layer on a flat plate. Transactions of the American Society of Mechanical Engineers, 79: 725-733.

Collins, D.C. and M.J. Williams. 1959. Two dimensional convection from heated wires at low Reynolds number. Journal of Fluid Mechanics, 6: 357-384.

Crawford, W.R. and T.R. Osborn. 1979. Microstructure Measurements in the Atlantic Equatorial Undercurrent during GATE. Submitted to Deep-Sea Research.

Freymuth, P. 1977. Frequency response and electronic testing for constant-temperature hot wire anemometers. Journal of Physics E; Scientific Instruments, 10: 705-710.

Freymuth, P. 1978. Theory of frequency optimization for hot film anemometers. Journal of Physics E; Scientific Instruments, 11: 177-179.

Gargett, A.E. 1978. Microstructure and fine structure in an upper ocean frontal regime. Journal of Geophysical Research, 83, C10: 5123-5134.

Grant, H.L., R.W. Stewart and A. Moilliet. 1962. Turbulence spectra from a tidal channel. Journal of Fluid Mechanics, 12: 241-268.

Grant, H.L., A. Moilliet and V.M. Vogel. 1968. Some observations of the occurrence of turbulence in and above the thermocline. Journal of Fluid Mechanics, 34: 443-448.

Gregg, M.C., T. Meagher, A. Pederson and E. Aagaard. 1978. Low noise temperature microstructure measurements with thermistors. Deep-Sea Research, 25: 843-856.

Gregg, M.C. and A.M. Pederson. 1978. High resolution salinity measurements, NATO Advanced Study Institute on Instrumentation for Air-Sea Interaction, in press.

Gust, G. 1976. Observations on turbulent-drag reduction in a dilute suspension of clay in sea-water. Journal of Fluid Mechanics, 75: 29-47.

Hill, P.G. and A.H. Stenning. 1960. Laminar boundary layers in oscillatory flow. Transactions of the ASME Series D, pp. 593-608.

Hinze, J.O. 1975. Turbulence. Second edition, McGraw-Hill, 790 pages.

Kramers, H. 1946. Heat transfer from spheres to flowing media. Physica, 12: 61-80.

Lighthill, M.J. 1954. The response of laminar skin friction and heat transfer to fluctuations in the stream velocity. Proceedings of the Royal Society of London, Series A, Vol. 224, pp. 1-23.

Ling, S-E. 1955. Measurement of flow characteristics by the hot-film technique. Ph.D. Thesis, State University of Iowa.

Marmorino, G.O. and D.R. Caldwell. 1978. Horizontal variation of vertical temperature gradients measured by thermocouple arrays. Deep-Sea Research, 25: 221-230.

Mangler, W. 1948. Zusammenhang zwischen ebenen und rotations-symmetrischen Grenzschichten in kampressiblen Flüssig-kirten, Zeitschrift für angewandte Mathematic und Mechanik, 28, 95.

Nowell, Arthur R.M. 1974. Some response characteristics of parabolic hot films in water. J. of Hydronautics 8: 4, pp. 169-171.

Osborn, T.R. 1978. Measurement of energy dissipation adjacent to an island. Journal of Geophysical Research, 83, C6, 2939-2957.

Rott, Nicholas and Martin L. Rosenzweig. 1960. On the response of the laminar boundary layer to small fluctuations of the free-stream velocity. J. of Aeronautical and Space Sci. 27: 741-747.

Tan-atichat, J., H.M. Nagib and J.W. Pluister. 1973. On the inter-pretation of the output of hot-film anemometers and a scheme of dynamic compensation for water temperature variations. Proceedings of the Symposium on Turbulence Measurements in Liquids, Department of Chemical Engineering, University of Missouri-Rolla.

White, Frank. 1974. Viscous Fluid Flow. McGraw-Hill, 725 pages.

Appendix A

The Unsteady Flux of Heat and Momentum from a Flat Plate

by Rolf G. Lueck

Institute of Oceanography

The University of British Columbia

Vancouver, B.C., Canada

V6T 1W5

March 1979

Abstract

The unsteady viscous stress on a flat plate computed numerically from a simplified unsteady momentum equation that is not restricted by frequency compares favourably with the frequency restricted calculations available. The unsteady heat flux from the same plate maintained at a constant temperature was also computed. The heat flux responds differently to oscillations of the ambient fluid's speed than it does to oscillations of the ambient fluid's temperature. The response to speed oscillations has a maximum value at low frequencies and a larger bandwidth than the response to temperature oscillations. An examination of the unsteady temperature equations shows that an oscillation of the plate's surface temperature does not generate a heat flux that is comparable to the heat flux in response to either speed oscillations or to temperature oscillations of the ambient fluid when the boundary layer is unsteady.

1. Introduction

A significant motive for understanding the unsteady heat flux from bodies exposed to streaming comes from the common use of heated sensors for high frequency turbulence flow measurements. Spectra of velocity and temperature may be significantly biased (filtered) if the sensor's unsteady response is different from its quasi-steady response, in which case, some data correction is required. Wire-shaped sensors have traditionally been used in air. In water, however, it is more common to use thin film sensors that are wedge-shaped (Nowell, 1974), cone-shaped (Gargett, 1976, Grant et al., 1962, 1968), and cylindrical.

The dimensions of film type sensors differ by several factors of 10 from wire sensors; wires have typical diameters of 10^{-6} meters, cylindrical film sensors 10^{-4} meters, and wedge and cone shaped sensors have films about 10^{-3} meters long. As shown later, a frequency parameter that characterizes the unsteady boundary layer is $\omega L/U_o$ where ω is the angular frequency of oscillation (in radians per second), L is a relevant dimension (diameter or length in the flow direction), and U_o is the ambient fluid's steady speed. If $\omega L/U_o \ll 1$ the flow is essentially quasi-steady, its behaviour at any instant is that appropriate to steady conditions at the instantaneous value of the fluid's speed and temperature. If $\omega L/U_o \gtrsim 1$ the flow is unsteady and may behave differently from the quasi-steady flow. It is readily seen that wire type sensors operate in the quasi-steady frequency range for all practical purposes. However, the boundary layer on cylindrical films is unsteady when $\omega \gtrsim 10^4\ U_o$ (U_o in meters/second) and is unsteady on wedge and cone shaped sensors when $\omega \gtrsim 10^3\ U_o$. Thus unsteady effects are within the frequency domain of typical measurements made with

wedge and cone shaped film turbulence sensors. Unsteady boundary layer effects have been reported by Nowell (1974) and Evans (1963). In both cases the response to external speed oscillations was measured by vibrating the probe in the direction of the steady stream. Nowell showed that the unsteady response of wedge shaped sensors diminished with increasing frequency when $\omega/U_o \geq 10^{-3}\text{metre}^{-1}$. The response was down by 3 dB at 120 cyles/sec for U_o=0.31 m/sec and 500 cycles/sec for U_o=1.12 m/sec. For cone shaped sensors with a narrow film at a distance L from the rear of the apex, Evans reported that the response rises when $\omega L/U_o \geq 0.9$

The frequency response of heated sensors is often inferred from internal heating methods; the probe is exposed to a steady streaming, its temperature is oscillated by an electric current and the resulting heat flux is measured. Whereas one wants to know the response to oscillations from outside of the boundary layer one is calibrating the response to an internal oscillation. The calibrations made by internal heating are related to the response to external speed and temperature oscillations by implicitly assuming that the response (to external oscillations) is quasi-steady (Freymuth, 1978). When the boundary layer is quasi-steady it does not matter whether the oscillations are external or internal because the inertia and the thermal inertia of the boundary layer are negligible. However, when the boundary layer is unsteady the heat flux in response to external oscillations is different from the heat flux in response to internal temperature oscillations; at unsteady frequencies ($\omega L/U_o \geq 1$) the former decreases with increasing frequency while the latter increases with increasing frequency (as shown later). At high frequencies the flux in response to internal oscillations depends only on the fluid's thermal properties and ω, whereas the flux in response to external oscillations always depends on the

fluid's speed and Prandtl number.

The point here is that if the response of a sensor is not affected by the inertia or the thermal inertia of the boundary layer then internal heating can give useful information. If the sensor is operated in a constant temperature mode then internal heating can tell about the electronics. If the sensor is operated in a constant current mode then internal heating can measure the thermal inertia of the probe and the limitation of the electronics. But if the response is limited by boundary layer processes then internal heating cannot give any information about the effect of the boundary layer because (1) the unsteady velocity in the boundary layer is not present during calibration and because (2) the heat flux from the probe responds differently to external oscillation than to internal oscillation. The probe's constant temperature electronics cannot control the behaviour of the boundary layer. Hence, frequency response calibrations of cylinder, wedge and cone shaped sensors made by internal heating may be erroneous in the frequency range where the boundary layer is unsteady.

In practice the response may be complicated by substrate effects (Bellhouse and Schultz, 1967), coating effects and possibly limitations of the electronics. However, an examination of the inherent hydrodynamic limitations of an ideal sensor like a flat plate has practical implications because these limitations must also apply to real sensors and other heated surfaces exposed to an unsteady streaming.

A considerable amount of work has been published on the plate's non-steady velocity boundary layer (Cheng and Elliott 1957, Hill and Stenning

1960, Rott and Resenzweig 1960). However, little of this work has been extended to the unsteady response of the heat flux to speed or to temperature oscillations in the ambient stream. Lighthill (1954) investigated the unsteady flow over a flat plate for the case of small oscillations in the magnitude, but not the direction, of the ambient fluid. By using the Kármán-Pohlhausen method, Lighthill derived an approximate analytic solution for the velocity field for low frequencies. The unsteady heat flux, however, could not be derived by the same method, mainly because of the plate's zero steady pressure gradient. Ostrach (1955), using a numerical method valid for low frequencies ($\omega L/U_o \ll 1$), found that the heat flux increases slightly in magnitude and has a phase advance over its quasi-steady value.

The author is unaware of any work on the response of heated sensors to temperature oscillations of the ambient fluid.

In the following, attention is restricted to the case where the magnitude but not the direction of the ambient fluid oscillates about a steady mean, and where the amplitude of oscillation is small enough to avoid harmonic distortions. The Reynolds number range is restricted to where the boundary layer approximations are valid and where the boundary layer is laminar. It is assumed that the temperature field does not influence the velocity field. The surface temperature of the plate is taken as constant at θ and the amplitude of oscillation of the ambient fluid's temperature is assumed to be small compared to θ. The analysis has applications for constant temperature sensors and other surfaces whose temperature remains constant or practically constant when exposed to unsteady streaming.

The viscous boundary layer is examined in section 2. Section 2a deals with the steady boundary layer velocity and 2b deals with unsteady flow in the boundary layer. The heat flux is calculated in section 3. The unsteady flux in response to speed oscillations in ambient fluid is calculated in 3a and the response to ambient fluid temperature oscillations is examined in 3b.

2. The Viscous Boundary Layer

The boundary layer equations for two dimensional incompressible flow with an ambient fluid speed U(t) parallel to the plate are (Lighthill, 1954)

$$\frac{\partial u}{\partial t} + \frac{u\partial u}{\partial x} + \frac{v\partial u}{\partial y} + \frac{1}{\rho}\frac{\partial P}{\partial x} = \nu \frac{\partial^2 u}{\partial y^2} \tag{1a}$$

$$\frac{\partial u}{\partial x} + \frac{\partial v}{\partial y} = 0 \tag{1b}$$

$$\frac{\partial U}{\partial t} + \frac{1}{\rho}\frac{\partial P}{\partial x} = 0 \tag{1c}$$

with boundary conditions

$u = v = 0$ @ $y = 0$ for $x > 0$ and

$u \to U(t)$ as $y \to \infty$

where ρ is the fluid density and ν the kinematic viscosity (Figure 1). We now let the quantities U, u, and v perform small oscillations about a steady mean and write

$$U(t) = U_o(1+\varepsilon e^{i\omega t}) \tag{2a}$$

$$u = u_o(x,y) + \varepsilon u_1(x,y,\omega)e^{i\omega t} \tag{2b}$$

$$v = v_o(x,y) + \varepsilon v_1(x,y,\omega)e^{i\omega t} \tag{2c}$$

where $\varepsilon << 1$ is the relative amplitude of the speed oscillations and is therefore a suitable perturbation parameter.

2a. Steady Flow

The well known Blasius transformation given in Schlichting (1955, p. 103), reduces the steady momentum equation (1a) to

$$ff'' + 2f''' = 0$$

$$f(0) = f'(0) = 0$$

$$f'(\infty) = 1, \tag{3}$$

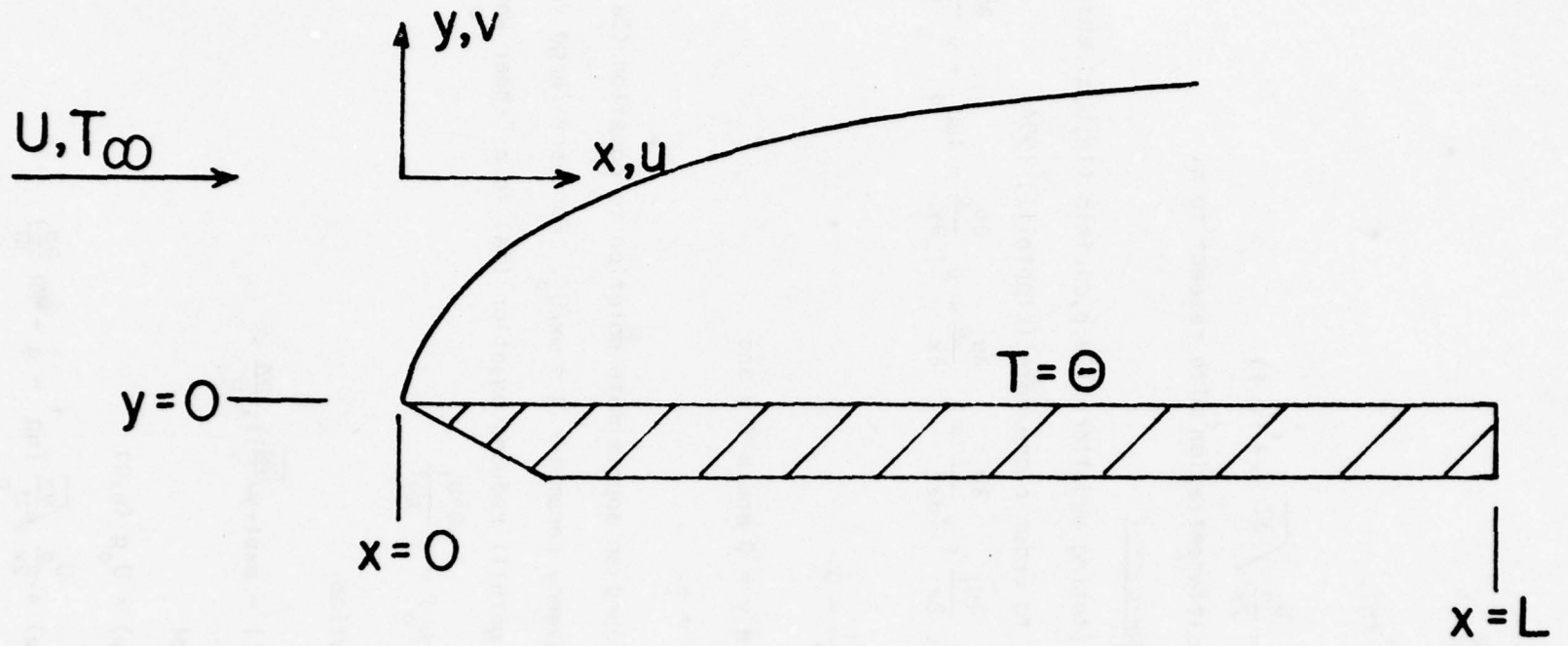

Figure 1. A sketch of the idealized plate showing the coordinate system employed for the analyses. The surface temperature is fixed at Θ, a constant.

where $\eta = y\sqrt{\frac{U_o}{\nu x}}$,

$$u_o = U_o f'(\eta),$$

and

$$v_o(x,y) = \frac{U_o}{2x}\sqrt{\frac{\nu x}{U_o}}(\eta f' - f) \tag{4}$$

and primes denote differentiation with respect to η.

2b. Non-Steady Flow $\varepsilon << 1$

By substituting equations (2a,b,c) into (1a,b,c) and by only retaining terms up to order ε one gets (Lighthill, 1954)

$$i\omega u_1 + u_o\frac{\partial u_1}{\partial x} + v_o\frac{\partial u_1}{\partial y} + u_1\frac{\partial u_o}{\partial x} + v_1\frac{\partial u_o}{\partial y} = i\omega U_o + \nu\frac{\partial^2 u_1}{\partial y^2} \tag{5a}$$

$$\frac{\partial u_1}{\partial x} + \frac{\partial v_1}{\partial y} = 0 \tag{5b}$$

where $u_1 = v_1 = 0$ @ $y = 0$ and $x > 0$ and

$u_1 = U_o$ as $y \to \infty$.

Lighthill (1954) found an approximate solution to equation (5a) for small values of the frequency parameter $\Omega = \omega x/U_o$. For very large values of the parameter $\omega x/U_o$ Lighthill reduced equation (5a) to a "shear wave" equation

$$i\omega(u_1 - U_o) = \nu\frac{\partial^2 u_1}{\partial y^2} \tag{6}$$

which has the solution

$$u_1 = U_o\{1 - \exp(-y\sqrt{\frac{i\omega}{\nu}})\},\ \frac{\omega x}{U_o} >> 1. \tag{7}$$

The substitution of

$$u_1(x,y,\omega) = U_o g'(\eta,\Omega) \tag{8a}$$

$$v_1(x,y,\omega) = \frac{U_o}{2x}\sqrt{\frac{\nu x}{U_o}}\{\eta g' - g - 2\Omega\frac{\partial g}{\partial \Omega}\} \tag{8b}$$

which satisfies continuity (5b), into (5a) yields

$$g''' + \frac{1}{2} fg'' - i\Omega g' + \frac{1}{2} f'' g - \emptyset = -i\Omega \tag{9a}$$

where

$$\emptyset = \Omega \frac{\partial}{\partial \Omega} (f'g' - f''g) \tag{9b}$$

$$g(0,\Omega) = g'(0,\Omega) = 0$$

$$g_1(\infty,\Omega) = 1$$

$$g(\eta,0) = \frac{1}{2} (f + \eta f') .$$

Rott and Rosensweig (1960) have partially solved equation (9b) numerically by writing g as a power series in Ω, that is

$$g(\eta,\Omega) = \sum_{n=0}^{\infty} (i\Omega)^n h_n(\eta) \qquad \text{for } \Omega < 1 ,$$

and calculated h_o and h_1. However, a power series expansion of the above type is impractical for $\Omega \sim 1$. Cheng and Elliott (1957) have solved the momentum equation (equation (5a)) to higher orders in Ω and have tabulated sufficient coefficients to evaluate the dimensionless surface stress $g''(0,\Omega)$ to the fourth order in Ω.

Equation (9a) becomes an ordinary differential equation where Ω is only a parameter if the term $\emptyset$ in equation (9a) can be ignored. Clearly as $\Omega \to 0$ $\emptyset \to 0$. For very high frequencies ($\Omega >> 1$) we have from equation (7), (8a), and (9b) that

$$\emptyset = \frac{1}{2} \{\eta f' g'' - \eta f'' g' + f'' g\}. \tag{10}$$

For $\eta < 2$ the function f is to a good approximation (Schlichting, 1954, p. 107)

$$f = \frac{1}{2} \eta^2 f''(0)$$

which makes the term $\emptyset$ for $\eta < 2$

$$\emptyset \approx \frac{1}{2} f''(0) \{\eta^2 g'' - \eta g' + g\}$$

whereas the advective term is

$$\frac{1}{2}\{fg'' + f''g\} \approx \frac{1}{2} f''(0)\{\frac{1}{2}\eta^2 g'' + g\}.$$

Because the magnitude of g' is never much larger than unity the term $\emptyset$ is comparable to the advective terms for $\eta<2$ at high frequencies. For $\eta<4$ an adequate approximation for f is (Schlichting 1954, p. 107)

$$f = \eta$$

which makes the term $\emptyset$ approximately

$$\emptyset \approx \frac{1}{2}\eta g''$$

and equal to the advective term. However, for high frequencies the advective term is small relative to the pressure gradient $i\Omega$, the inertia term $-i\Omega g'$ and the diffusion term g'''. The resulting equation, valid for $\Omega>>1$, is

$$g''' = i\Omega(g'-1)$$

which is equivalent to the "shear wave" equation 6.

For low frequencies, that is $\Omega<<1$, a first order expression for g is given by Lighthill (1954) and can be written as

$g(\eta,\Omega) = g(\eta,0) + i\Omega h(\eta)$, where h is a real function of order unity. Consequently.

$$\emptyset = i\Omega\{f'h' - f''h\} \qquad \text{(IIa)}$$

whereas the advective term is

$$\frac{1}{2}\{[fg''(\eta,0) + f''g(\eta,0)] + i\Omega(fh'' + f''h)\}. \qquad \text{(IIb)}$$

The term $\emptyset$ is small compared to the advective term because $\Omega<<1$ and because the negative sign in (IIa) causes a partial cancelling except for large η where h' may be slightly negative. In summary then, $\emptyset$ is identically zero at $\Omega=0$, is small compared to the advective terms for small Ω, and is comparable to the advective terms for large Ω but small compared to the

dominant terms which are diffusion, inertia and pressure.

If the velocity field does not have any singularities with respect to Ω, such as resonances and notches, then one can reasonably expect that the magnitude of $\emptyset$ transits smoothly, if not monotonically, from zero at $\Omega=0$ to a value comparable to the advective term at very large values of Ω. Thus the deletion of the term $\emptyset$ from equation (9) cannot lead to serious errors in computing g, its inclusion on the other hand would lead to formidable computational difficulties near $\Omega=1$. (In comparison the advective terms are easily handled by numerical routines.)

The simplified unsteady momentum equation

$$g''' + \frac{1}{2} fg'' - i\Omega g' + \frac{1}{2} f''g = i\Omega$$

$$g(0,\Omega) = g'(0,\Omega) = 0,\ g'(\infty,\Omega) = 1 \qquad (12)$$

and the steady momentum equation (3) have been solved numerically to an accuracy of 1 part in 10^6 or better, by a collocation routine currently being phased into operation at the Computing Science Department of The University of British Columbia (Ascher, Christiansen, and Russell, 1977). The frequencies Ω examined range from 0 to 8^2 in steps of $(0.1)^2$. The computed values for f, f', and f'' agree with the values tabulated in Schlichting to within one unit in the least significant digit. An estimate of $\emptyset$ at $\Omega=1$ based on the solution to equation (12) will be given later. The unsteady velocity profile g' is plotted in Figure 2 for $\Omega=0$, 0.25, 1.00 and 5.29.

Figure 3 compares Lighthill's low frequency solution at his critical frequency of $\Omega=0.588$, which in the notation used here is

$$1 - (1 - 0.171\eta)^2\{(1 - 0.171\eta - 0.0882\eta^2) - i\ 0.515\eta(1 - 0.229\eta)\}$$

against the computed velocity profile at the same frequency. The frequency

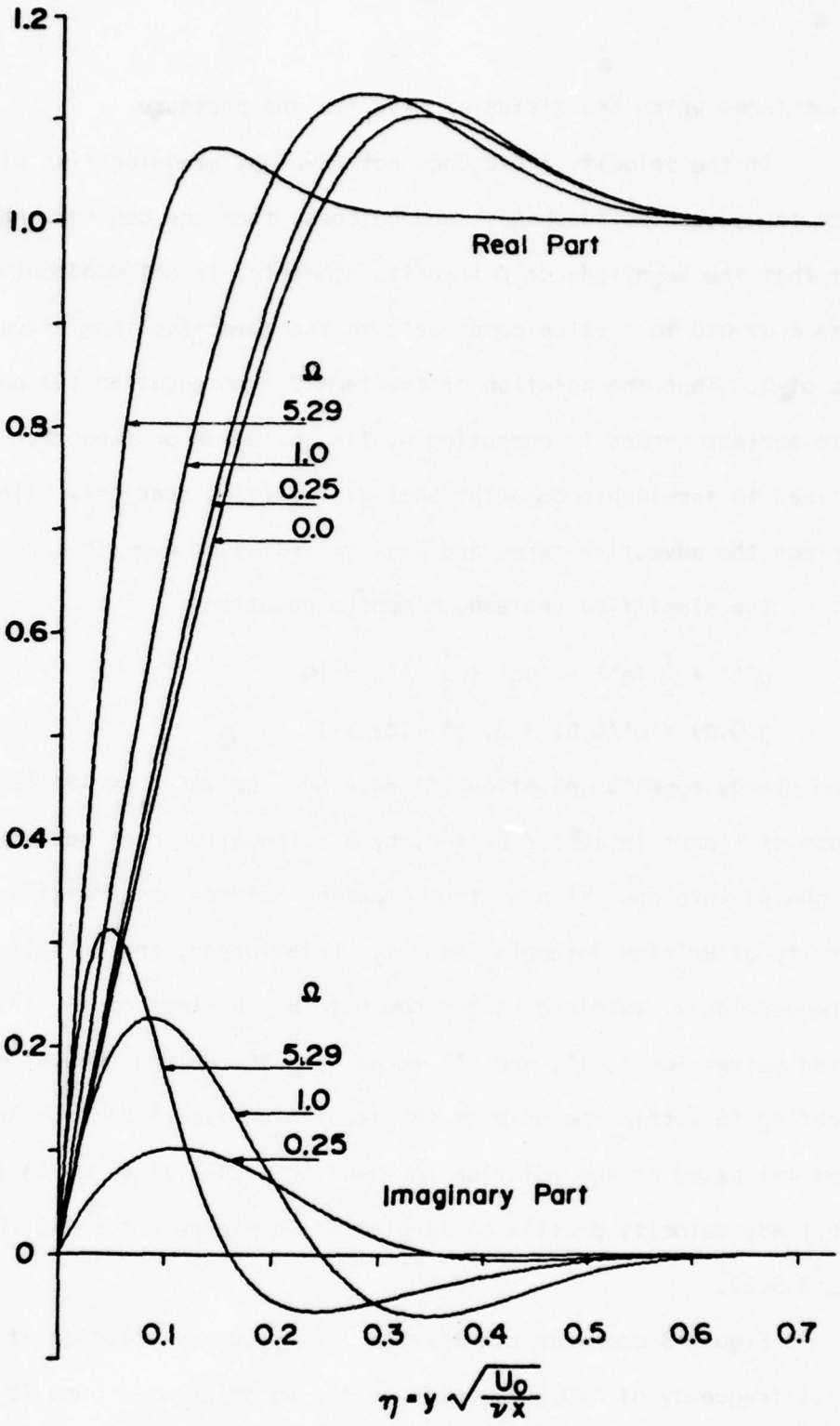

Figure 2. The real and imaginary components of the boundary layer perturbation velocity profiles at values of the frequency parameters Ω=0.0, 0.25, 1.0 and 5.29. The imaginary component of g' is zero for Ω=0.

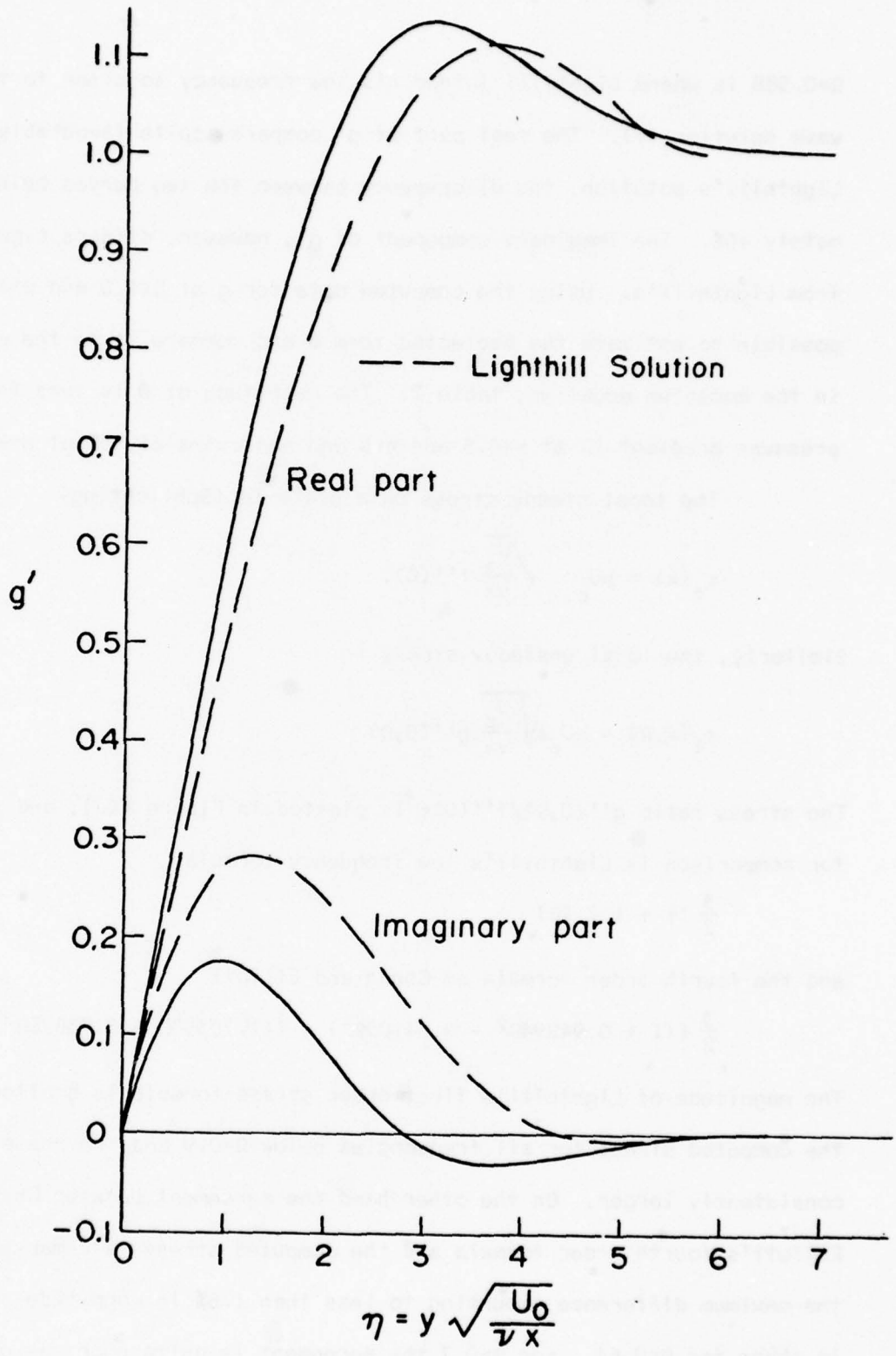

Figure 3. A comparison between the computed perturbation velocity profile and Lighthill's profile at the "critical" frequency Ω=0.588.

Ω=0.588 is where Lighthill joined his low frequency solution to the shear-wave solution (7). The real part of g' compares quite favourably with Lighthill's solution, the discrepancy between the two curves being approximately 10%. The imaginary component of g', however, differs significantly from Lighthill's. Using the computed data for g at Ω=1.0 and Ω=1.24 it is possible to estimate the neglected term $\emptyset$ and compare it to the other terms in the momentum equation, table 2. The magnitude of $\emptyset$ is less than 1% of the pressure gradient $i\Omega$ at η=0.5 and η=5 and approximately 5% at η=2.

The local steady stress on a plate is (Schlichting)

$$\tau_o(x) = \mu U_o \sqrt{\frac{U_o}{\nu x}}\, f''(0).$$

Similarly, the local unsteady stress is

$$\tau_1(x,\Omega) = \mu U_o \varepsilon \sqrt{\frac{U_o}{\nu x}}\, g''(0,\Omega)$$

The stress ratio $g''(0,\Omega)/f''(0)\varepsilon$ is plotted in Figure 4(a), and included for comparison is Lighthill's low frequency formula

$$\frac{3}{2}(1 + 1.7\, i\Omega)$$

and the fourth order formula of Cheng and Elliott

$$\frac{3}{2}\{(1 + 0.94294\Omega^2 - 0.54105\Omega^4) + i(1.70353\Omega - 0.73828\Omega^3)\}$$

The magnitude of Lighthill's first order stress formula is smaller than the computed stress for all frequencies below Ω=0.9 and the phase is consistently larger. On the other hand the agreement between Cheng and Elliott's fourth order formula and the computed stress is remarkable, the maximum difference amounting to less than 1.6% in magnitude and 1.4% in phase for $\Omega \leq 0.64$. For $\Omega > 0.7$ the agreement is quite poor; as expected their series expression diverges. Table I summarizes the unsteady

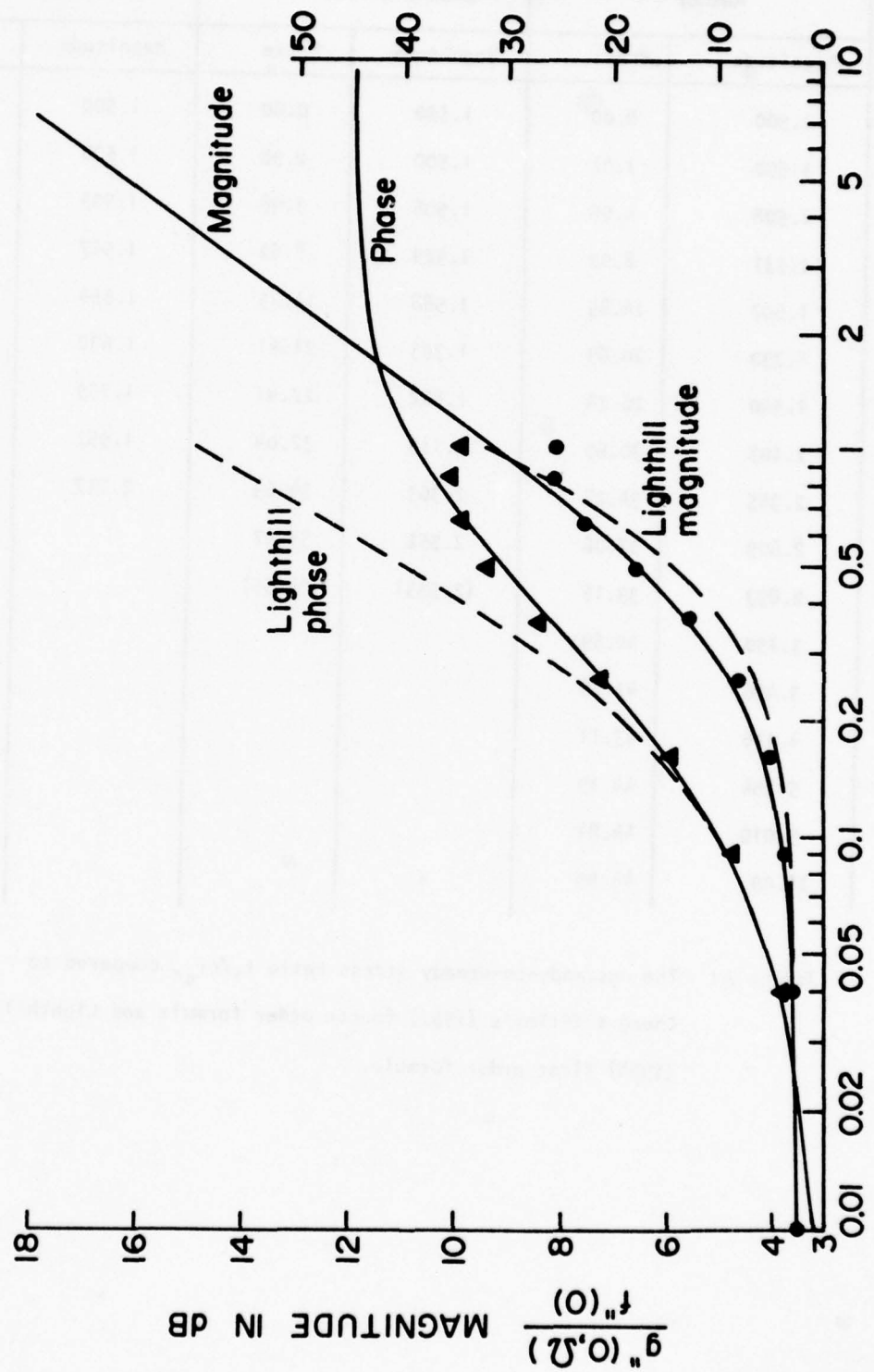

Figure 4(a). A comparison of the unsteady-to-steady local surface stress ratio (solid curves) against Lighthill's result (dashed curves) and Cheng and Elliott's results (solid dots for the magnitude and solid triangles for the phase).

	Author		Chen & Elliot		Lighthill	
Ω	Magnitude	Phase	Magnitude	Phase	Magnitude	Phase
0.0	1.500	0.00	1.500	0.00	1.500	0.00
0.01	1.500	1.02	1.500	0.98	1.500	0.97
0.04	1.508	4.06	1.506	3.98	1.503	3.89
0.09	1.537	8.90	1.529	8.62	1.517	8.70
0.16	1.607	14.85	1.588	14.75	1.554	15.22
0.25	1.730	20.89	1.703	21.41	1.630	23.00
0.36	1.900	26.24	1.882	27.47	1.759	31.47
0.49	2.107	30.69	2.115	32.04	1.952	39.79
0.64	2.345	34.27	2.363	34.69	2.217	(47.41)
0.81	2.609	37.06	2.552	35.47		
1.00	2.893	39.16	(2.553)	(34.55)		
1.21	3.190	40.69				
1.44	3.496	41.78				
1.96	4.116	43.11				
3.24	5.354	44.19				
9.00	9.010	44.84				
64.00	24.09	44.99				

Table AI The unsteady-to-steady stress ratio $\tau_1/\varepsilon\tau_0$, compared to Cheng & Elliot's (1957) fourth order formula and Lighthill's (1954) first order formula.

	η=0.5		η=2.0		η=5.0	
	Real	Imaginary	Real	Imaginary	Real	Imaginary
g'''	-0.237	-0.62	-0.30	+0.069	+0.034	-0.022
$\frac{1}{2}fg''+$ $+\frac{1}{2}f''g$	-0.29	+0.013	+0.232	-0.014	-0.016	+0.043
$-i\Omega g'$	+0.193	-0.362	+0.074	-1.043	-0.019	-1.021
$i\Omega$	--	+1.0	--	+1.0	--	+1.0
$\emptyset$	+0.010	+0.006	-0.023	-0.056	-0.024	-0.003

Table AII A comparison of the deleted term $\emptyset$ against the retained terms of the unsteady momentum equation (9a) at the frequency $\Omega=1.0$ for positions $\eta=0.5$, 2.0, and 5.0 . The values for g''' are approximations.

dimensionless surface stress ratios. For very large frequencies the non-dimensional surface stress approaches

$$g''(0,\Omega) = \sqrt{i\Omega}$$

in agreement with the "shear wave" solution given in equation (7).

The total steady drag per unit width on a plate of length L wetted on both sides is (Schlichting, 1955, p. 108)

$$D_o = 4\,\mu U_o \sqrt{\frac{U_o L}{\nu}}\; f''(0).$$

Similarly the total unsteady drag is

$$D_1 = 2\varepsilon\mu U_o \int_0^L \sqrt{\frac{U_o}{\nu x}}\; g''(0,\Omega)dx$$

$$= 4\varepsilon\mu U_o \sqrt{\frac{U_o L}{\nu}}\; \frac{1}{\xi^{\frac{1}{2}}} \int_0^{\xi^{\frac{1}{2}}} g''(0,\Omega)d\sqrt{\Omega}$$

where $\xi^{\frac{1}{2}} = \omega L/U_o$ is the non-dimensional plate frequency. The ratio of these two drags, namely

$$\frac{D_1}{\varepsilon D_o} = \frac{1}{f''(0)\xi^{\frac{1}{2}}} \int_0^{\xi^{\frac{1}{2}}} g''(0,\Omega)\; d\sqrt{\Omega}$$

is plotted in figure 4(b), and exhibits characteristics similar to the local stress ratio, namely an asymptotic trend to $\sqrt{i\xi}$ at large frequencies.

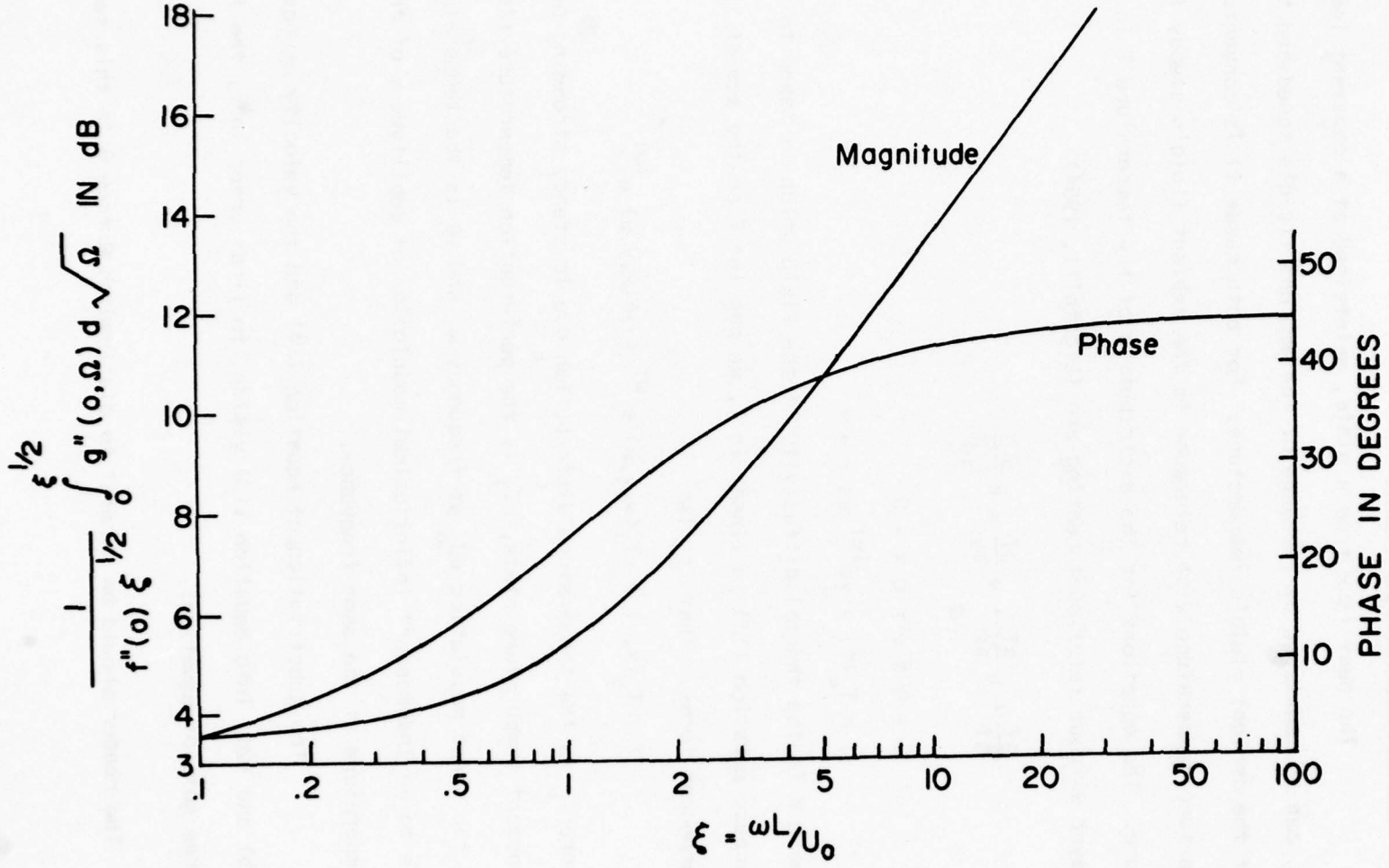

Figure 4(b). The unsteady-to-steady total stress ratio for a plate of length L.

3. The Thermal Boundary Layer

The heat flux from a plate, maintained at a constant temperature Θ, can be modulated by a change of the ambient fluid's speed and by a change of the ambient fluid's temperature. For both cases it is convenient to measure temperature with reference to the ambient fluid's steady temperature. The equations for the distribution of the temperature T in a boundary layer without frictional heating are (Lighthill, 1954)

$$\frac{\partial T}{\partial t} + u\frac{\partial T}{\partial x} + v\frac{\partial T}{\partial y} = K\frac{\partial^2 T}{\partial y^2} \tag{13}$$

$$T = \Theta \ @ \ y = 0 \quad x > 0$$

$$T = T_\infty(t) = \gamma e^{i\omega t} \text{ as } y \to \infty$$

where K is the thermal diffusivity of the fluid which is taken to be uniform. Because equation (13) is linear in T, we can let T be the sum of three component terms. That is, let

$$T = T_o(x,y) + \varepsilon T_1(x,y,\omega)\, e^{i\omega t} + \gamma\theta(x,y,\omega)\, e^{i\omega t}{}^{*} \tag{14}$$

where T_o is the temperature distribution due to steady streaming over the constant temperature plate, εT_1 is the perturbation temperature field due to the speed modulation εU_o at frequency ω, and $\gamma\theta$ is the temperature field due to an independent infinitesimal modulation of amplitude γ of the ambient temperature at the same frequency.

The substitution of equation (14) and the velocity expressions (2b) and (2c) into equation (13) yields, to first order in ε, the following three sets of equations.

* The reader should be careful to distinguish Θ from θ in this section.

$$\left.\begin{aligned} u_o \frac{\partial T_o}{\partial x} + v_o \frac{\partial T_o}{\partial y} &= K \frac{\partial^2 T_o}{\partial y^2} \\ T_o &= \Theta \ @ \ y = 0 \ x > 0 \\ T_o &= 0 \text{ as } y \to \infty \end{aligned}\right\} \tag{15}$$

$$\left.\begin{aligned} i\omega T_1 + u_o \frac{\partial T_1}{\partial x} + v_o \frac{\partial T_1}{\partial y} - K \frac{\partial^2 T_1}{\partial y^2} &= -u_1 \frac{\partial T_o}{\partial x} - v_1 \frac{\partial T_o}{\partial y} \\ T_1 &= 0 \ @ \ y = 0 \\ T_1 &= 0 \text{ as } y \to \infty \end{aligned}\right\} \tag{16}$$

and

$$\left.\begin{aligned} i\omega\theta + u_o \frac{\partial \theta}{\partial x} + v_o \frac{\partial \theta}{\partial y} - K \frac{\partial^2 \theta}{\partial y^2} &= 0 \\ \theta &= 0 \ @ \ y = 0 \\ \theta &= 1 \text{ as } y \to \infty \end{aligned}\right\} \tag{17}$$

A comparison of equations (16) and (17) makes it quite clear that the anemometric response (T_1) must be very different from the temperature response (θ). Equation (16) is non-homogeneous but has homogeneous boundary conditions. The unsteady heating source that generates the temperature field T_1 is not at the boundaries but is intrinsically distributed throughout the entire boundary layer and results from the advection of the steady boundary layer temperature gradient ($\partial T_o/\partial x$, $\partial T_o/\partial y$) by the unsteady boundary layer velocity (u_1,v_1). This heating source $\underset{\sim}{u}_1 . \nabla T_o$, as shown later, is a function of Prandtl number, frequency and position. The temperature response (θ) equation (17), on the other hand, is a homogeneous equation driven by a non-homogeneity at the boundary $y=\infty$. The heating source is outside of the boundary layer and can only penetrate the boundary layer through advection by the steady velocity field (u_o and v_o) and by diffusion.

Proper frequency response calibration requires a faithful simulation of the generating term, $\underset{\sim}{u}_1 \cdot \nabla T_o$ when determining the anemometric response and a simulation of the boundary condition $\theta=1$ at $y\to\infty$ when determining the temperature response. The equations for an internal temperature oscillation of $\exp(i\omega t)$ are

$$\left.\begin{aligned} & i\omega T_i + u_o \frac{\partial T_i}{\partial x} + v_o \frac{\partial T_i}{\partial y} - K \frac{\partial^2 T_i}{\partial y^2} = 0 \\ & T_i(x,0,\omega) = 1 \\ & T_i(x,\infty,\omega) = 0. \end{aligned}\right\} \qquad (18)$$

For quasi-steady frequencies ($\omega x/U_o \ll 1$) the thermal inertia of the boundary layer $i\omega T_i$ is small compared to the other terms and it is clear that $T_i = 1-\theta$ and, using equation (15), that

$$\theta = 1 - \frac{T_o}{\theta} .$$

Using equation (16) one has for $\omega x/U_o \ll 1$

$$T_1 = U_o \frac{\partial T_o}{\partial U_o}$$

and hence there is a simple relationship between T_1, θ, and T_i when $\omega x/U_o \ll 1$. When $\omega x/U_o \gtrsim 1$ there does not exist any simple relationship between T_1, θ and T_i, because (1) the generating term $\underset{\sim}{u}_1 \cdot \nabla T_o$ becomes unsteady but is not present in the equation for T_i and (2) the thermal inertia of the boundary layer becomes important. For very high frequencies ($\omega x/U_o \gg 1$) equation (18) reduces to

$$i\omega T_i - K \frac{\partial^2 T_i}{\partial y^2} = 0, \quad \begin{matrix} T(0,\omega) = 1 \\ T(\infty,\omega) = 0 \end{matrix}$$

because only terms involving ω and the derivatives of highest order need

to be retained. The solution is

$$T_i(y,\omega) = \exp\left\{-y\sqrt{\frac{i\omega}{K}}\right\}$$

The effect of the internal temperature oscillations on the fluid is restricted to a layer whose thickness decreases with increasing frequency. The surface heat flux is $k(i\omega/K)^{\frac{1}{2}}$ which increases with increasing frequency and does not depend on the fluid's speed or Prandtl number. Solutions for T_1 and θ (section 3 a & b) show that the heat flux in response to speed or temperature oscillations in the main stream decreases with increasing frequency when $\omega x/U_o \geq 0.3$ and always depends on the speed and Prandtl number of the main stream. In summary, the response as measured by an internal heating method can only be related to the response to external oscillations when $\omega x/U_o << 1$. When $\omega x/U_o \geq 1$ internal heating methods do not correctly measure the response to either speed or temperature oscillations in the main stream.

Using the Blasius transformation, equation (15) can be written as (Schlichting, 1954, p. 264)

$$\begin{aligned} &T_o'' + \frac{1}{2} Pr f T_o' = 0 \\ &T_o = \Theta \quad \eta = 0 \\ &T_o = 0 \quad \eta \to \infty \end{aligned} \tag{19}$$

which has the solution

$$T_o(\eta,Pr) = \frac{\Theta}{F(Pr)} \int_{z=\eta}^{\infty} [f''(z)]^{Pr} dz$$

where

$$Pr = \nu/K$$

and

$$F(Pr) = \int_0^\infty [f''(z)]^{Pr} dz$$

By making use of the Blasius transformation and equations (8a), (8b) and (20), the perturbation temperature equation (16) becomes

$$\frac{1}{Pr} T_1'' + \frac{1}{2} f T_1' - i\Omega T_1 = \frac{\theta}{2} \frac{[f''(\eta)]^{Pr}}{F} \{g + 2\Omega \frac{\partial g}{\partial \Omega}\} + f'\Omega \frac{\partial T_1}{\partial \Omega} \tag{20}$$

$$T_1(0,\Omega) = 0$$

$$T_1(\infty,\Omega) = 0$$

$$T_1(\eta,0) = U_o \frac{\partial T_o}{\partial U_o} = -\frac{\eta}{2} \frac{\theta}{F} [f''(\eta)]^{Pr}$$

and similarly the temperature response equation becomes

$$\frac{1}{Pr} \theta'' + \frac{1}{2} f\theta' - i\Omega\theta = f'\Omega \frac{\partial \theta}{\partial \Omega}$$

$$\theta(0,\Omega) = 0$$

$$\theta(\infty,\Omega) = 1$$

$$\theta(\eta,0) = 1 - \frac{\partial T_o}{\partial \theta} = \frac{1}{F} \int_0^{z=\eta} [f''(z)]^{Pr} dz \tag{21}$$

3a. <u>The Anemometric Response</u>

A perturbation temperature field solution (T_1) for very high frequencies that is valid where the steady temperature T_o, is a linear function of η was given by Lighthill (1954) and is

$$T_1(\eta,\Omega) = \frac{-i}{2\Omega} \frac{\theta[f''(0)]^{Pr}}{(1-Pr)\,F} \{\eta(1-Pr)^2 + Pr[\eta(1-Pr) + \frac{2}{\sqrt{i\Omega}}] e^{-\eta\sqrt{i\Omega}}$$

$$- \frac{2Pr}{\sqrt{i\Omega}} e^{-\eta\sqrt{i\Omega Pr}} \}$$

Thus for high frequencies the last term in equation 20

$$f'\Omega \frac{\partial T_1}{\partial \Omega} = -\frac{1}{2} f' \{3T_1 - \eta T_1'\}$$

and has the same magnitude as the advective term $\frac{1}{2} fT_1'$ but is small compared to the dominant terms diffusion, thermal inertia and heating. The reasons given for dropping the term $\emptyset$ from the momentum equation apply equally to the term $f'\Omega\partial T_1/\partial\Omega$ in equation (20).

The simplified perturbation temperature equation is

$$T_1'' + \frac{1}{2} fPrT_1' - i\Omega PrT_1 = \frac{\Theta Pr[f''(\eta)]^{Pr}}{2F(Pr)} \{g + 2\Omega \frac{\partial g}{\partial \Omega}\} \qquad (22)$$

$$T_1 = 0 \text{ @ } \eta = 0,\infty.$$

The term $g + 2\Omega\ \partial g/\partial\Omega$ can be evaluated from the solution of the non-steady momentum equation. Equation (22) has been solved numerically by a finite difference formulation with 881 points for η in the range 0 to 8.8. The tri-diagonal matrix representing the finite difference term of (22) was solved by Gaussian elimination. The generating term

$$\frac{1}{2} \frac{Pr}{F} [f''(\eta)]^{Pr} \{g + 2\Omega \frac{\partial g}{\partial \Omega}\}$$

which represents the heat source for the anemometric effect is calculated from the solutions to the momentum equations (4 and 12) and is plotted in Figure 5 for Prandtl numbers 1 and 8 at frequencies Ω= 0 and 1. The forcing increases in magnitude and phase advance with increasing frequency; it has vanishing boundary values and an amplitude maximum with a value and location that depends strongly on the Prandtl number. When $\omega x/U_o \geq 1$ the unsteady anemometer response can only be measured by a method that

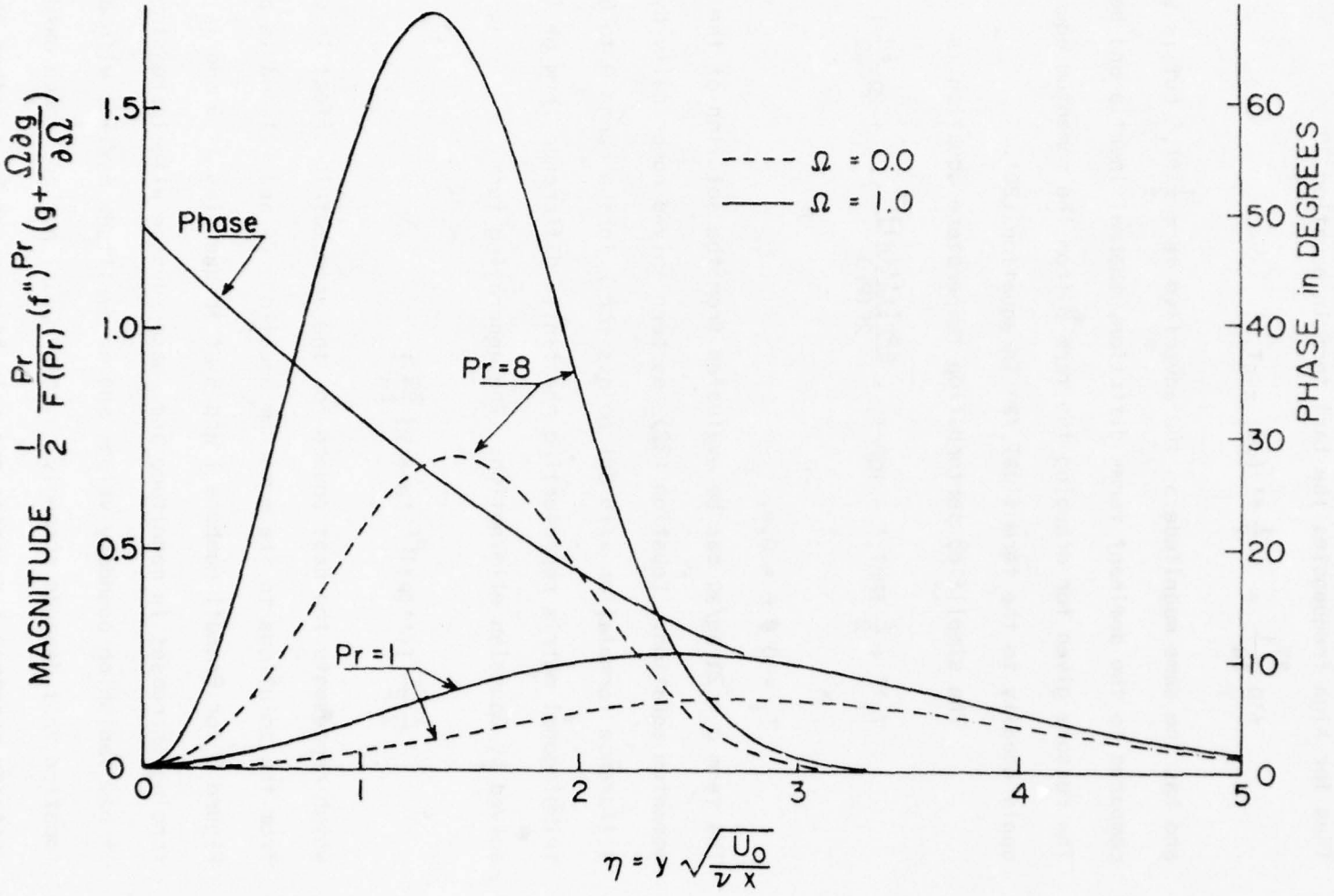

Figure 5. The profile of the function that generates the unsteady anemometric effect, for Prandtl numbers 1 and 8 at Ω=0 (dashed line) and Ω=1 (solid line). The phase is the same for Pr=1 and Pr=8.

simulates this generating term.

The steady local heat flux from the plate is

$$-k\sqrt{\frac{U_o}{\nu x}}\ T_o'(0,Pr)$$

where k is the fluid's conductivity. Similarly the local perturbation heat flux, that produces the non-steady anemometric effect, is

$$-\varepsilon k\sqrt{\frac{U_o}{\nu x}}\ T_1'(\Omega,Pr)\Big|_{\eta=0}$$

The perturbation-to-steady local heat flux ratio

$$\frac{T_1'(\Omega,Pr)\Big|_{\eta=0}}{\varepsilon T_o'(Pr)\Big|_{\eta=0}}$$

which is effectively the local unsteady Nusselt number is plotted in Figure 6(a). The heat flux magnitude rises above the quasi-steady value of 0.5 for all Prandtl numbers from 0.7 to 15. The highest heat flux peak is attained at a Prandtl number of two, for larger Prandtl numbers the peak height decreases and its location shifts to lower frequencies. A more detailed plot is in Figure 6(b). A power series expression for the local perturbation heat flux would have to be of third or higher order to duplicate the low frequency curves shown in Figure 6(b). For high frequencies the heat flux is proportional to $(i\Omega)^{-1}$. The phase is negative for all frequencies in spite of the low frequency amplitude rise. The ratio of the perturbation-to-steady local heat flux has been plotted in Figure 6(c) against a frequency axis scaled by

$$\frac{(1+\sqrt{Pr})^2}{1+2\sqrt{Pr}} \tag{23}$$

Except for some discrepancies associated with the various low frequency

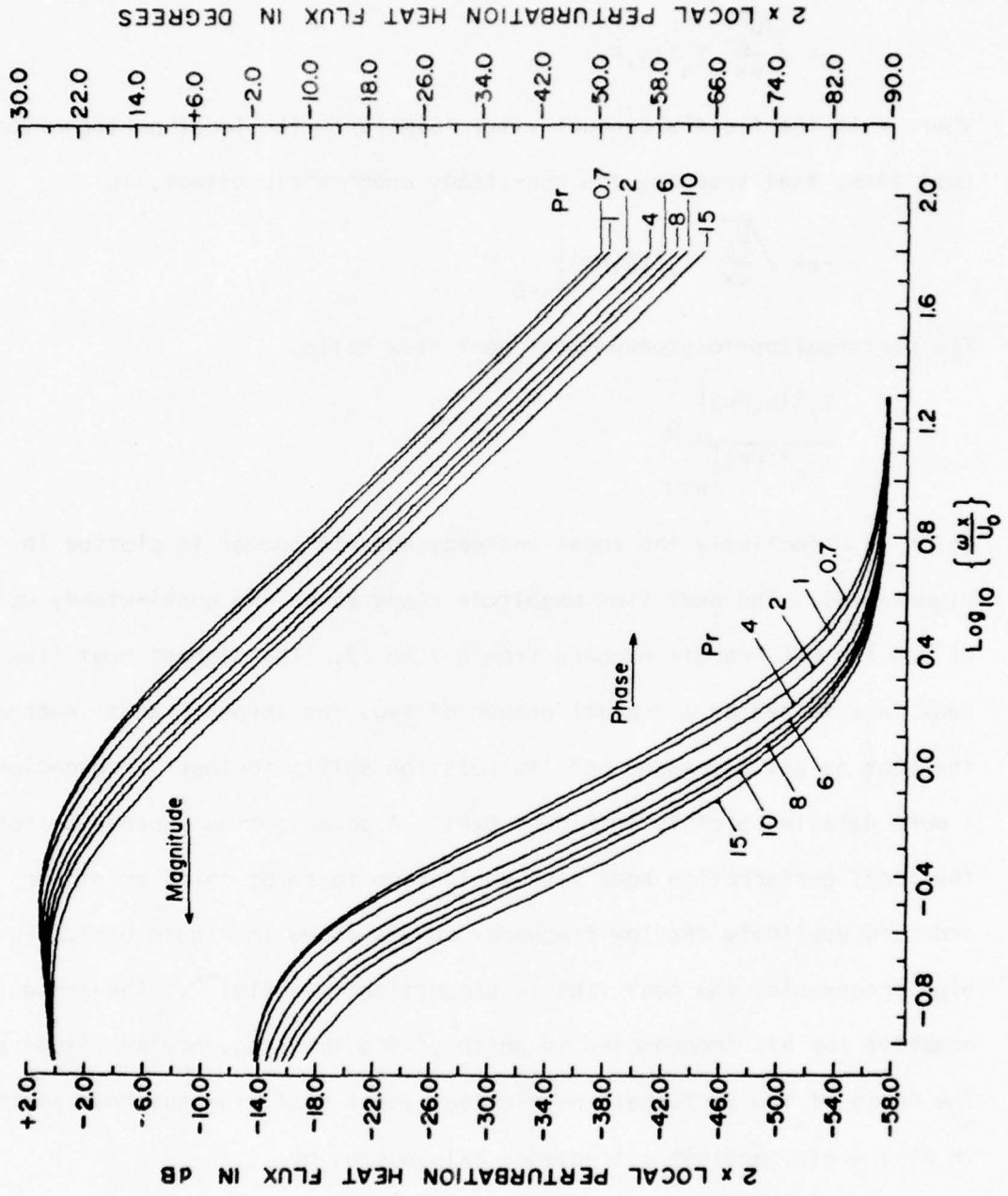

Figure 6(a). The local perturbation heat flux response to speed modulations, normalized by the steady heat flux; logarithmic plot.

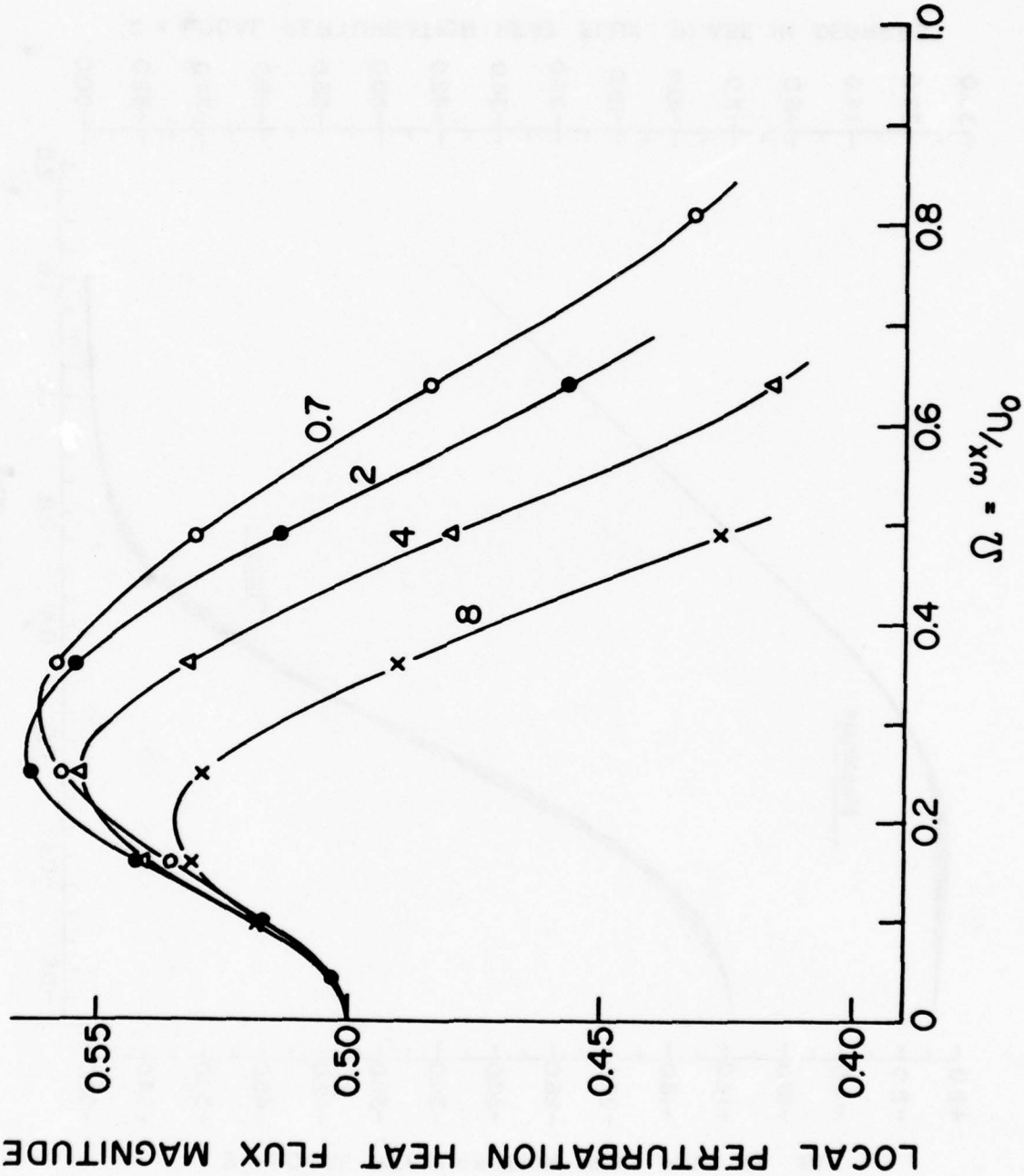

Figure 6(b). The local perturbation heat flux response to speed modulations, normalized by the steady heat flux; linear plot detailing the heat flux maxima.

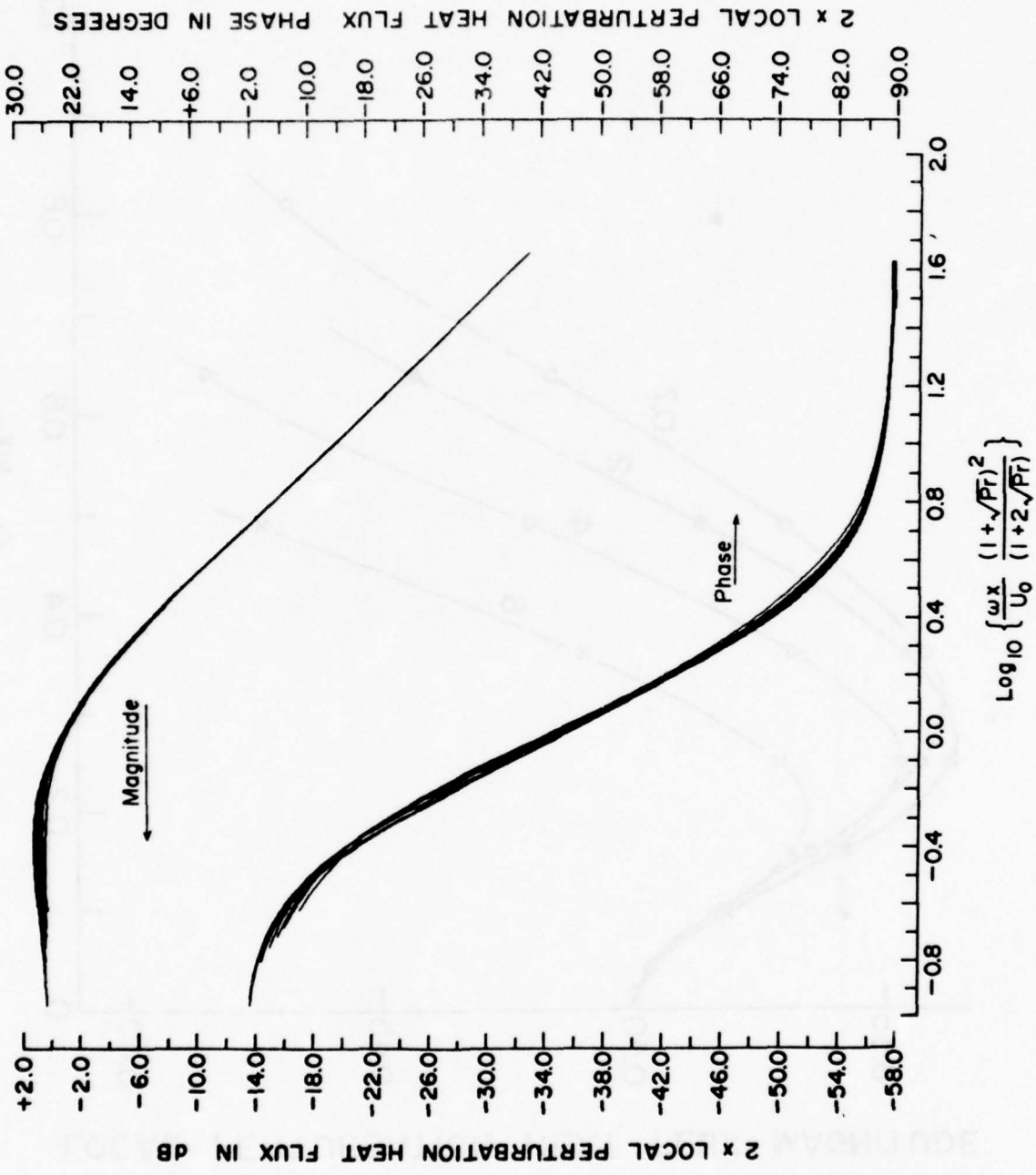

Figure 6(c). The local perturbation heat flux response to speed modulations, normalized by the steady heat flux; a frequency scaled version of (a).

peaks, both the magnitude and phase of the heat flux for the various Prandtl numbers satisfactorily collapse into one curve. The 3 dB bandwidth of the local perturbation heat flux is

$$\Omega_{3dB} = 1.45 \left\{ \frac{1 + 2\sqrt{Pr}}{(1 + \sqrt{Pr})^2} \right\}$$

In practice one senses only the total heat flux. The total heat flux, per unit width, from a plate wetted on both sides is (Schlichting 1955, pp. 268-269)

$$4k \sqrt{\frac{U_o L}{\nu}} \; T_o' \Big|_\eta = 4k \, R_e^{\frac{1}{2}} \frac{\Theta}{F} [f''(0)]^{Pr}$$

where $R_e = U_o L/\nu$. Similarly the total perturbation heat flux is

$$2\varepsilon k \int_0^L \sqrt{\frac{U_o}{\nu x}} \; T_1'(0,\Omega,Pr)\,dx$$

$$= 2 \, k \, R_e^{\frac{1}{2}} \; \frac{1}{\xi^{\frac{1}{2}}} \int_0^{\frac{1}{2}} T_1'(0,\Omega,Pr)\, d\sqrt{\Omega}$$

where $\xi = \omega L/U_o$. The ratio of the perturbation-to-steady total heat flux

$$\frac{F}{2\varepsilon [f''(0)]^{Pr} \xi^{\frac{1}{2}}} \int_0^{\xi^{\frac{1}{2}}} T_1'(0,\Omega,Pr)\, d\sqrt{\Omega}$$

is plotted in Figure 7(a). Asymptotically, the total heat flux is proportional to $(i\xi)^{-\frac{1}{2}}$, in contrast to the local heat flux ratio which is asymptotically proportional to $(i\Omega)^{-1}$. The peaks are less pronounced than the local heat flux peaks. The Prandtl number scaling of equation (23) satisfactorily collapses the curves for various Prandtl numbers into

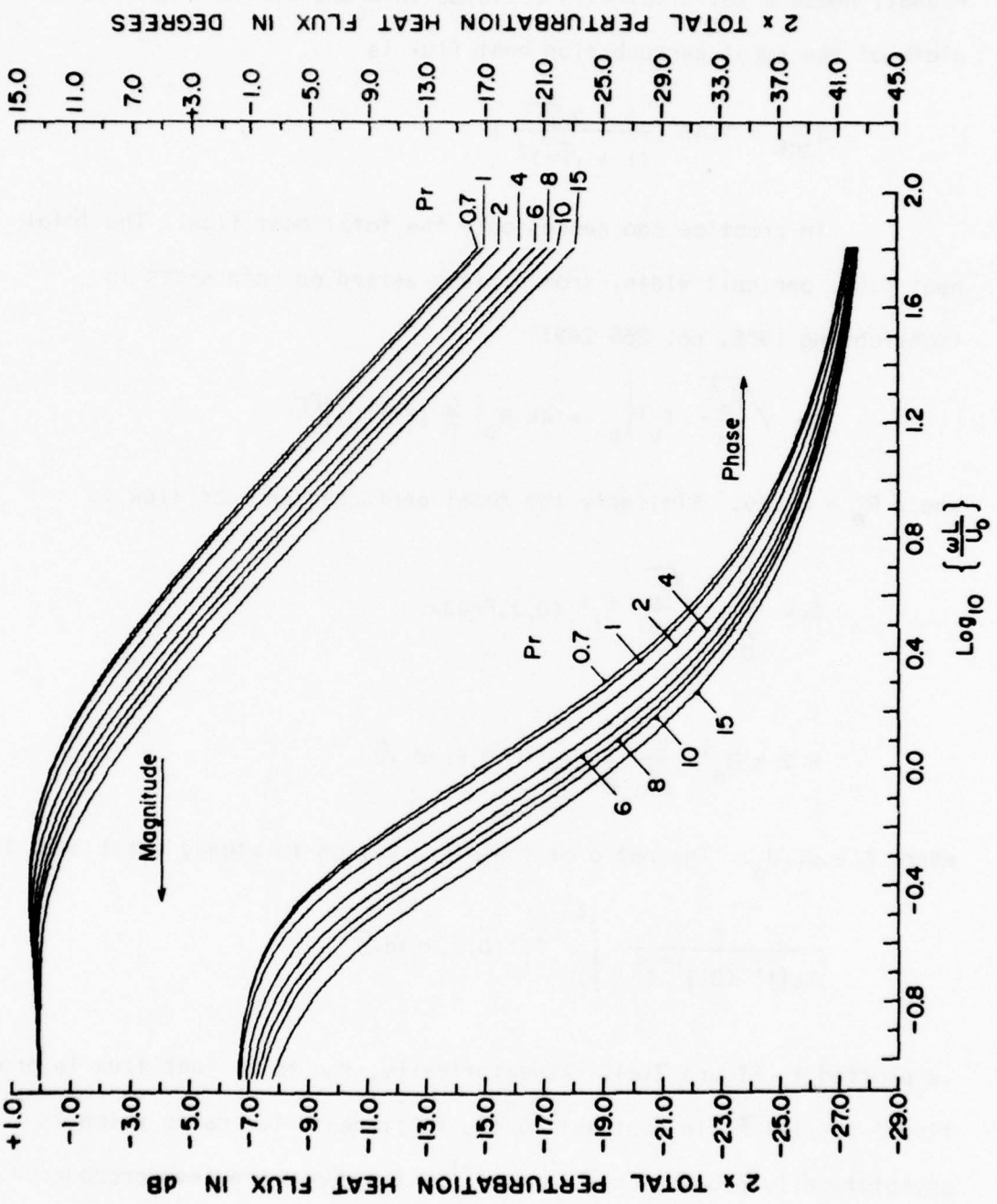

Figure 7(a). The perturbation-to-steady total heat flux ratio for speed modulations; unscaled frequency axis.

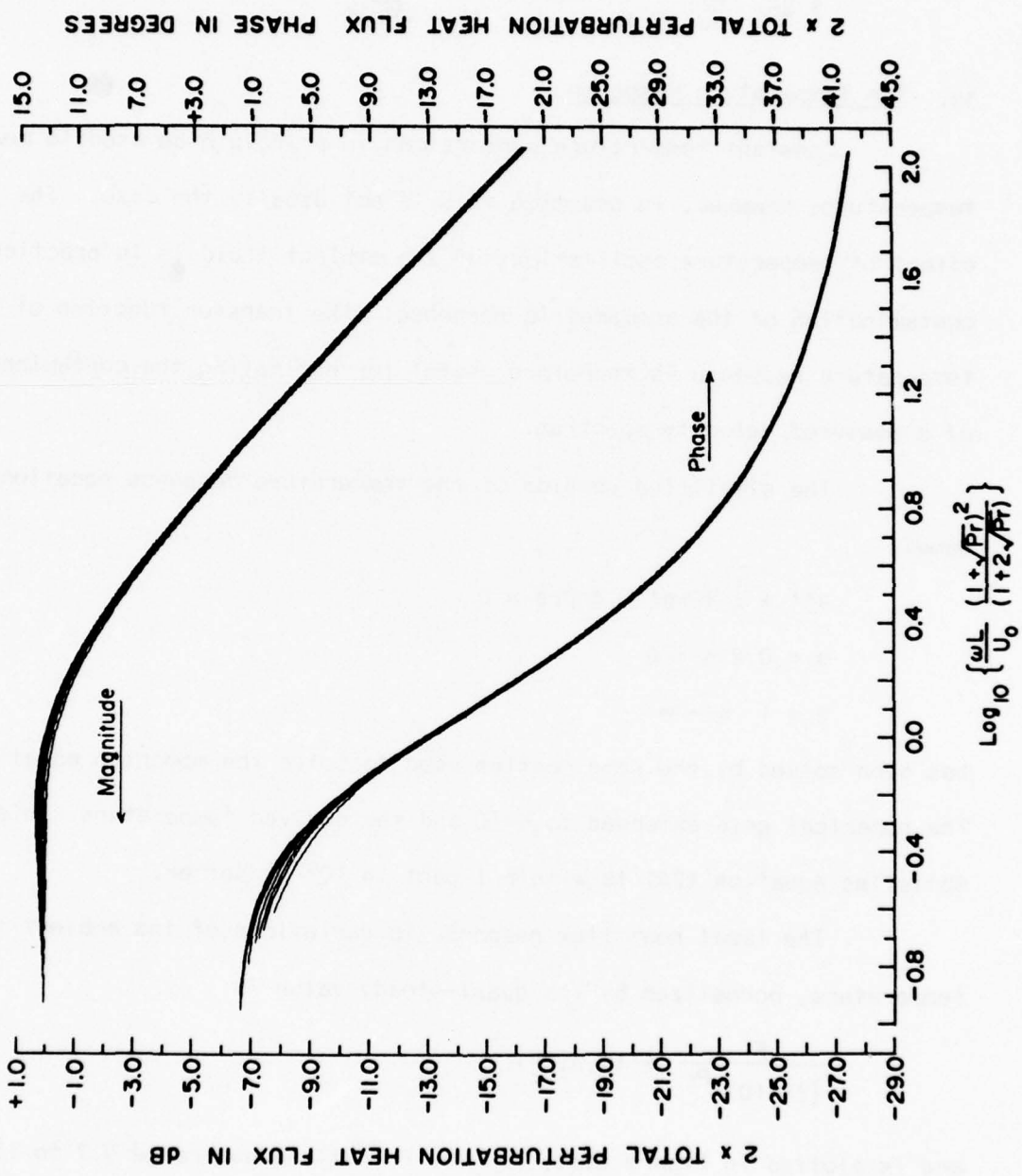

Figure 7(b). The perturbation-to-steady total heat flux ratio for speed modulations; scaled frequency axis.

one curve (Figure 7(b)). The 3 dB bandwidth of the total perturbation heat flux, the anemometric response bandwidth, is

$$\xi_{3\ dB} = \frac{\omega L}{U_o}_{3\ dB} = 3.7 \left\{ \frac{1 + 2\sqrt{Pr}}{(1 + \sqrt{Pr})^2} \right\}$$

3b. The Temperature Response

Constant temperature sensors can in principle be used to measure temperature; however, in practice this is not usually the case. The effect of temperature oscillations of the ambient fluid is in practice a contamination of the anemometric response. The transfer function of the temperature response is therefore useful for estimating the contamination of a measured velocity spectrum.

The simplified version of the temperature response equation (21), namely

$$\theta'' + \frac{1}{2} f Pr \theta' - i\Omega Pr \theta = 0$$

$$\theta = 0 \ @ \ \eta \approx 0$$

$$\theta = 1 \quad \eta \to \infty \qquad (24)$$

has been solved by the same routine used to solve the momentum equation (12). The numerical grid extended to η=10 and the derived temperature field satisfies equation (24) to within 1 part in 10^6 or better.

The local heat flux response to variations of the ambient fluid temperature, normalized by its quasi-steady value is

$$\frac{F}{[f''(0)]^{Pr}} \ \theta'(0,\Omega,Pr)$$

and is plotted in Figure 8(a), for the Prandtl number range 0.7 to 15. In contrast to the anemometer response, the local heat flux response to temperature decreases rapidly with increasing frequency. The phase shift

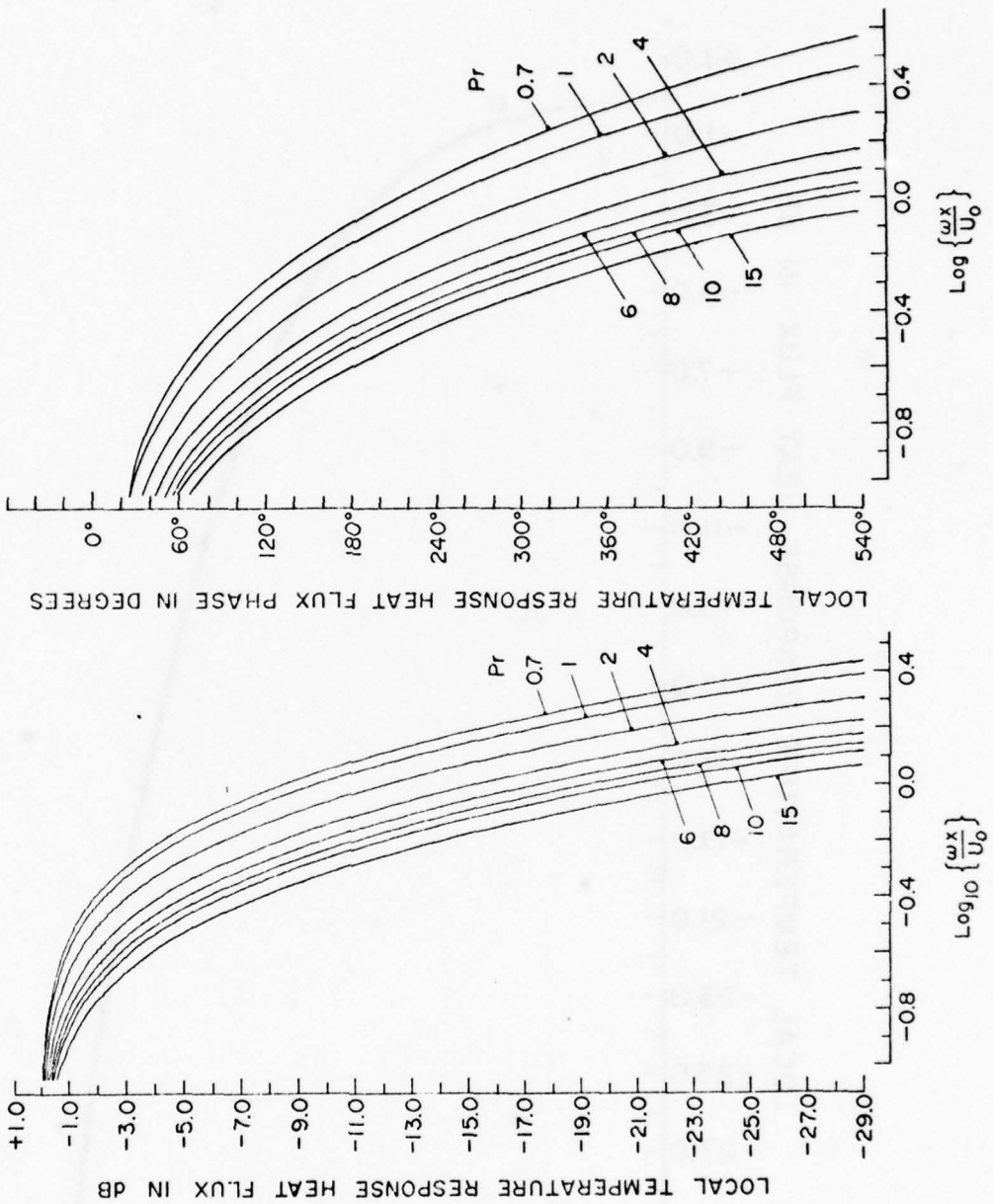

Figure 8(a). The local heat flux response to a temperature modulation of the ambient fluid, normalized by its quasi-steady value; magnitude and phase.

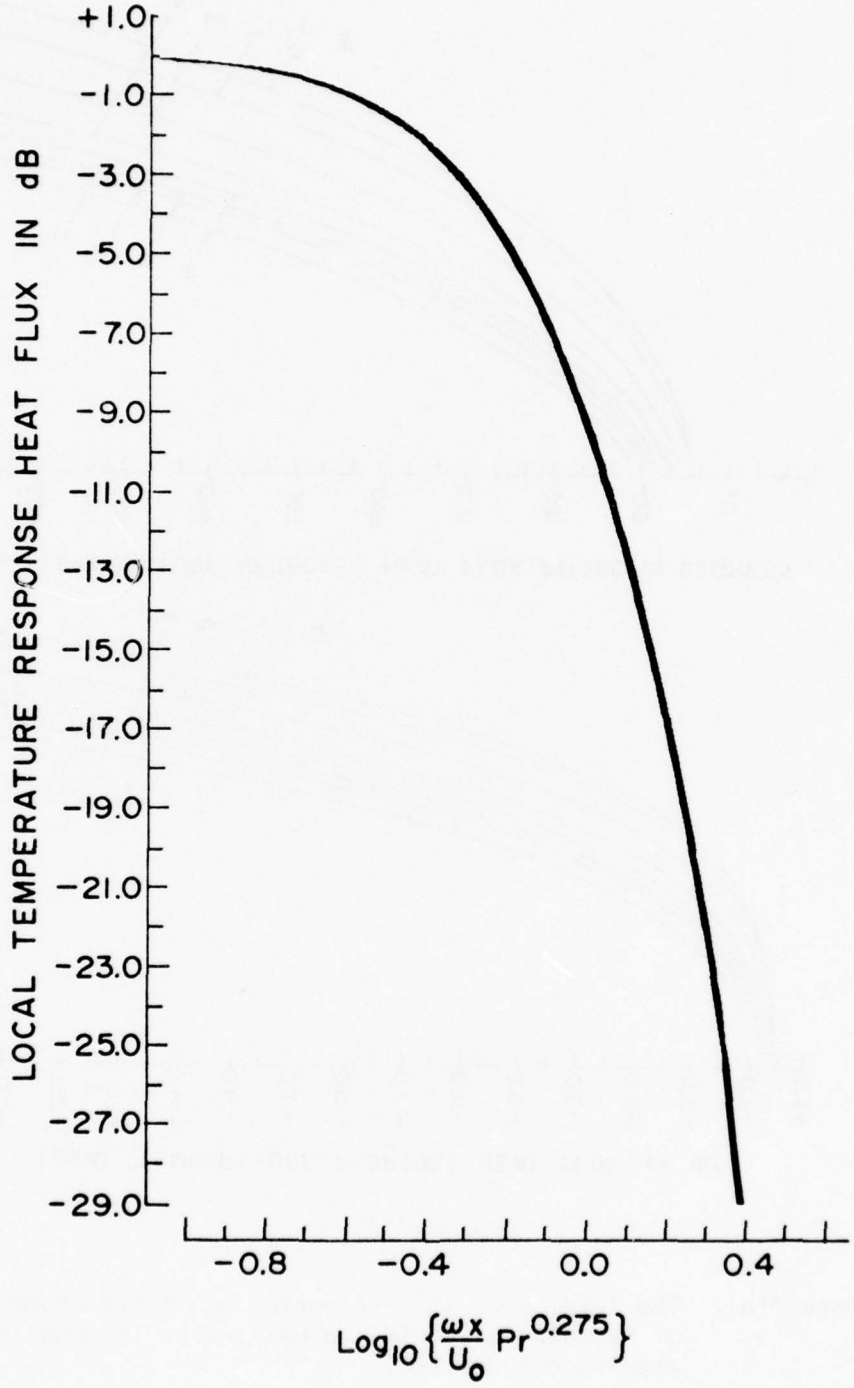

Figure 8(b). The local heat flux response to a temperature modulation of the ambient fluid, normalized by its quasi-steady value; magnitude only plotted against a scaled frequency axis.

and the rate of decrease of magnitude (in decibels per decade) do not tend towards an asymptotic limit. The curve for the magnitude of the local heat flux for various Prandtl numbers nearly collapses into one curve when the frequency axis is scaled by $Pr^{0.275}$, Figure 8(b). The phase, however, does not have a Prandtl number exponent scaling. The phase shift is large, even at very low frequencies. Consequently there are regions on the plate where the heat flux direction is opposite to that at the leading edge, where the phase shift is zero..

The total heat flux response to variations of the ambient fluid's temperature, normalized by its quasi-steady value, is

$$\frac{F}{[f''(0)]^{Pr}} \frac{1}{\xi^{\frac{1}{2}}} \int_0^{\xi^{\frac{1}{2}}} \theta'(0,\Omega,Pr)\, d\sqrt{\Omega}$$

and is plotted in Figure 9(a). The character of the curves changes around $\xi=1$. In this frequency region the local heat flux phase delay near the trailing edge of the plate exceeds 270^{o}. This local "in phase" flux moderates the rate of flux decrease with increasing frequency. For frequencies above $\Omega=1$ the relative local heat flux magnitude is, however, quite small and consequently the total heat flux is proportional to $(i\xi)^{-\frac{1}{2}}$ for $\xi>>1$.

A satisfactory frequency scaling, for both the magnitude and phase, is given by $Pr^{0.38}$, Figure 9(b). There is, however, some spreading of the curves near $\xi Pr^{0.38}=1$ where the character of the individual curves depends strongly on the Prandtl number.

The 3 dB bandwidths for the response to temperature oscillations in the main stream is

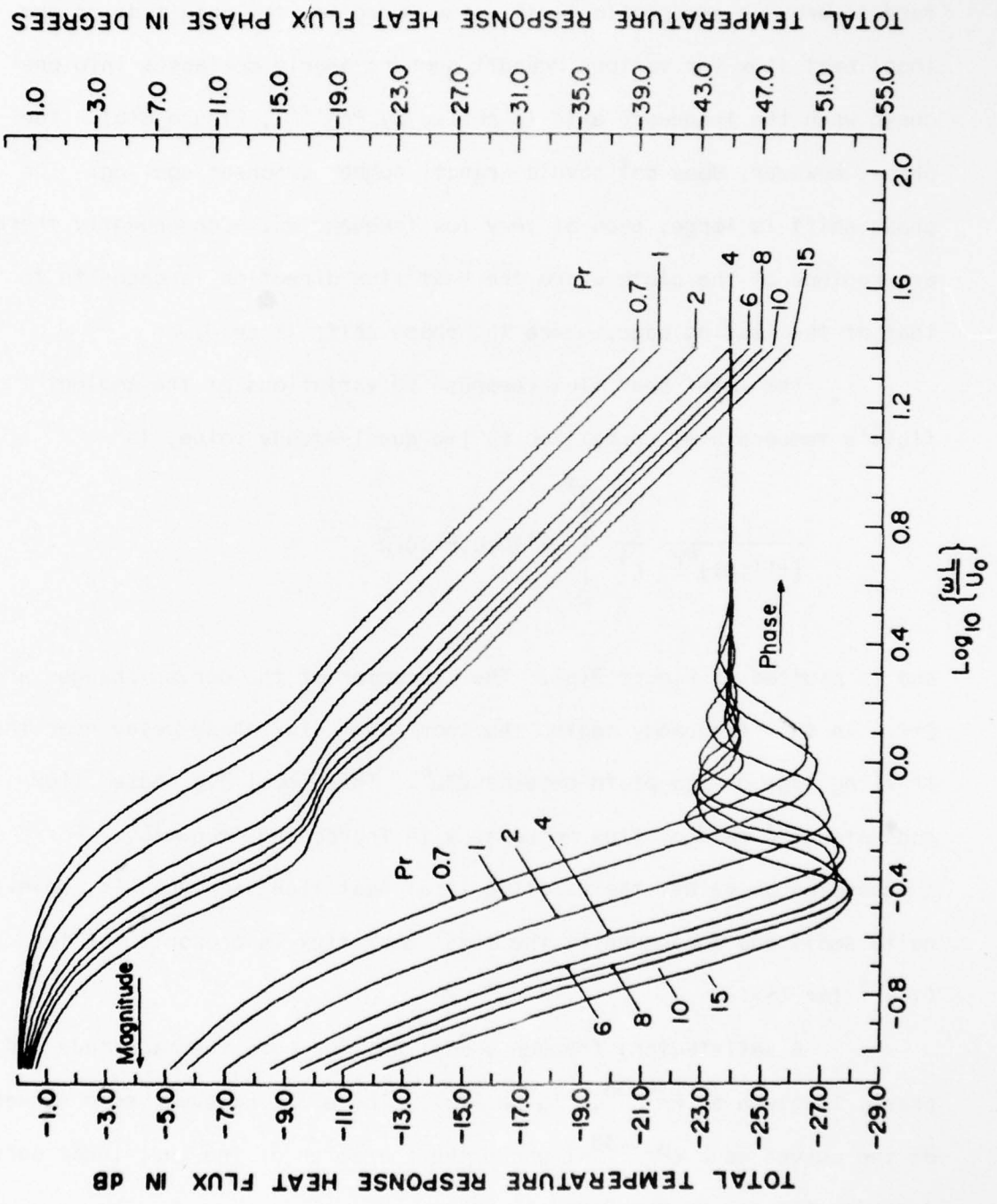

Figure 9(a). The total heat flux response to a temperature modulation of the ambient fluid, normalized by its quasi-steady value; unscaled frequency axis.

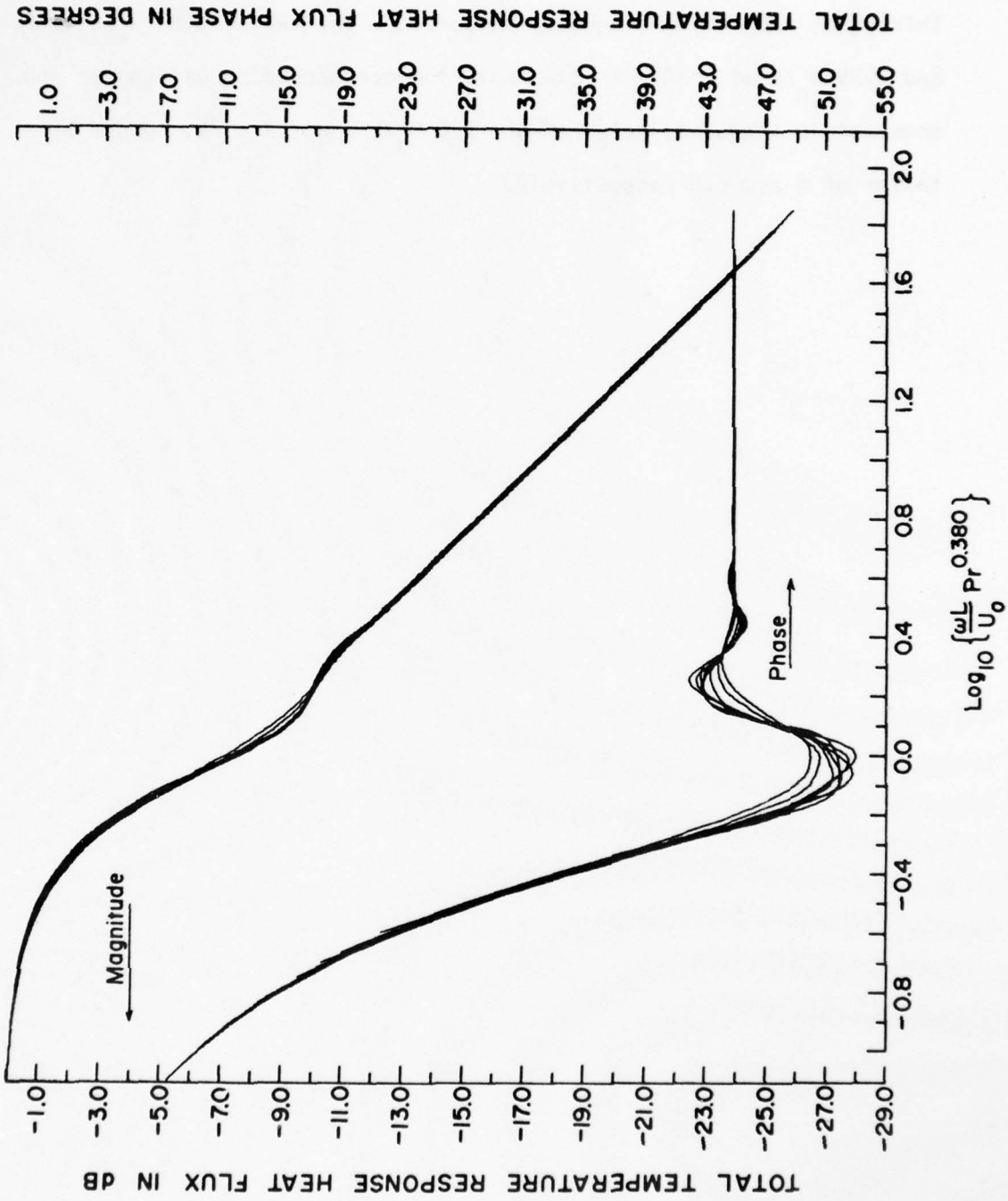

Figure 9(b). The total heat flux response to a temperature modulation of the ambient fluid, normalized by its quasi-steady value; scaled frequency axis.

$$\xi_{3\ dB} = \left(\frac{\omega L}{U_o} \right)_{3\ dB} = 0.56\ Pr^{-0.38}.$$

This makes the radian frequency temperature band-width 0.56 U_o/L at Pr=1 and 0.25 U_o/L at Pr=8. In contrast, the corresponding values for the anemometric frequency response are 2.8 U_o/L and 1.7 U_o/L, larger by a factor of 5 and 6.8 respectively.

4. Conclusions

The unsteady viscous stress computed numerically from a simplified unsteady momentum equation that is not restricted by frequency compares favourably with the frequency restricted results of Cheng and Elliott (1957) and Lighthill (1954).

When the boundary layer is unsteady ($\omega x/U_o >> 1$) the equation governing the heat flux from the plate in response to speed oscillations in the main streams is significantly different from the equation governing the response to temperature oscillations in the main stream. Both equations are also different from the equation governing the response to oscillations of the plate's temperature. The unsteady heating source that generates the anemometric response is intrinsically distributed throughout the boundary layer and has a profile that depends strongly on the Prandtl number and the frequency of the speed oscillation. The heating source that generates the temperature response, on the other hand, is constant for all frequencies and is at the boundary $y=\infty$ for external temperature oscillations and at $y=0$ for internal temperature oscillations.

The anemometric heat flux response increases in magnitude with increasing frequency (from its quasi-steady value of 0.5) to a maximum value. The heat flux then decreases with increasing frequency to an asymptotic value proportional to $(i\Omega)^{-1}$ for the local heat flux and $(i\xi)^{-\frac{1}{2}}$ for the total heat flux from the plate. The location and the value of the heat flux maxima depend on the Prandtl number. The largest maximum occurs at a Prandtl number of 2. The phase of the heat flux is always negative.

The local heat flux in response to external temperature oscillations decreases with increasing frequency and has neither an asymptotic logarithmic rate of decrease nor an asymptotic phase shift at high frequencies. The total heat flux in response to temperature oscillations decreases rapidly from its quasi-steady value with increasing frequency up to the frequency $\xi=1.4\ Pr^{0.38}$ and then becomes proportional to $(\xi Pr^{0.38})^{-\frac{1}{2}}$ for larger frequencies.

The -3 dB bandwidth is $3.7(1+2\sqrt{Pr})/(1+\sqrt{Pr})^2$ for the total heat flux in response to speed oscillations and is $0.56Pr^{-0.38}$ for the total heat flux in response to temperature oscillations in the main stream.

Frequency response calibrations made by internal heating methods cannot correctly measure the response to speed or temperature oscillations in the main stream, for constant temperature anemometers or thermometers, when the boundary layer is not quasi-steady.

Bibliography

Ascher, U., J. Christiansen and R.D. Russell. 1977. A collocation solver for mixed order systems of boundary value problems. Technical Report 77-13, Department of Computer Science, The University of British Columbia.

Bellhouse, B.J. and D.L. Schultz. 1967. The determination of fluctuating velocity in air with heated thin film gauges, Journal of Fluid Mechanics, 29, 2, pp. 289-295.

Cheng, Sin-I and D. Elliott. 1957. The unsteady laminar boundary layer on a flat plate. Transactions of the American Society of Mechanical Engineers, 79: 725-733.

Evans, D. 1963. An instrument for the measurement of ocean turbulence, Technical Memorandum 63-8, Pacific Naval Laboratory, Defense Research Board, Canada.

Freymuth, Peter. 1978. A comparative study of the signal-to-noise ratio of hot-film and hot-wire anemometers. J. Physics E: Sci. Instrum. 11: 915-18.

Gargett, A.E. 1976. An investigation of the occurrence of oceanic turbulence with respect to finestructure. J. of Phys. Oceanog. 6:2, 139-156.

Grant, H.L., R.W. Stewart and A. Moilliet. 1962. Turbulence spectra from a tidal channel. J. of Fluid Mech. 12: 241-268.

Grant, H.L., A. Moilliet and W.M. Vogel. 1968. Some observations of the occurrence of turbulence in and above the thermocline. J. of Fluid Mech. 34:443-448.

Hill, P.G. and A.H. Stenning. 1960. Laminar boundary layers in oscillatory flow. Transactions of the ASME Series D, pp. 593-608.

Lighthill, M.J. 1954. The response of laminar skin friction and heat transfer to fluctuations in the stream velocity. Proceedings of the Royal Society of London, Series 4, 224: 1-23.

Nowell, Arthur R.M. 1974. Some response characteristics of parabolic hot films in water. J. of Hydronautics 8: 4, pp. 169-171.

Ostrach, Simon. 1955. Compressible laminar boundary layer and heat transfer for unsteady motions of a flat plate. National Advisory Committee for Aeronautics, Technical Note 3569.

Rott, Nicholas and Martin L. Rosenzweig. 1960. On the response of the laminar boundary layer to small fluctuations of the free-stream velocity. J. of Aeronautical and Space Sci. 27: 741-747.

Schlichting, M. 1955. Boundary Layer Theory, Pergamon Press, 535 pages.

Acknowledgements

I would like to express appreciation to the following:

Dr. U. Ascher and Mr. Chris Hermansen of the Computing Science Department of the University of British Columbia for providing the numerical routines for solving the equations and for other co-operation that they have shown;

Professors P.H. LeBlond and L.A. Mysak of the Institute of Oceanography at U.B.C. for their reviews and criticisms; and

Professor T.R. Osborn for his encouragement and support throughout this work.

This work has been supported by the Office of Naval Research, Contract Number 00014-083-207.

Appendix B

The Calibration of a Hot Film Turbulence Probe

by

Rolf G. Lueck

Institute of Oceanography

University of British Columbia

Vancouver, B.C., V6T 1W5

Canada

Abstract

The steady flow calibration data of two platinum thin film turbulence probes show that their thermal conductance $Q/\Delta T$ is not proportional to $U_o^{\frac{1}{2}}$ as expected for a constant temperature conical surface. A thermal model of the probes that agrees favourably with the calibration data indicates that this non-proportionality is due to the thermal effect of the glass coating over the film and glass substrate below it. The unsteady heat flux from the film in response to variations in the ambient fluid's speed increases with increasing frequency above 100 Hertz. It is shown that the unsteady heat flux is proportional to the unsteady viscous surface stress over the film which increases in magnitude with increasing value of the frequency parameter $\omega L/3U_o$. The ratio of the temperature-to-velocity sensitivity is highest at zero frequency.

1. Introduction

The steady and unsteady calibration of two (similar) conical platinum thin film turbulence sensors used for oceanic measurements are discussed in this paper. Comparable probes have been used by Grant, Stewart and Moilliet (1962) to derive the Kolmogorov spectrum from direct turbulence measurements in a tidal channel, and by Grant, Moilliet and Vogel (1968) to measure turbulence in and above the thermocline. More recently, the same probes discussed here have been mounted on a towed body for open ocean measurements (Nasmyth, 1970) and have been mounted on a small submersible for coastal and estuarine studies (Gargett, personal communication).

The most outstanding feature of the conical hot film probe is its high frequency response. The frequency response is calibrated from 10 to 1000 Hertz by vibrating the probe in the direction of the steady flow in a low turbulence water tunnel. All of the calibration data presented here have been taken by the Ocean Mixing Group of the Institute of Ocean Science at Patricia Bay, British Columbia, Canada. In calibration, the modulation in velocity, as seen by the probe, arises from the oscillation of the probe parallel to a steady stream. However, during field measurements the modulation in velocity stems from the oscillation of the ambient fluid speed parallel to the steady motion of the probe. This flow difference is not important; the behaviour of the boundary layer is the same in both cases when the fluid is incompressible (Lighthill, 1954). Hence, calibration by probe vibration correctly simulates the probe's frequency response to ambient fluid speed oscillations.

It is more common to measure the frequency response of heated sensors by electronically modulating its internal temperature in the presence of steady streaming (Freymuth, 1977, 1978). However, this method does not measure a probe's frequency response when the boundary layer is not quasi-steady (Lueck, 1979). The unsteady calibration data presented indicates that the boundary layer is not quasi-steady at frequencies above approximately 100 Hertz.

A reproduction of the probes is in Figure 1. The basis of the probe is a blunt glass cone having a half-angle of 15 degrees. The sensing element is a narrow thin platinum film which is deposited around the entire circumference at a position 'downstream' from the cone's apex. Electrical contact with the film is made on opposite sides of the cone via two platinum sponges in the glass substrate. That portion of the film that overlays the sponges (hashed area in Figure 1) is not considered as part of the film's sensing surface. A thin quartz layer of unknown thickness covers the entire probe to provide electrical insulation from the fluid being probed. The probes were made under special contract at the University of British Columbia. The probes are operated in a constant temperature mode by an AC servo-amplifier centered at 12.5 kHz. A detailed account of the probe's electronics and its operation has been given by Evans (1962).

The steady flow calibration curves for the two probes (V-31 and V-38) are given in Figure 2. Plotted is the probe's thermal conductance $Q/\Delta T$ against the square root of the Reynolds number where Q is the electric power dissipated in the film and ΔT is the temperature difference

V - 31

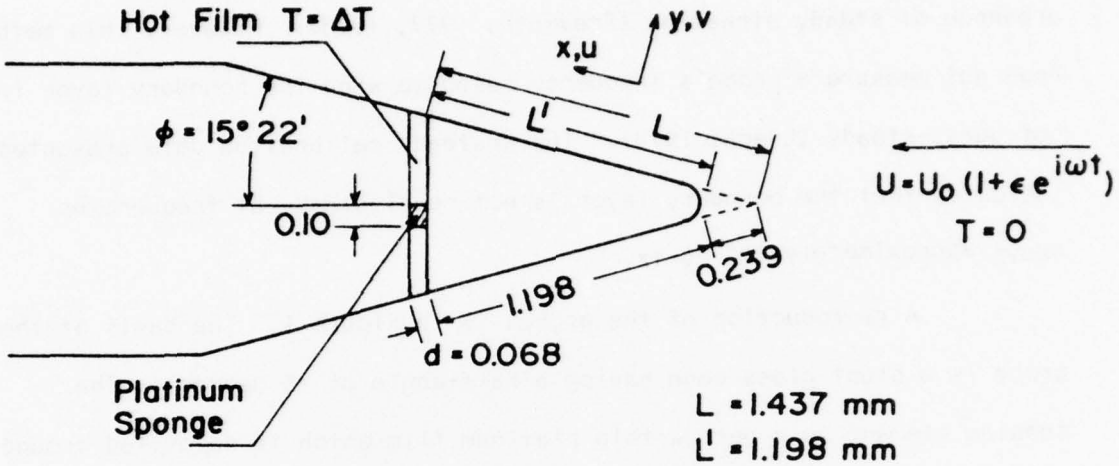

L = 1.437 mm
L' = 1.198 mm
d/L = 0.047

Film Surface Area ≅ 0.92 (2π) L d sin φ
= 1.5 x 10^{-3} cm^2

V - 38

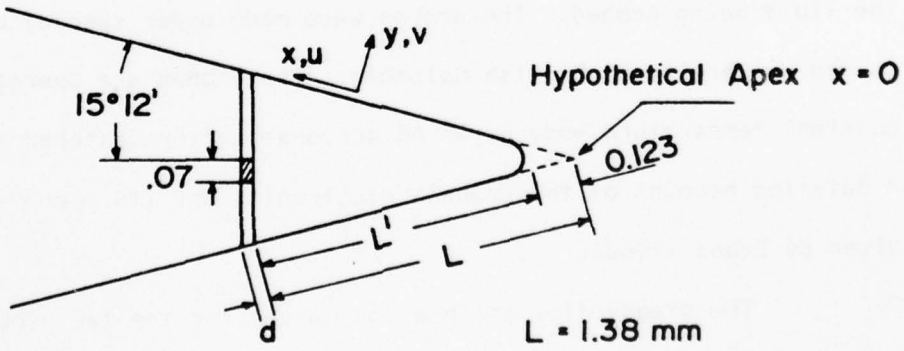

L = 1.38 mm
L' = 1.17 mm
d = 0.056 mm

Film Surface Area = 0.94 (2π) L d sin φ

1. A sketch of probes V-31 and V-38, their relevant dimensions and the coordinate system employed in the analyses.

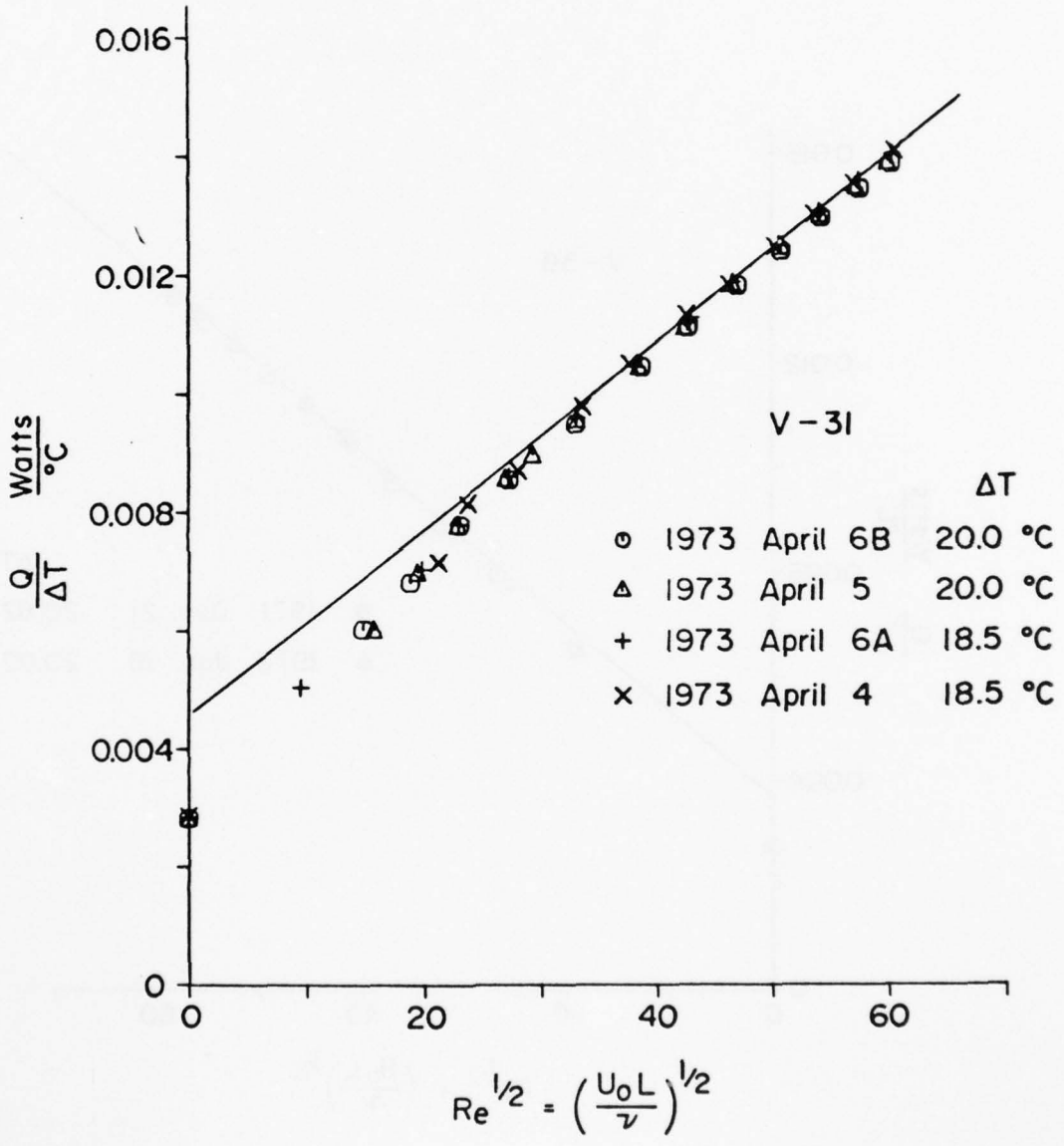

2(a). The probes' thermal conductance $Q/\Delta T$ versus $R_e^{\frac{1}{2}}$ for V-31.

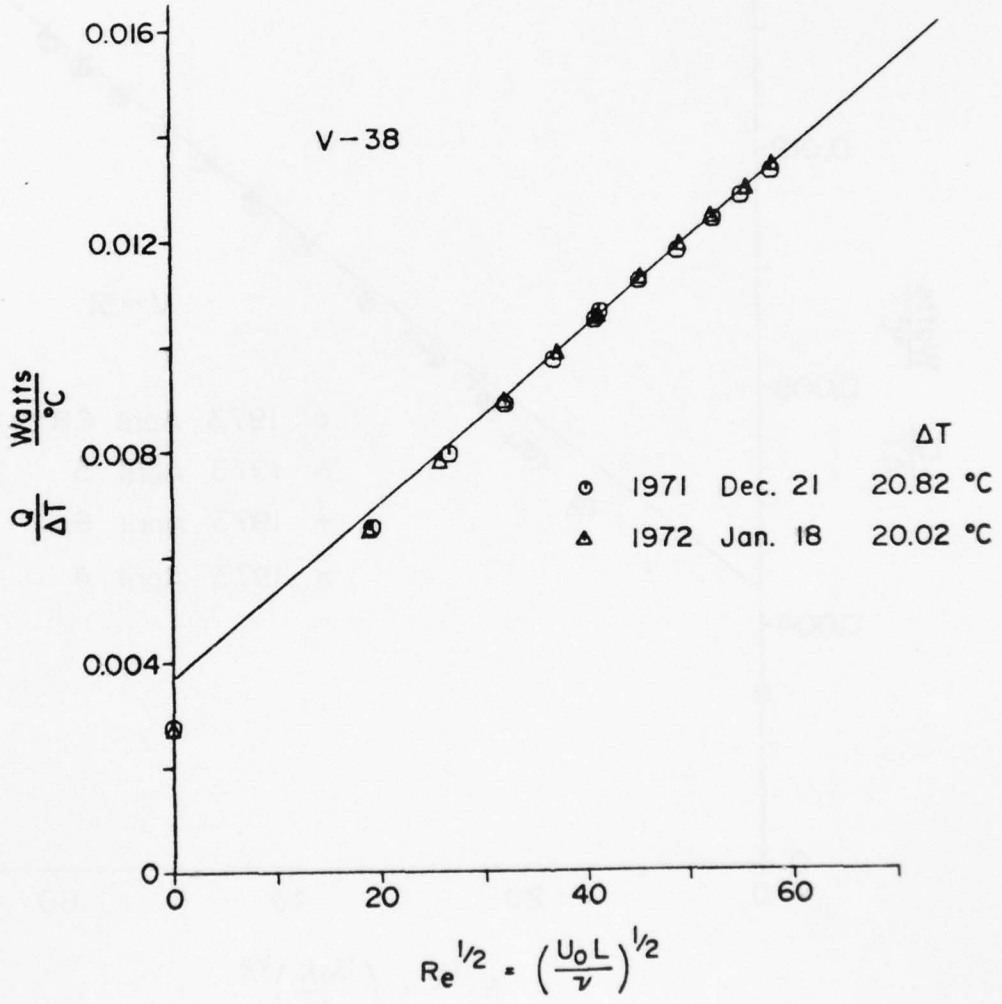

2(b). The probes' thermal conductance $Q/\Delta T$ versus $R_e^{\frac{1}{2}}$ for V-38.

AD-A071 376 BRITISH COLUMBIA UNIV VANCOUVER INST OF OCEANOGRAPHY F/G 8/3
HEATED ANEMOMETRY AND THERMOMETRY IN WATER.(U)
MAY 79 R G LUECK N00014-76-C-0446

UNCLASSIFIED NL

2 OF 2
AD A071376

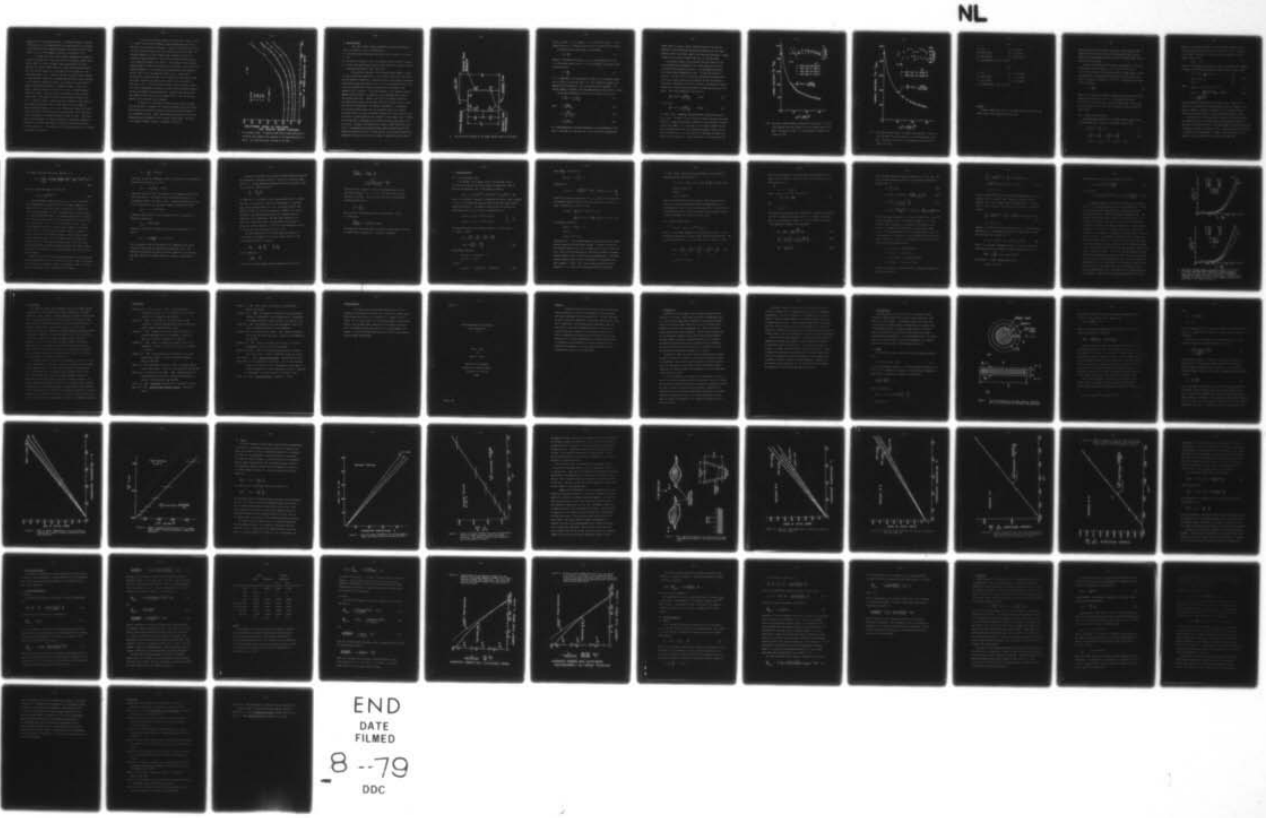

END
DATE FILMED
8 -79
DDC

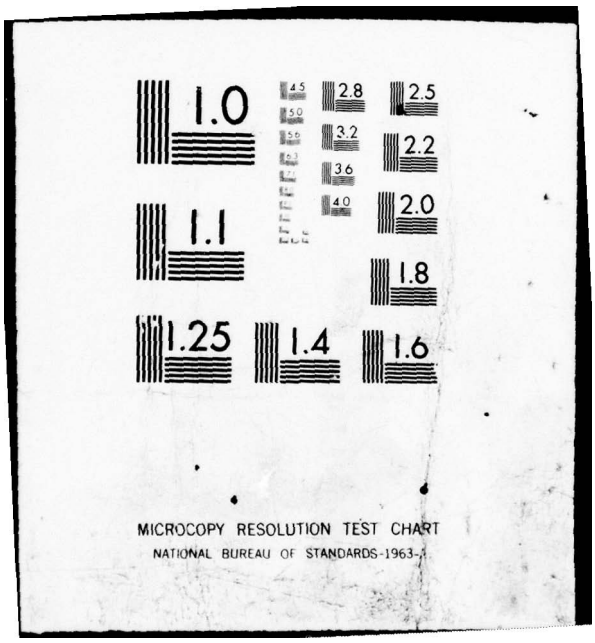
1.0
1.1
1.25
1.4
1.6
1.8
2.0
2.2
2.5
2.8
3.2
3.6
4.0
4.5
5.0
5.6
MICROCOPY RESOLUTION TEST CHART
NATIONAL BUREAU OF STANDARDS-1963-A

between the film and the ambient water. The Reynolds number is defined as $\frac{U_o L}{\nu}$ where U_o is the steady ambient fluid speed relative to the probe, L the distance from the hypothetical apex to the start of the film (see Figure 1) and ν is the kinematic viscosity of the ambient fluid.

The heat flux from an ideal constant temperature axi-symmetric surface is proportional to the square root of the Reynolds number (White, 1974, p. 282) if the usual boundary layer approximations are valid. Bellhouse and Schultz (1967) reported a linear relationship between the heat flux and the square root of the ambient fluid's speed for a two-dimensional sensor in air. However, the data in Figure 2 show curvature at large Reynolds numbers and a systematic deviation away from a straight line for Reynolds numbers below 500. This deviation at lower Reynolds numbers cannot be attributed to a fundamental change in the Nusse't number - Reynolds number relationship of the flow. Although changes in the Nusselt number - Reynolds number relationship have been reported (Hinze, 1975), they appear to be restricted to Reynolds numbers below 0.5. In addition, Kramers (1946) reported for spheres a linear relationship between the Nusselt number and the square root of the Reynolds number to Reynolds numbers as low as 50. Tan-atichat, Nagib and Pluister (1973) had similar difficulties with fitting the heat flux to the square root of the speed, for a coated cylindrical sensor in water. They found that plotting the heat flux against U_o^m where m = 0.225 gave a moderately successful fit to the data; however, no physical explanation was given for their choice of m. An explanation for the observed steady flow response is presented in Section 2.

A plot of the unsteady response of probe V-38 is shown in Figure 3. Plotted is the probe's unsteady voltage-to-speed amplitude ratio in arbitrary units against the frequency, in Hertz, of the speed oscillation. The lines joining the data points are a casual fairing of the data. The unsteady response, at a given steady speed, decreases slightly with increasing frequency between 10 and 50 Hertz and then increases sharply with increasing frequency up to 1000 Hz. The character of the frequency response depends strongly on the ambient fluid's speed. A more significant response decrease at low frequencies has been reported by Bellhouse and Schultz (1967) for a two-dimensional probe in air. These authors attributed the response decrease to an attenuation of heat waves through the probe's substrate and predicted the effect to be much smaller in water than in air. A small difference between the quasi-steady response of a hot wire anemometer calculated by differentiating the steady response and the low frequency response observed by vibrating the probe has also been reported by Morrison, Perry and Samuel (1972). Their calibrations, however, were restricted to one frequency.

An analysis of the bridge circuitry by Evans (1963) indicates that the increase in response with increasing frequency above 50 Hz cannot be attributed to the probe's electronics and must therefore represent a real hydrodynamic effect. Evans (1963) showed that the heat flux at high frequencies may be connected to the unsteady surface shear. The nature of the probe's unsteady response is examined in Section 3.

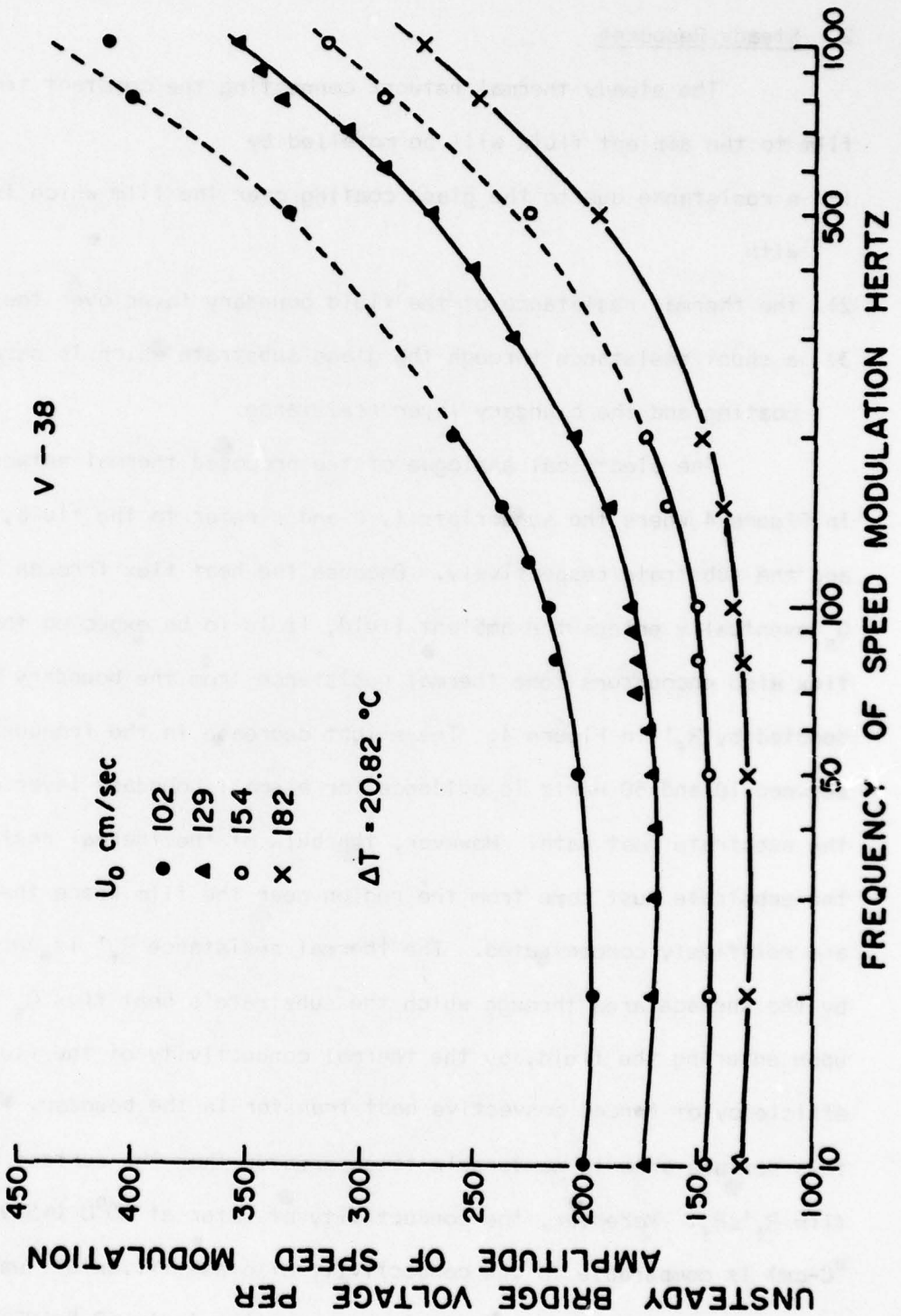

3. The unsteady probe voltage per amplitude of speed modulation in arbitrary units against the frequency of the speed modulation in Hertz. The lines are casual fairings to the data.

2. Steady Response

The steady thermal network connecting the constant temperature film to the ambient fluid will be modelled by

1) a resistance due to the glass coating over the film which is in series with
2) the thermal resistance of the fluid boundary layer over the film and by
3) a shunt resistance through the glass substrate which is parallel to the coating and the boundary layer resistance.

The electrical analogue of the proposed thermal network is shown in Figure 4 where the subscripts f, c and s refer to the fluid, the coating and the substrate respectively. Because the heat flux through the substrate Q_s eventually enters the ambient fluid, it is to be expected that this heat flux also encounters some thermal resistance from the boundary layer denoted by R_f' in Figure 4. The slight decrease in the frequency response between 10 and 50 Hertz is evidence for a small boundary layer effect in the substrate heat path. However, the bulk of the thermal resistance of the substrate must come from the region near the film where the flux lines are relatively concentrated. The thermal resistance R_f' is determined by the surface area through which the substrate's heat flux Q_s passes upon entering the fluid, by the thermal conductivity of the fluid and by the efficiency of forced convective heat transfer in the boundary layer. Because this surface area is comparable to or greater than the surface area of the film $R_f' \leq R_f$. Moreover, the conductivity of water at 20°C ($\sim 5.9 \times 10^{-3}$ watts/°C-cm) is comparable to the conductivity of glass ($\sim 1.0 \times 10^{-2}$ watts/°C-cm) whereas the conductivity of air is much smaller (only $\sim 2.5 \times 10^{-4}$ watts/°C-cm). Subsequent analyses show that for the probes in question $R_f << R_s$ and hence

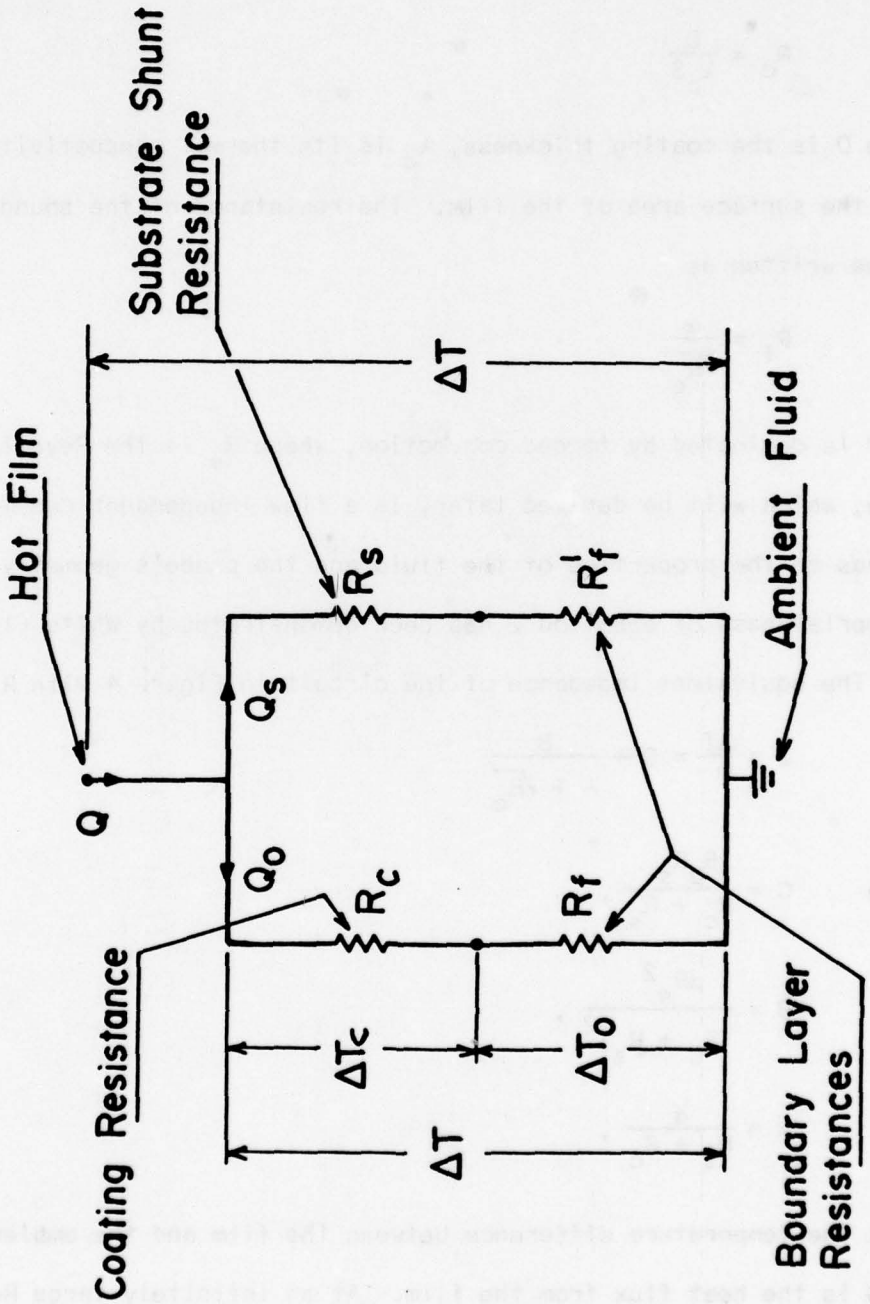

4. The electrical analogue to the steady thermal model of the probes.

$R_f' << R_s$ in water. In air, however, it is possible that $R_f' \sim R_s$. In the remaining work R_f' is ignored relative to R_s, the substrate's resistance.

The probe's coating resistance is approximately

$$R_c = \frac{D}{\lambda_c S} \tag{1}$$

where D is the coating thickness, λ_c is its thermal conductivity and S is the surface area of the film. The resistance of the boundary layer can be written as

$$R_f = \frac{\alpha}{\sqrt{R_e}} \tag{2}$$

if it is dominated by forced convection, where R_e is the Reynolds number and α, which will be derived later, is a flow independent constant that depends on the properties of the fluid and the probe's geometry. The appropriateness of equation 2 has been demonstrated by White (1974, p. 282).

The equivalent impedance of the circuit in Figure 4 with $R_f'=0$ is

$$Z = \frac{\Delta T}{Q} = C + \frac{B}{A + \sqrt{R_e}} \tag{3}$$

where $$C = \frac{R_c R_s}{R_c + R_s}, \tag{4a}$$

$$B = \frac{\alpha R_s^2}{(R_c + R_s)^2}, \tag{4b}$$

$$A = \frac{\alpha}{R_s + R_c}, \tag{4c}$$

ΔT is the temperature difference between the film and the ambient fluid and Q is the heat flux from the film. At an infinitely large Reynolds

number equation 3 gives a thermal resistance equal to the parallel equivalent of the coating and substrate resistance and at very small Reynolds numbers a resistance equal to the substrate resistance. Thermal convection, which must be present when $R_e \leq 1$, is not considered.

The available steady flow calibration data for probes V-31 and V-38 has been fitted to equation 3 by a least square error routine to determine the constants A, B and C. All measurements were made at an ambient water temperature of 20°C. The data are plotted in Figure 5. The solid line is the thermal resistance $Z=\Delta T/Q$ determined by the least square routine and the symbols represent the observed resistances. The quality of the fit in terms of the percent difference between the fit and the observed values is plotted near the top of the graphs. The fitted impedance of the probes are

$$\frac{\Delta T}{Q} = 25.4 + \frac{3220}{7.77 + \sqrt{R_e}} \quad {}^{\circ}C/watt \tag{5a}$$

for V-31 and

$$\frac{\Delta T}{Q} = 12.5 + \frac{4410}{12.3 + \sqrt{R_e}} \quad {}^{\circ}C/watt \tag{5b}$$

for V-38. Table I summarizes the experimentally determined values of R_s, R_c and α. The data of zero flow were not used to calculate the least square fit. Some care was taken to attempt to minimize thermal convection at zero flow speeds. All of the data for V-31 agree to better than 4% and all except three of the lower speed points agree to better than 2% with the fitted curve. All of the data for V-38 agrees to better than 0.8% with the fitted curve. The two data sets for V-38 were taken one

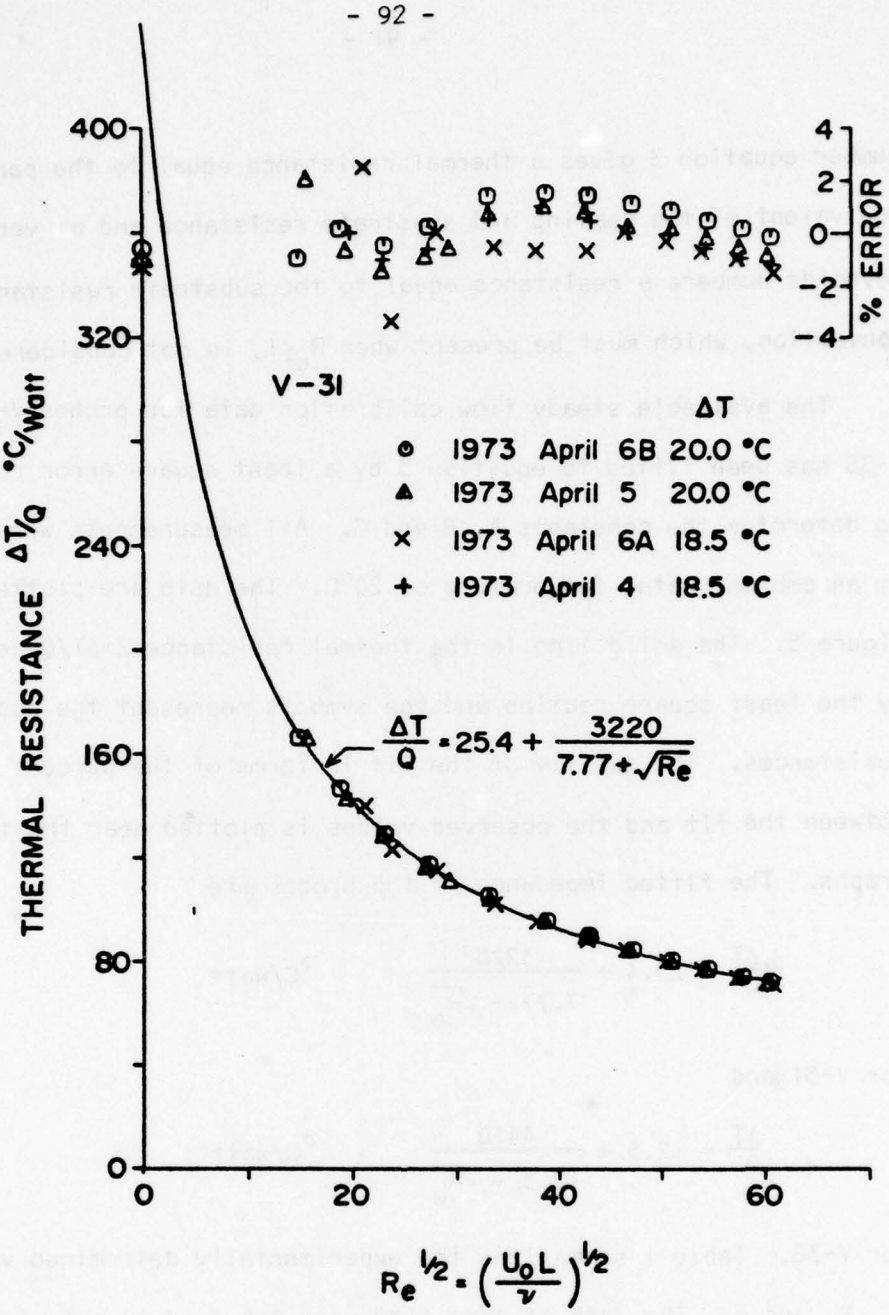

5(a) The probes' steady thermal resistance ΔT/Q versus $R_e^{\frac{1}{2}}$. The solid lines represent the least square fit of the thermal model to the data. The quality of the fit is indicated near the top of the figure; for V-31.

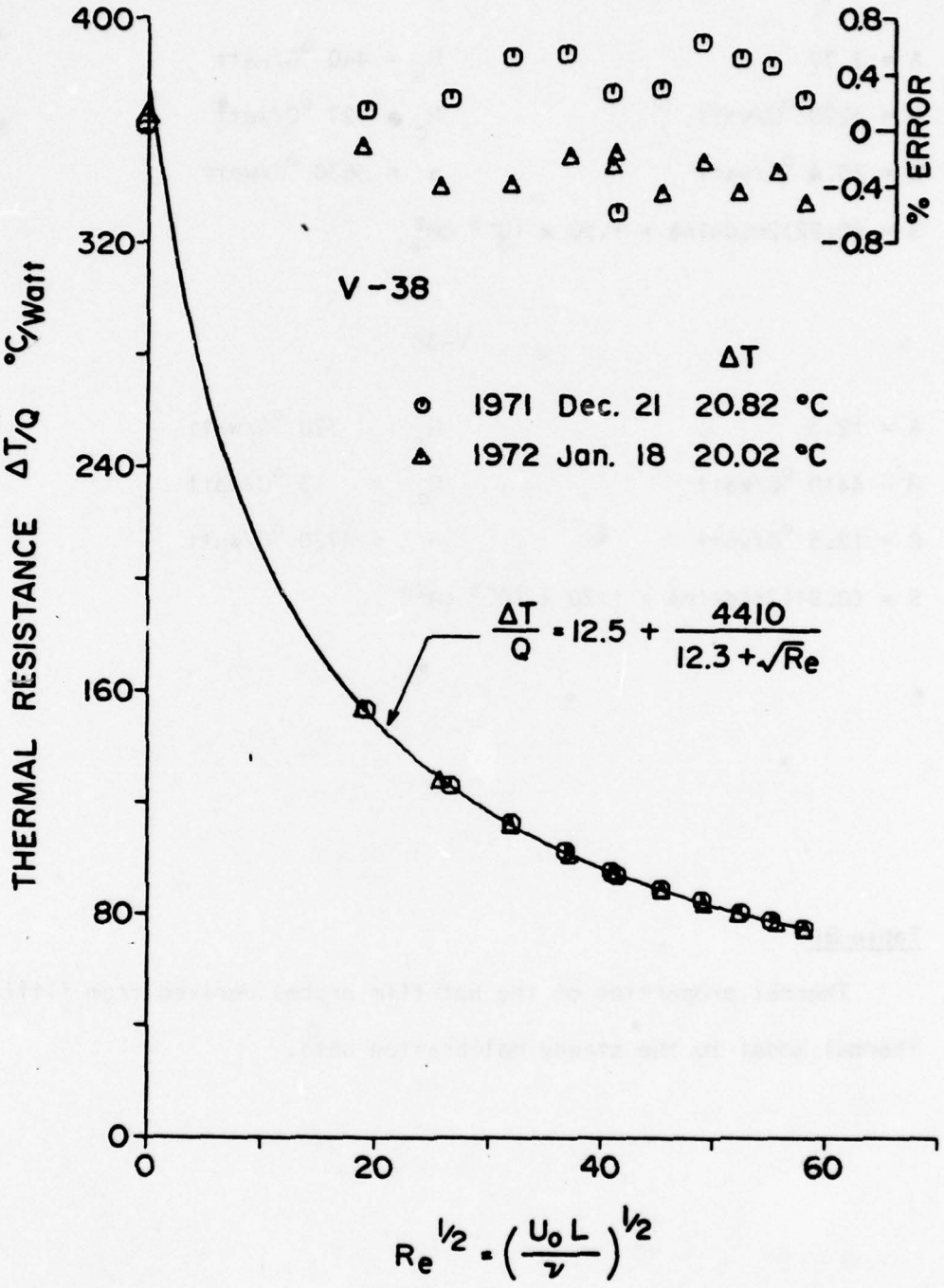

5(b). The probes' steady thermal resistance $\Delta T/Q$ versus $R_e^{\frac{1}{2}}$. The solid lines represent the least square fit of the thermal model to the data. The quality of the fit is indicated near the top of the figure; for V-38.

V-31

$A = 7.77$ $\qquad R_s = 440\ ^{o}C/watt$

$B = 3220\ ^{o}C/watt$ $\qquad R_c = 27\ ^{o}C/watt$

$C = 25.4\ ^{o}C/watt$ $\qquad \alpha = 3630\ ^{o}C/watt$

$S = (0.92)2\pi L d \sin\phi = 1.50 \times 10^{-3}\ cm^2$

V-38

$A = 12.3$ $\qquad R_s = 370\ ^{o}C/watt$

$B = 4410\ ^{o}C/watt$ $\qquad R_c = 13\ ^{o}C/watt$

$C = 12.5\ ^{o}C/watt$ $\qquad \alpha = 4720\ ^{o}C/watt$

$S = (0.94)2\pi L d \sin\phi = 1.20 \times 10^{-3}\ cm^2$

Table BI

Thermal properties of the hot film probes derived from fitting the thermal model to the steady calibration data.

month apart and show a systematic difference of approximately 0.8%. It appears that the difficulty with fitting the probe's heat flux to a proportionate relationship with $U_o^{\frac{1}{2}}$ is due to the thermal effect of the coating and the substrate.

The coating thickness over the probes, using equation (1) and the surface areas listed in Table 1, is 4.1×10^{-4} cm for V-31 and 1.6×10^{-4} cm for V-38. The coating thickness on these probes is otherwise unknown but two commercial manufacturers of similar probes coat theirs to a nominal thickness of 2×10^{-4} cm. The substrate resistance should be given by

$$R_s \simeq \frac{D'}{\lambda_s S} \tag{6}$$

where D' is a characteristic depth of thermal penetration and should be comparable to the width of the film. Using equation (6) gives $D' = 67 \times 10^{-4}$ cm for V-31 which is almost exactly equal to the width of the film and $D' = 46 \times 10^{-4}$ cm for V-38 which is 20% less than the film's width.

2(a). Boundary Layer Resistance

The hydrodynamic equations for the probe's boundary layer, using the coordinates shown in Figure 1, are (White, 1974, p. 340)

$$\frac{\partial}{\partial x}(Ru_o) + R\frac{\partial}{\partial y}v_o = 0 \tag{7}$$

$$u_o\frac{\partial u_o}{\partial x} + v_o\frac{\partial u_o}{\partial y} = \nu\frac{\partial^2 u_o}{\partial y^2} + V_o\frac{dV_o}{dx} \tag{8}$$

$$u_o(x,y) = v_o(x,y) = 0\,, \quad u_o(x,\infty) = V_o(x)$$

where V_o is the steady potential flow at the probe's surface, u_o and v_o are the steady boundary layer velocities and $R = R(x)$ is the radius of the probe. The potential flow over an ideal axisymmetric cone is (White, 1974, p. 341)

$$V_o(x) = Ex^n \tag{9}$$

where E is a constant and n=0.035 for a cone of half-angle 15^o. Equation 8 reduces to the ordinary differential equation (White, 1974, p. 242)

$$\left.\begin{aligned} &f''' + ff'' + \frac{2n}{3+n}(1-f'^2) = 0 \\ &f'(0) = f(0) = 0 \\ &f'(\infty) = 1 \end{aligned}\right\} \tag{10}$$

where

$$u_o(x,y) = V_o(x)\, f'(\eta) = Ex^n f'(\eta) \tag{11}$$

$$v_o(x,y) = -\sqrt{\frac{2}{3+n} Ex^{n-1}}\left\{\frac{n+3}{2} f + \frac{n-1}{2}\eta f'\right\} \tag{12}$$

$$\eta = y\sqrt{\frac{3+n}{2\nu} Ex^{n-1}}$$

and prime denotes differentiation with respect to η. Equation 10 is identical to the equation for two-dimensional flow over a wedge of half-angle 2.1 degrees. Solutions to equation (10) for various values of η can be found in White (1974, p. 276) and Schlichting (1955, p. 129).

At the blunt tip of the cone and at the rear of the conical section the potential flow at the surface cannot be represented by equation 9. Over most of the conical section of the probe equation 9 should be accurate, and because $n=0.035 \ll 1$ the potential flow V_o should not differ significantly from the free-stream speed U_o. However, a detailed analysis of the potential flow over probes V-31 and V-38 has not been made.

The equation governing the boundary layer temperature $T_o(x,y)$, measured with respect to the ambient fluid's steady temperature, is (Lighthill, 1954)

$$u_o \frac{\partial \theta}{\partial x} + v_o \frac{\partial \theta}{\partial y} - \kappa \frac{\partial^2 \theta}{\partial y^2} = 0 \qquad (14)$$

where $\theta = \Delta T_o - T_o(x,y)$, ΔT_o is the temperature difference between the probe's wetted surface and the ambient fluid, and κ is the thermal diffusivity of the fluid. Assuming negligible heating upstream of the film and a uniform temperature ΔT_o at the wetted surface over the film, the boundary conditions on equation 14 are

$$\left.\begin{aligned} \theta &= 0 \quad \text{at } y = 0 \quad L \leq x \leq L+d \\ \theta &= \Delta T_o \quad \text{for all } x < L \\ \theta &= \Delta T_o \quad \text{as } y \to \infty \text{ for all } x. \end{aligned}\right\} \qquad (15)$$

Because the momentum boundary layer starts at the tip of the cone whereas the thermal boundary layer starts at the film ($x = L$) the similarity variable η is not appropriate for the temperature equation (14).

Following Kays (1966) let the velocity profile be approximated by the cubic parabola

$$f'(\eta) = \frac{u_o(x,y)}{V_o(x)} = \frac{3}{2}\left(\frac{y}{\delta}\right) - \frac{1}{2}\left(\frac{y}{\delta}\right)^3 \qquad (16)$$

where δ is an artificial viscous boundary layer thickness. The choice

$$\delta = 3.04 \sqrt{\frac{2\nu}{(3+n)\, E x^{n-1}}} \qquad (17)$$

makes the surface velocity gradient calculated from equation (16) agree with the value tabulated in White (1974, p. 270). Assuming a similar profile for temperature we can write

$$\frac{\theta}{\Delta T_o} = \frac{3}{2}\left(\frac{y}{\delta_T}\right) - \frac{1}{2}\left(\frac{y}{\delta_T}\right)^3 \qquad (18)$$

where δ_T is the artificial thermal boundary layer thickness. The thermal-to-viscous boundary layer thickness ratio $r = \delta_T/\delta$ is (Kays, 1966, p. 218)

$$r = \frac{\delta_T}{\delta} = \frac{1}{Pr^{1/3}}\left\{1 - \left(\frac{L}{x}\right)^c\right\}^{1/3} \qquad (19)$$

where

$$c = \frac{3}{4}\left(\frac{3+n}{3}\right) \simeq 3/4 \qquad (20)$$

and $Pr = \nu/\kappa$ is the Prandtl number.

The steady heat flux from the probe's surface can be calculated using equations 17, 18 and 19, and is

$$\hat{Q}_o(x) = \lambda_f \left.\frac{\partial\theta}{\partial y}\right|_{y=0} = \frac{3}{2}\frac{\Delta T_o}{3.04}\sqrt{\frac{3+n}{2}}\frac{1}{x}\frac{\lambda_f Pr^{1/3}}{[1-(\frac{L}{x})^c]^{1/3}}\sqrt{\frac{U_o x}{\nu}} \qquad (21)$$

where λ_f is the thermal conductivity of the fluid. The variation of the heat flux over the wetted surface is dominated by the factor

$$\left(1 - (\tfrac{L}{x})^c\right)^{1/3}$$

because the film is relatively narrow ($d/L \ll 1$). Accordingly, x can be set equal to L where it occurs outside of the above factor and this factor can be set equal to $(c\beta / L)^{1/3}$ where $\beta = x - L \ll L$. The total heat flux into the fluid above the film is then obtained by integrating equation 21 over the surface area of the film;

$$Q_o = S\int_L^{L+d}\hat{Q}_o(x)dx = \left(\frac{0.92}{0.94}\right)2\pi L\sin\phi\int_L^{L+d}\hat{Q}_o(x)dx \qquad (22)$$

$$= \frac{9}{4}\left(\frac{0.92}{0.94}\right)\frac{2\pi L\sin\phi}{3.04}\left(\frac{3+n}{2}\right)^{1/2}\left(\frac{4}{3+n}\right)^{1/3}\left(\frac{d}{L}\right)^{2/3}\lambda_f\Delta T_o R_e^{\frac{1}{2}}Pr^{1/3}.$$

The thermal resistance coefficient, equation 2, is

$$\alpha^{-1} = \frac{Q_o}{\Delta T_o R_e^{\frac{1}{2}}} = \frac{9}{4}\left(\frac{0.92}{0.94}\right)\frac{2\pi L \sin\phi}{3.04}\left(\frac{3+n}{2}\right)^{1/2}\left(\frac{4}{3+n}\right)^{1/3}\left(\frac{d}{L}\right)^{2/3}\lambda_f Pr^{1/3}, \tag{23a}$$

which for both probes equals (to within 1%)

$$1.53\,\lambda_f\, L\left(\frac{d}{L}\right)^{2/3} Pr^{1/3}. \tag{23b}$$

Using the probes' dimensions (figure 1), $\lambda_f = 6.3 \times 10^{-3}$ watts/ ^{o}C-cm (appropriate for water at 40^{o}C), and a Prandtl number of 7.1 (water at 20^{o}C) in equation 23 predicts values for α of 2880^{o}C/watt for V-31 and 3320^{o}C/watt for V-38. The experimentally derived values for α are 3630 and 4720 ^{o}C/watt. The boundary layer heat flux infered from fitting the thermal model to the calibration data is smaller than the calculated heat flux by 21% for V-31 and 30% for V-38. Some of this discrepancy is due to a variable Prandtl number in the thermal bounday layer. At 40^{o}C the Prandtl number is 4.3, for instance. In addition the origin of the momentum boundary layer has been assigned to the hypothetical apex (x=0) rather than the real (blunted) apex. Placing the origin of the momentum boundary layer at the real apex would accentuate the discrepancy whereas decreasing the Prandtl number to account for the warming of the thermal boundary layer would diminish the discrepancy.

Some implications of the proposed thermal model can now be examined. Oceanic measurements with V-31 and V-38 are typically taken at 130 cm/sec. This corresponds to a Reynolds number of approximately 1800. A typical value for the boundary layer resistance at that speed is

$$R_f = \frac{\alpha}{\sqrt{R_e}} \simeq 85^{\circ}C/watt.$$

Taking $R_c = 27$ and $R_s = 440^{\circ}C/watt$ (Table I) one calculates the temperature drop across the coating, ΔT_c, from

$$\Delta T_c = \Delta T \frac{R_c}{R_f + R_c} \simeq 0.24\Delta T.$$

Twenty-four percent of the film-to-ambient fluid temperature drop occurs across the coating. The boundary layer resistance coefficient, α, is considerably larger in air than in water. Placing the appropriate values of fluid conductivity, λ_f, and Prandtl number into equation 23 gives

$$\alpha_{air} \simeq 1.7 \times 10^5 \ ^{\circ}C/watt$$

A Reynolds number based on a more representative air flow speed of 10 meters per second gives

$$R_{f_{air}} \simeq 4500 \ ^{\circ}C/watt.$$

According to the model the temperature drop across the coating in air then is

$$\Delta T_c = \Delta T \frac{27}{27+4500} = 6 \times 10^{-3} \Delta T.$$

Only 0.6 percent of the film-to-ambient fluid temperature drop occurs across the coating when the same probes are operated in air. The coating's thickness and the coating's thermal conductivity are obviously much more important to a probe's heat flux response in water than in air.

A fraction of the heat flux from the film goes through the substrate and consequently contributes nothing, if $R_f' << R_s$, to the probe's speed sensitivity. Let Q_s denote the substrate flux and Q_o the boundary layer flux (Figure 4). The flux ratio is

$$\frac{Q_s}{Q_o} = \frac{R_f + R_c}{R_s} .$$

For water at U_o = 130 cm/sec, Q_s/Q_o is approximately 0.25; i.e. 20% of the total flux from the film goes into the substrate. In contrast, Q_s/Q_o should be approximately 14 in air, indicating that more than 90% of the total flux is into the substrate. However, this part of the model is not completely applicable in air because R_f' may be comparable to R_s. Nonetheless, the same probes operated in air would lose a significant amount of speed sensitivity because of conduction into the substrate. A thin film turbulence probe suitable for use in water may be unsuitable for use in air.

The quasi-steady sensitivity to both speed and temperature fluctuations in the ambient fluid are now readily attained. The quasi-steady sensitivity to speed is

$$\frac{\partial Q}{\partial U_o} = \frac{\partial Q}{\partial R_e} \frac{\partial R_e}{\partial U_o} = \frac{R_e}{U_o} \frac{\partial Q}{\partial R_e}$$

and to temperature is

$$\frac{\partial Q}{\partial (\Delta T)} = \frac{Q}{\Delta T} .$$

The ratio of the quasi-steady speed-to-temperature sensitivity is

$$\frac{\partial Q/\partial U_o}{\partial Q/\partial(\Delta T)} = \frac{R_e}{Q}\frac{\partial Q}{\partial R_e}\left(\frac{\Delta T}{U_o}\right)$$

$$= \frac{B\,R_e^{\frac{1}{2}}}{(A+R_e^{\frac{1}{2}})(AC+B+CR_e^{\frac{1}{2}})}\left\{\frac{\Delta T}{2U_o}\right\}.$$

The ideal conical probe has no coating resistance and an infinite substrate resistance, i.e. $A = C = 0$. Thus the optimum relative sensitivity is $\Delta T/2U_o$. The real probe (V-31) has at U_o=130 cm/sec a relative sensitivity of

$$0.61\left(\frac{\Delta T}{2U_o}\right),$$

which is 61% of the optimum sensitivity at 130 cm/sec. Using $\Delta T = 20^{\circ}C$ gives

$$\frac{\partial Q/\partial U_o}{\partial Q/\partial(\Delta T)} = 0.047^{\circ}C \text{ per cm/sec}$$

which means that the probe cannot distinguish a quasi-steady fluctuation of $0.047^{\circ}C$ from a fluctuation of 1 cm/sec at 130 cm/sec.

3. Unsteady Response

3(a). Viscous Boundary Layer

If the ambient fluid's speed, relative to the probe, has an infinitesimal sinusoidal oscillation about its steady mean, then one can write the potential flow at the probe's surface as

$$V(x,t) = V_o(x)(1+\varepsilon e^{i\omega t}) = Ex^n(1+\varepsilon e^{i\omega t}) \simeq U_o(1+\varepsilon e^{i\omega t}) \quad (24)$$

where ω is the angular frequency in radians/sec and where ε, small compared to unity, is the normalized speed amplitude of the probe shaker used for response calibrations. The boundary layer velocity will consist of a steady mean velocity plus a sinusoidal perturbation, i.e.

$$\left.\begin{aligned} u(x,y,t) &= u_o(x,y) + \varepsilon e^{i\omega t}\, u_1(x,y,\omega) \\ v(x,y,t) &= v_o(x,y) + \varepsilon e^{i\omega t}\, v_1(x,y,\omega) \end{aligned}\right\} \quad (25)$$

The appropriate perturbation momentum equation, to first order in ε is (Lighthill, 1954)

$$i\omega u_1 + u_o\frac{\partial u_1}{\partial x} + v_o\frac{\partial u_1}{\partial y} + u_1\frac{\partial u_o}{\partial x} + v_1\frac{\partial u_o}{\partial y}$$

$$= i\omega V_o + 2V_o\frac{dV_o}{dx} + \nu\frac{\partial^2 u_1}{\partial y^2} \quad (26)$$

with boundary conditions

$$u_1(x,o,\omega) = v_1(x,o,\omega) = 0$$

$$u_1(x,\infty,\omega) = V_o(x)$$

If we let

$$u_1(x,y,\omega) = V_o(x)g'(\eta,\Omega) = Ex^n g'(\eta,\Omega) \quad (27)$$

where $\Omega=\frac{\omega x}{3V_o}$, then continuity

$$\frac{\partial}{\partial x}(Ru_1) + R\frac{\partial v_1}{\partial y} = 0$$

requires that

$$v_1(x,y,\omega) = -\sqrt{\frac{2\nu}{3+n}Ex^{n-1}}\left\{\frac{3+n}{2}g + (\frac{n-1}{2})\eta g' + (1-n)\Omega\frac{\partial g}{\partial\Omega}\right. \tag{28}$$

Substituting the above expressions for u_1, v_1, and Ω into the perturbation momentum equation (26) and using the expressions for u_o and v_o given in equations (11) and (12) yields

$$g'''+fg'' - \frac{2}{3+n}\{2nf' + 3i\Omega\}g' + f''g =$$

$$= \frac{-2}{3+n}\{2n + 3i\Omega\} - 2(\frac{1-n}{3+n})\Omega\frac{\partial}{\partial\Omega}\{f''g - f'g'\} \tag{29}$$

with boundary conditions

$$g(o,\Omega) = g'(o,\Omega) = 0$$

$$g'(\infty,\Omega) = 1$$

$$g(\eta,0) = \tfrac{1}{2}(f + \eta f').$$

The presence of n in the momentum equation (29) results from the steady pressure gradient along the cone's surface. Its effect relative to a zero pressure gradient flow, is an increase in the fluid's inertia (the third term on the left-hand side in (29)) and an increase in unsteady pressure gradient (the first term on the right-hand side). The steady pressure gradient along a cone of half-angle 15^o is evidently quite small because n = 0.035. Thus n can be ignored relative to 3 and, because $0 \le f' \le 1$, 2n can also be ignored relative to $3i\Omega$ when

$\Omega >> 2n/3 = 0.023$. Within the above constraints, the perturbation momentum equation (29) simplifies to

$$g''' + fg'' - 2i\Omega g' + f''g = -2i\Omega + \frac{2}{3}\Omega \frac{\partial}{\partial \Omega}(f''g - f'g') \quad (30)$$

$$g(0,\Omega) = g'(0,\Omega) = 0$$

$$g'(\infty,\Omega) = 1$$

$$g(\eta,0) = \tfrac{1}{2}(f+\eta f').$$

Except for the definition of the variables η and Ω equation (30) is identical to the corresponding perturbation momentum equation for two-dimensional flow over a flat plate (Lueck, 1979). The solution for the unsteady flow over a plate also applies to the unsteady flow over a cone of half-angle 15^{o}, within the limits cited.

3(b). Thermal Boundary Layer

Let

$$T(x,y,t) = T_o(x,y) + \varepsilon e^{i\omega t} T_1(x,y,\omega)$$

where T_o is the steady temperature field given earlier and T_1 is the perturbation temperature field due to main stream flow oscillations. The governing equation for T_1, to first order in ε, is (Lighthill, 1954)

$$i\omega T_1 + u_o \frac{\partial T_1}{\partial x} + v_o \frac{\partial T_1}{\partial y} - \kappa \frac{\partial^2 T_1}{\partial y^2} = -u_1 \frac{\partial T_o}{\partial x} - v_1 \frac{\partial T_o}{\partial y} \quad (32)$$

(a) (b) (c) (d)

$$T_1 = 0 \text{ at } y = 0 \text{ and } \infty.$$

The artificial concept of a finite boundary layer thickness will be used to solve T_1 because η cannot be a similarity variable for T_1, as was the case for T_o.

Let

$$T_1(x,y,\omega) = T_1(\xi,\Omega)$$

where, using equations (13), (17) and (19)

$$\xi = \frac{y}{\delta_T} = \frac{y}{r\delta} = \frac{\eta}{3.04r} \tag{33}$$

and

$$0 \leq \xi \leq 1.$$

The steady viscous boundary layer thickness, δ, is essentially constant over the film because the aspect ratio $d/L \ll 1$. Hence, x can be set equal to L except where it appears in r. The differential operators in the temperature equation (32) then become

$$\frac{\partial}{\partial y} = \frac{1}{r\delta}\frac{\partial}{\partial \xi} = \frac{1}{3.04r}\sqrt{\frac{3U_o}{2\nu L}}\frac{\partial}{\partial \xi} \tag{34a}$$

$$\frac{\partial^2}{\partial y^2} = \frac{1}{(r\delta)^2}\frac{\partial^2}{\partial \xi^2} = \frac{1}{(3.04r)^2}\frac{3U_o}{2\nu L}\frac{\partial^2}{\partial \xi^2} \tag{34b}$$

$$\frac{\partial}{\partial x} = -\frac{\xi}{4Lr^3 Pr}\frac{\partial}{\partial \xi} \tag{34c}$$

Using the above operators along with equations (11), (12), (18), (19), (27) and (28) transforms the terms in the perturbation temperature equation (32) to

$$(a)\quad \frac{U_o}{L} \times 3i\Omega T_1 \tag{35a}$$

$$(b)\quad -\frac{U_o}{L} \times \{(1+2r^3Pr)\xi f' - \frac{6r^2Prf}{3.04}\} \frac{1}{4r^3Pr} \frac{\partial T_1}{\partial \xi} \tag{35b}$$

$$(c)\quad -\frac{U_o}{L} \times \frac{3}{2(3.04)^2 r^2 Pr} \frac{\partial^2 T_1}{\partial \xi^2} \tag{35c}$$

$$(d)\quad -\frac{U_o}{L} \times \frac{3(\Delta T_o)(1-\xi^2)}{8r^3Pr} \{(1+2r^3Pr)\xi g' - \frac{r^2 Pr}{3.04} (6g+4\Omega\frac{\partial g}{\partial \Omega}). \tag{35d}$$

For the two probes considered, r is always less than 0.17. Thus $2r^3Pr$ is small compared to unity. Throughout the domain $0 \leq \xi \leq 1$ the variable η never exceeds 0.51; consequently, the steady velocity profile f' is essentially proportional to η (Schlichting, 1955, p. 107). A linear approximation for the unsteady velocity profile g' is reasonable up to frequencies Ω not much greater than unity (Lueck, 1979). Thus for $\eta < \frac{1}{2}$ and $\Omega \leq 1$ the boundary layer velocity profiles over the film can be approximated by

$$f = \tfrac{1}{2}\eta f''(0) = \tfrac{1}{2}(3.04)^2 r^2 \xi^2 f''(0)$$

$$f' = \eta f''(0) = 3.04\, r\xi f''(0)$$

$$g = \tfrac{1}{2}\eta g''(0,\Omega) = \tfrac{1}{2}(3.04)^2 r^2 \xi^2 g''(0,\Omega)$$

$$g' = \eta g'(0,\Omega) = 3.04\, r\xi\, g''(0,\Omega)$$

Substituting the above into the perturbation temperature equation (35 and 32) yields finally

$$\frac{\partial^2 T_1}{\partial \xi^2} + \frac{(3.04)^3 \xi^2}{6} f''(0) \frac{\partial T_1}{\partial \xi} - 2(3.04)^2 r^2 Pri\Omega T_1 =$$

$$= \frac{(3.04)^3}{4} \xi^2 (1-\xi)^2 (\Delta T_o) g''(0,\Omega) + \sim O(r^3 Pr) \qquad (36)$$

$$T_1 = 0 \text{ at } \xi = 0, 1$$

The term $2(3.04)^2 r^2 Pri\Omega T_1$ which represents the thermal inertia of the boundary layer, is evidently small compared to the other terms in equation 36 for the frequency range considered here $\Omega \leq 1$. Dropping the third term in equation 36 reduces it to the ordinary differential equation

$$\frac{dT_1}{d\xi^2} + \frac{(3.04)^3}{6} \xi^2 f''(0) \frac{dT_1}{d\xi} = \frac{(3.04)^3}{4} \xi^2 (1-\xi^2)(\Delta T_o) g''(0,\Omega) \qquad (37)$$

$$T_1 = 0 \text{ at } \xi = 0, 1.$$

Equation 37 does not have to be solved explicitly. The perturbation temperature, T_1, is everywhere proportional to $(\Delta T_o) g''(0,\Omega)$. Hence the total heat flux from the film is

$$Q = Q_o + q(\Omega) e^{i\omega t} = Q_o + \varepsilon e^{i\omega t} F(\Delta T_o) g''(0,\Omega) \qquad (38)$$

where F is a frequency independent constant. In the limit $\Omega \to 0$, the perturbation heat flux must equal the quasi-steady heat flux, i.e.

$$\frac{q(0)}{\varepsilon} = U_o \frac{\partial Q_o}{\partial U_o} = \tfrac{1}{2} Q_o = F(\Delta T_o) g''(0,0)$$

The constant F is readily determined by using

$$g''(0,0) = \frac{3}{2} f''(0).$$

The total heat flux into the fluid above the film then is

$$Q = Q_o \left[1 + \frac{\varepsilon}{3} e^{i\omega t} \frac{g''(0,\Omega)}{f''(0)}\right] \tag{39}$$

or using (23b)

$$Q = 1.53\lambda_f L\left(\frac{d}{L}\right)^{2/3} Pr^{1/3} R_e^{1/2} \Delta T_o \left[1 + \frac{\varepsilon}{3} e^{i\omega t} \frac{g''(0,\Omega)}{f''(0)}\right] \tag{40}$$

The unsteady response of the two thin film probes is plotted in figure 6 for the steady speeds 102, 129, 154 and 182 cm/sec. Plotted is the unsteady thermal conductance $q/\Delta T_o$ divided by $U_o^{\frac{1}{2}}$ and the fractional amplitude ε against the frequency parameter $\omega L/3U_o$. The unsteady conductance has been scaled by an arbitrary factor, γ, to bring the low frequency values close to 0 dB. (The calibration for the velocity monitor on the shaker is unavailable.) The solid line in figure 6 is $2/3\ g''(0,\Omega) / f''(0)$ which according to equation 40 is proportional to $q/(\varepsilon \Delta T_o U_o^{\frac{1}{2}})$. The dashed line has been drawn to show the quality of the fit if the frequency parameter $\omega L'/3U_o$ had been used instead of $\omega L/3U_o$ (figure 1). The data for both V-31 and V-38 exhibit a rise with increasing frequency characteristic of $g''(0,\Omega)$ but appear to be shifted by approximately 40% to the right along the frequency axis (less if scaled by $\omega L'/3U_o$). This shift along the frequency axis may reflect some inadequacies with modelling the flow over a blunted cone by the flow over an ideal "needle sharp" cone. The scatter among the data points for $\Omega > 1.5$ is noticeable. This scatter may be due to some spurious motions of the probe support at high frequencies (Evans, personal communication); $\Omega > 1.5$ corresponds to real frequencies of 500 to 1000 Hertz. Thermal inertia should become important for $\Omega > 1$ and

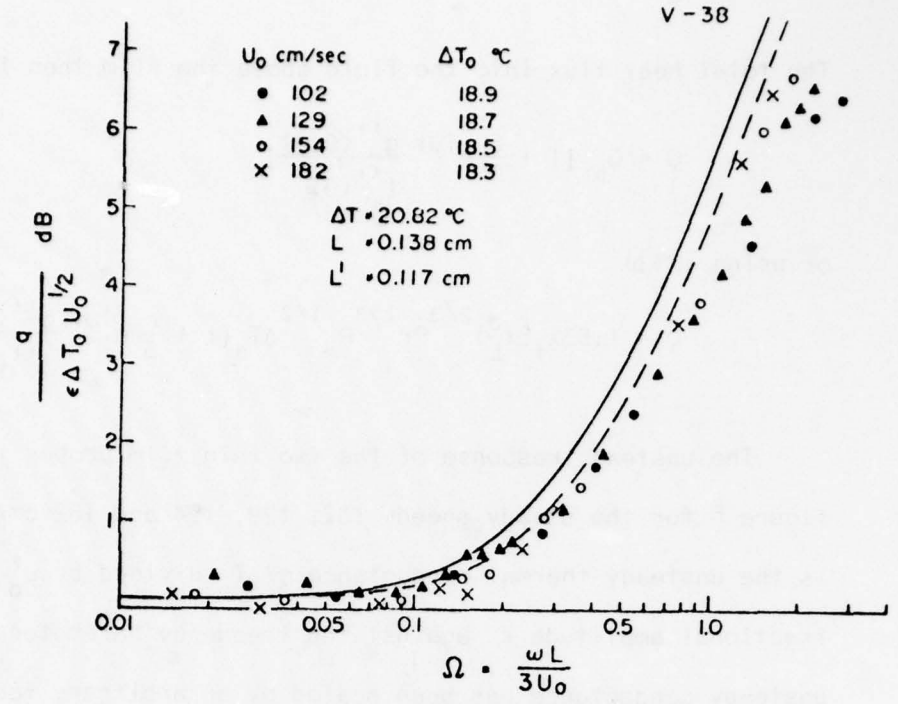

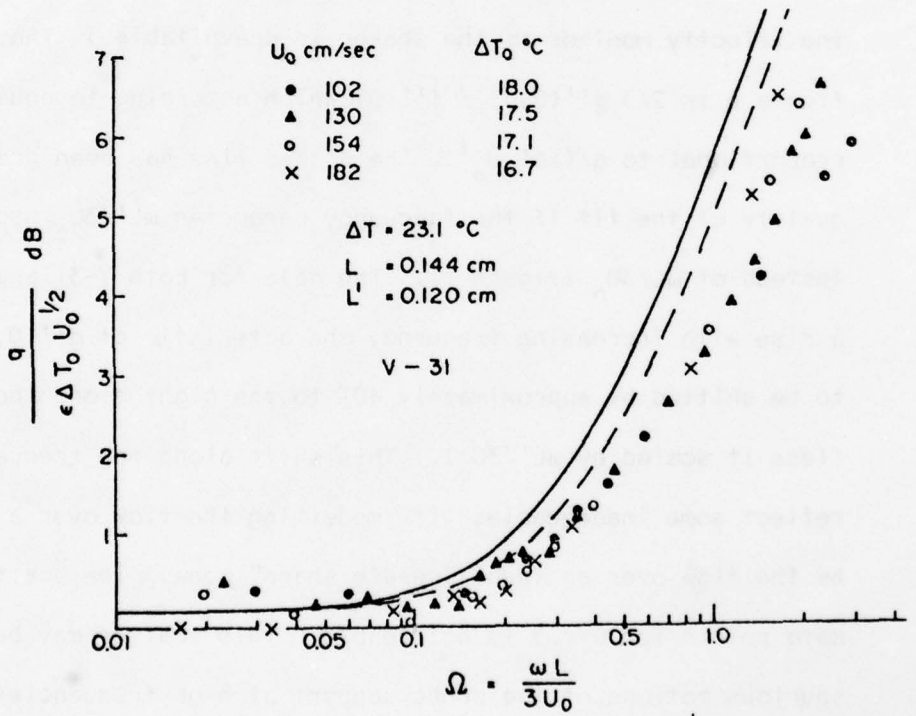

6. The probes' unsteady thermal conductance scaled by $U_0^{\frac{1}{2}}$ and the fractional speed amplitude ε versus the frequency parameter $\Omega = \omega L/3U_0$. The solid line is two-thirds of the unsteady-to-steady surface stress ratio after Lueck (1979). The dashed line indicates the quality of the fit if the frequency had been scaled by $\omega L'/3U_0$. L' is shown in figure 1.

cause a "roll-off" in the frequency response, but only the data for U_o=102 cm/sec shows a definite trend to roll-off. Although the match between the data and the theoretically predicted response is not complete it does appear that the unsteady heat flux from the film is strongly influenced by the unsteady viscous boundary layer and that for probes V-31 and V-38 it is proportional to the unsteady surface shear $g''(0,\Omega)$.

The peculiar rise of the response with increasing frequency is due to the probes' aspect ratio $d/L<<1$. Most commercial probes have aspect ratios closer to unity and therefore should show much less if any rise, at high frequencies due to the thermal inertia of the boundary layer. Observations by Nowell (1974) of commercial constant temperature hot film probes show a decrease in response with increasing frequency above approximately 100 Hertz.

The sensitivity of these probes to temperature oscillations in the main stream causes a contamination of the measured velocity signal which can be very severe (Gargett, 1978). The response of these probes to temperature oscillations is difficult to calculate. However, at least three aspects of the response to infinitesimal external temperature oscillations can be deduced. Firstly, the heat flux into the boundary layer above the film cannot increase with increasing frequency because there is no mechanism to accentuate the response to temperature oscillations in the main stream. As well, calculations for an ideal flat plate sensor by Lueck (1979) show that the bandwidth of the response to temperature oscillations is smaller than the bandwidth for the response to speed oscillations. Secondly, the heat flux into

the substrate induced by external temperature oscillations will decrease with increasing frequency because of the substrate's finite diffusivity. The effective depth of penetration into the substrate is approximately the width of the film $d \approx 6 \times 10^{-3}$ cm, hence the heat flux decreases when $\omega d^2/K_s \geq 1$, i.e. above approximately 30 Hertz. Thirdly, the glass upstream from the film acts as a passive heat sink and reduces somewhat the temperature oscillations of the fluid close to the surface before this fluid reaches the area above the film. Thus the ratio of temperature-to-velocity sensitivity is highest at zero frequency and decreases with increasing frequency. An upper bound to the contamination of a measured velocity spectrum by temperature fluctuations can be calculated from the ratio of quasi-steady temperature-to-velocity sensitivity and an independent estimate of the temperature spectrum.

4. Conclusions

The steady calibration data presented show that the probes' thermal conductance $Q/\Delta T$ is not proportional to $U_o^{\frac{1}{2}}$ as expected for a constant temperature conical surface. A thermal model of the probes indicates that $Q/\Delta T$ is neither proportional nor linearly related to $U_o^{\frac{1}{2}}$ because of the thermal effects of the coating over the film and the substrate below it. The model predicts that a glass coating of only $\sim 1 \times 10^{-4}$ cm can significantly reduce the temperature difference between the probe's wetted surface and the ambient fluid and that the heat flux into the substrate is moderately important for probes operated in water. For probes operated in air, on the other hand, the model predicts the opposite characteristics: a relatively small effect due to the coating and a very large heat flux into the substrate. The coating and the substrate reduce the quasi-steady speed-to-temperature sensitivity of the probes by about 40% from its optimum value of $\Delta T/2U_o$.

The unsteady heat flux from the hot film probes in response to variations of the ambient fluid's speed is strongly influenced by the unsteady viscous boundary layer. For the probes considered, the unsteady heat flux is proportional to the unsteady viscous surface stress over the film. The unsteady heat flux from the probes examined increases in magnitude, over its quasi-steady value, with increasing frequency. The ratio of temperature-to-velocity sensitivity is highest at zero frequency and decreases with increasing frequency. An upper bound to the contamination of a measured velocity spectrum by temperature fluctuations in the main stream can be calculated from the ratio of the quasi-steady temperature-to-velocity sensitivity and an independent estimate of the tempeature spectrum.

Bibliography

Bellhouse, B.J. and D.L. Schultz. 1967. The determination of fluctuating velocity in air with heated thin film gauges. Journal of Fluid Mechanics, 29: 289-295.

Evans, D.J. 1963. An instrument for the measurement of ocean turbulence. Technical Memorandum 63-8, Pacific Naval Laboratory, Defense Research Board, Canada.

Freymuth, P. 1977. Frequency response and electronic testing for constant-temperature hot wire anemometers. Journal of Physics E; Scientific Instruments, 10: 705-710.

Freymuth, P. 1978. Theory of frequency optimization for hot film anemometers. Journal of Physics E; Scientific Instruments, 11: 177-179.

Gargett, A.E. 1978. Microstructure and finestructure in an upper ocean frontal regime. Journal of Geophysical Research, 83(C10): 5123-5134.

Grant, H.L., R.W. Stewart and A. Moilliet. 1962. Turbulence spectra from a tidal channel. Journal of Fluid Mechanics, 12: 241-288.

Grant, H.L., A. Moilliet and V.M. Vogel. 1968. Some observations of the occurrence of turbulence in and above the thermocline. Journal of Fluid Mechanics, 34: 443-448.

Hinze, J.O. 1975. Turbulence, second edition. McGraw-Hill, 790 pp.

Kays, W.M. 1966. Convective Heat and Mass Transfer. McGraw-Hill, 387 pp.

Kramers, H. 1946. Heat transfer from spheres to flowing media. Physics, 12: 61-80.

Lighthill, M.J. 1954. The response of laminar skin friction and heat transfer to fluctuations in the stream velocity. Proceedings of the Royal Society of London, Series A, vol. 224, pp. 1-23.

Lueck, R.G. 1979. The unsteady flux of heat and momentum from a flat plate. Submitted to Journal of Fluid Mechanics.

Morrison, G.L., A.E. Perry and A.E. Samuel. 1972. Dynamic Calibration of Inclined and Crossed Hot Wires. Journal of Fluid Mechanics, 52: 405-474.

Nasmyth, P.W. 1970. Oceanic Turbulence. Ph.D. Thesis, Institute of Oceanography, University of British Columbia.

Nowell, Arthur R.M. 1974. Some response characteristics of parabolic hot films in water. Journal of Hydronautics 8:4, pp. 169-171.

Schlichting, H. 1955. Boundary Layer Theory. Pergamon Press, 535 pp.

Tan-atichat, J., H.M. Nagib and J.W. Pluister. 1973. On the interpretation of the output of hot-film anemometers and a scheme of dynamic compensation for water temperature variation. Symposium on Turbulence in Liquids, University of Missouri, Rolla.

White, F.M. 1974. Viscous Fluid Flow. McGraw-Hill, 725 pp.

Acknowledgements

This paper could not have been produced without the co-operation of the Ocean Mixing Group at the Institute of Ocean Sciences, Patricia Bay, particularly Dr. A. Gargett, Dr. P. Nasmyth and Mr. G. Chase. Mr. D. Evans, formerly with the Defense Research Establishment, Pacific, has provided needed information on the probes' electronics. Prof. T.R. Osborn deserves appreciation for his encouragements and support. This work has been supported by the Office of Naval Research, Contract Number 00014-083-207.

Appendix C

The Characteristics of Internally Heated Thermistors

by

Rolf G. Lueck

and

Thomas R. Osborn

Institute of Oceanography

University of British Columbia

Vancouver, B.C. V6T 1W5

Canada

January 1979

Abstract

A model for the heat flux from coated spherical and plate-shaped thermistors to their fluid environment has been developed and agrees favourably with the available data. The heat flux model is used to derive the thermistor's quasi-steady sensitivity to speed and to temperature. The coating reduces significantly both the sensitivity to speed and to temperature as well as the ratio of speed-to-temperature senstivity. The available values for the rates of temperature and kinetic energy dissipation in the ocean indicate that (1) velocity measurements by heated thermistors may be contaminated by temperature in the main thermocline and (2) temperature measurements by a nearly unheated thermistor may be contaminated by velocity in the mixed layer.

1. Introduction

Thermistors are now commonly used to measure temperature microstructure in the ocean. Their large sensitivity to temperature, due to a high fractional temperature coefficient of resistance (approximately 0.04/°C) and a large resistance (up to 25 x 10^6 ohms), make thermistors attractive for oceanographic use. There are, however, several problems with using thermistors. Three of these problems are (1) the thermistor's signal-to-noise ratio which has been examined by Gregg, Meagher, Pederson, and Aagaard (1978), (2) its frequency (and spatial) response which has been examined by Lueck, Hertzman, and Osborn (1977), and (3) the sensitivity to velocity due to self-heating which has been raised by Gregg, et al. (1978).

Inevitably, a small but finite electrical current must be passed through the thermistor to measure its electrical resistance and hence its temperature. The electric power dissipated by the ohmic-heating raises the temperature of the thermistor above the ambient fluid's temperature and thereby subjects the thermistor to a velocity-dependent forced convective cooling.

At a given resistance, the sensitivity to temperature is proportional to the current passing through the thermistor. Hence, the signal-to-noise ratio is readily increased by increasing the thermistor current. The limit to which the current can be increased is governed by the thermistor's relative velocity-to-temperature sensitivity, the relative velocity-to-temperature activity in the fluid being probed, and the level of velocity contamination in the temperature signal that one is willing to accept.

A deliberate large self-heating is also interesting because it turns the thermistor into an anemometer with some level of temperature contamination. The use of thermistors as anemometers has so far been limited. Caldwell (1968) reported on an indirectly heated thermistor to measure bottom currents. Lange (personal communication) has mounted both 0.015 cm micro-bead and 0.05 cm flake thermistors on a free-fall vehicle for microstructure measurements. The thermistors were heated by a constant current source to approximately 50°C above the ambient temperature.

Their relatively large temperature coefficient and large resistance compared to thin metal film sensors also make thermistors attractive for measuring velocity microstructure. In this paper we propose, in section 2, a thermal model for the heat flux from thermistors. Section 3 compares the model with the available data. The quasi-steady sensitivity of the thermistor to speed and temperature in the ambient fluid is derived in section 4 both for constant temperature operation, 4a, and constant current operation, 4b. The implications for thermometry and anemometry in the ocean are discussed in section 5.

2. Steady Response

Following Lueck, et al. (1977) we will use a sphere to model microbead thermistors and a flat plate for flake thermistors. Both models are shown in Figure 1. The models consist of an inner core of metal-oxide, a uniform coating of thickness Δ and a boundary layer of unspecified thickness. Because the ohmic heating in the metal-oxide is distributed over the volume of the core we will assign a spatially uniform temperature T to the metal-oxide core. The temperature of the wetted surface is θ_s and the temperature in the ambient fluid, at the outside limit of the boundary layer, is θ.

2a. Sphere

The heat flux, Q, from a sphere with a uniform surface temperature θ_s is

$$Q = 2\pi(R + \Delta)\lambda_2 (\theta_s - \theta)Nu \qquad (1)$$

where Nu is the Nusselt number, λ_2 the fluid's thermal conductivity, and $2(R + \Delta)$ is the diameter of the sphere. In the coating the temperature distribution, if spherically symmetric, is governed by

$$\frac{1}{r^2} \frac{\partial}{\partial r} \left(r^2 \frac{\partial T_c}{\partial r} \right) = 0$$

which is satisfied by

$$T_c(r) = T - (T - \theta_s) \frac{R + \Delta}{\Delta} \left\{ 1 - \frac{R}{r} \right\} .$$

$$R \leq r \leq R + \Delta$$

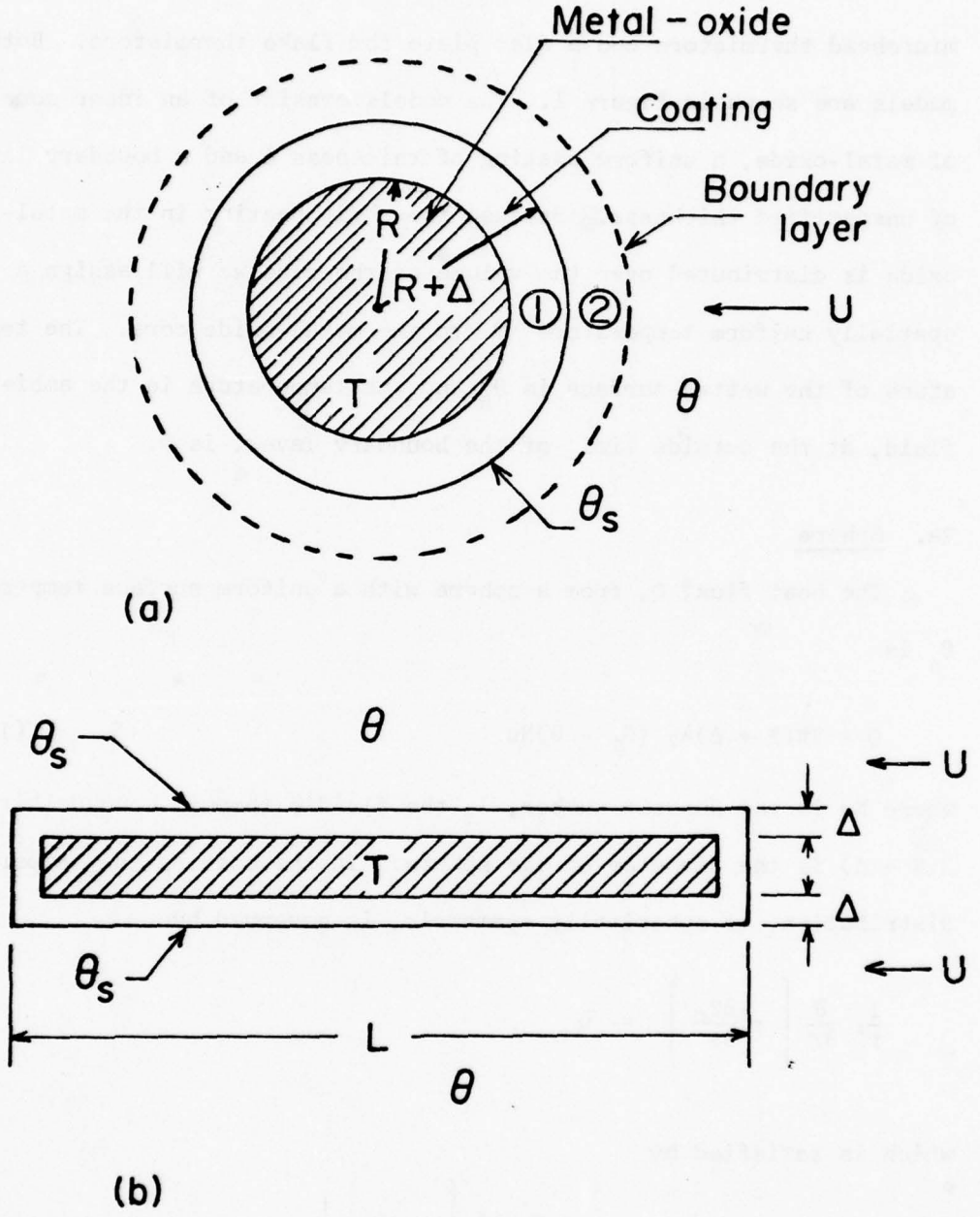

Figure 1. (a) A cross-section of the model spherical thermistor, and (b) a cross-section of the model plate thermistor.

Under steady conditions the heat flux through the coating must equal the heat flux, Q, into the fluid. Hence, we use

$$-\lambda_1 \, 4\pi \, R^2 \frac{\partial T_c}{\partial r}\bigg|_R = Q$$

where λ_1 is the thermal conductivity of the coating, to eliminate the surface temperature, θ_s, and derive

$$\frac{T - \theta}{Q} = \frac{\Delta/R}{4\pi(R + \Delta)\lambda_1} + \frac{1}{2\pi(R + \Delta)\lambda_2 Nu} \quad . \tag{2}$$

Equation 2 relates the heat flux from the model thermistor to the temperature difference $(T - \theta)$, to the properties of the coating and to the properties of the flow. If the ratio $(T - \theta)/Q$ is regarded as a thermal resistance, in analogy to Ohm's Law, where $T - \theta$ is the thermal "voltage" and Q the thermal "current", then the first term on the right side in equation 2 represents the thermal resistance of the coating and the last represents the thermal resistance of the boundary layer. The thermistor's inner core thus "sees" two thermal resistances between it and the ambient fluid, namely the coating and the boundary layer.

The velocity dependence of the heat flux is implicit in the Nusselt number. The Nusselt number for spheres of approximately uniform surface temperature was empirically determined by Kramers (1946) as

$$Nu = 2.0 + 1.3 \, Pr^{0.15} + 0.66 \, Pr^{0.31} \, Re^{1/2} \tag{3}$$

where

$$Re = \frac{2(R + \Delta)}{\nu} U$$

$$Pr = \frac{\nu}{\kappa}$$

Re is the Reynolds number, Pr the Prandtl number, U the ambient fluid's speed, ν the ambient fluid's kinematic viscosity, and κ its thermal diffusivity.

The effect of the coating on the thermistor's heat flux is more readily determined by rearranging equation 2 to read

$$Q = \frac{2\pi(R + \Delta)\lambda_2 (T - \theta)Nu}{[1 + \frac{\lambda_2}{\lambda_1} \frac{\Delta Nu}{2R}]} \qquad (4)$$

For an uncoated sphere $\Delta = 0$ and hence the heat flux relates to the fluid's speed in a fashion after King's Law because of the Nusselt-Reynolds number relationship shown in equation 3. A finite coating thickness, however, reduces the heat flux's dependence on speed through the term

$$DF = \frac{\lambda_2}{\lambda_1} \frac{\Delta Nu}{2R} \qquad (5)$$

The term DF depends on the ratio of the fluid-to-coating conductivity, the relative coating thickness, $\Delta/2R$, and the Nusselt number of the flow. It can also be regarded as the ratio of the coating-to-boundary layer resistance. Evidently, DF is an important design parameter because if $DF << 1$, there is no coating effect, and if $DF >> 1$, the heat flux is independent of the flow. In addition, equation 4 shows that the ratio

$(T - \theta)/Q$ is a constant at a given Nusselt number and that the heat flux does not follow King's Law if DF is not small compared to unity.

The term DF can be quite large for commonly available thermistors. For example, 0.015 cm appears to be the lower limit for the diameter of the metal-oxide core (M. Sapoff, personal communication) and at a speed of 10 cm/sec the Nusselt number is approximately 10 in water. Accordingly, a 0.015 cm diameter microbead coated with paralene-C (λ_1 = 0.0010 watts/^{o}C cm) to a thickness of Δ = 0.0018 cm has a DF value of 7. The same thermistor under the same flow conditions but coated with 0.0025 cm of glass (λ_1 = 0.0105 watts/^{o}C cm) has a DF value of 0.9.

2b. Plate

The total heat flux from both wetted surfaces of a plate held at a uniform temperature θ_s is (Schlichting, 1955, p. 269)

$$Q = 2b\lambda_2(\theta_s - \theta)Nu$$

where

$$Nu = 0.664\ Pr^{1/3}Re^{1/2}$$

$$Re = \frac{UL}{\nu}$$

b is the plate's width and L its length in the flow direction. The heat flux through the coating is

$$Q = \frac{2bL\lambda_1}{\Delta}(T - \theta_s) \qquad (6)$$

The surface temperature is readily eliminated to yield the plate's thermal resistance as

$$\frac{T - \theta}{Q} = \frac{\Delta/L}{2b\lambda_1} + \frac{1}{2b\lambda_2 Nu}\ . \qquad (7)$$

3. Observations

3.a Plate

Lange (personal communication) measured the temperature of a flake thermistor for various heating currents. The flake thermistor had the nominal dimensions of 0.051 by 0.051 by 0.0025 cm and was coated with paralene-C to a nominal thickness of 0.0018 cm. The measurements were made by towing the thermistor, with its face parallel to the flow, down the length of a 30 by 2.4 by 0.24 metre tow tank at speeds of 10, 20, 30, 40, 50 and 60 cm/sec. The accuracy of the speed measurements is 15% or better. We used Lange's data to calculate the heat flux and the thermistor's (metal-oxide's) temperature for the various heating currents and flow speeds. The results are shown in Figure 2. The slopes of the temperature vs heat flux plots for a given speed equal the thermal resistance $(T - \theta)/Q$ (because $T = \theta$ when $Q = 0$). The thermistor's thermal resistance is plotted against $U^{-1/2}$ in Figure 3. The observed relationship, by a least square fit, is

$$\frac{T - \theta}{Q} = 0.437 \pm 0.001 + \frac{0.538 \pm 0.005}{U^{1/2}} \frac{^{\circ}C}{mw} \qquad (8)$$

Using the appropriate parameter values listed in Table 1 yields, according to equation 7,

$$\frac{T - \theta}{Q} = 0.35 + \frac{0.59}{U^{1/2}} \frac{^{\circ}C}{mw} \quad .$$

The observed and the predicted thermal resistances agree favorably considering that the flake's dimensions are known only by the nominal values specified by the manufacturer.

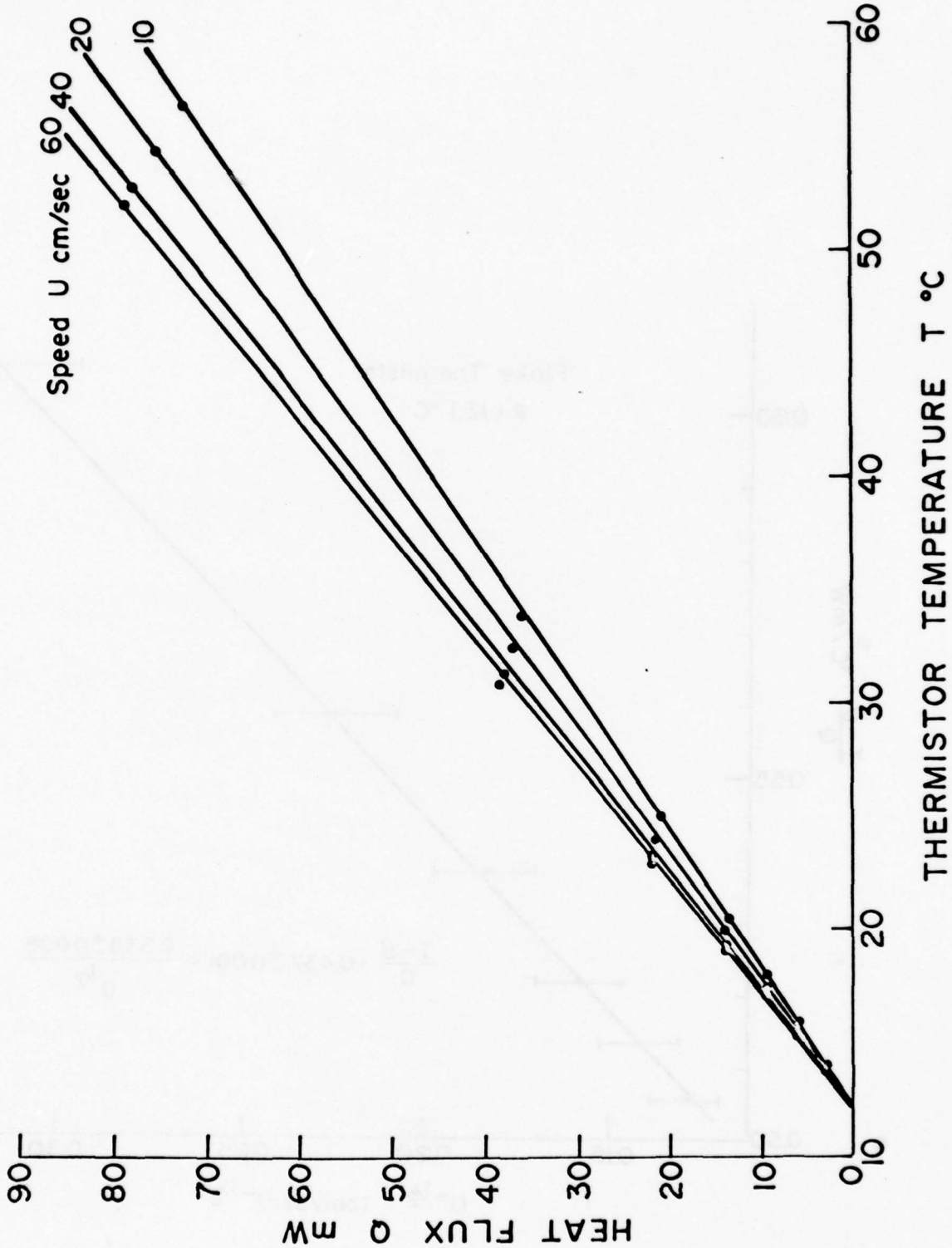

Figure 2. Heat flux versus temperature for various speeds for Lange's 0.051 x 0.051 x 0.0025 cm paralene-c coated flake thermistor.

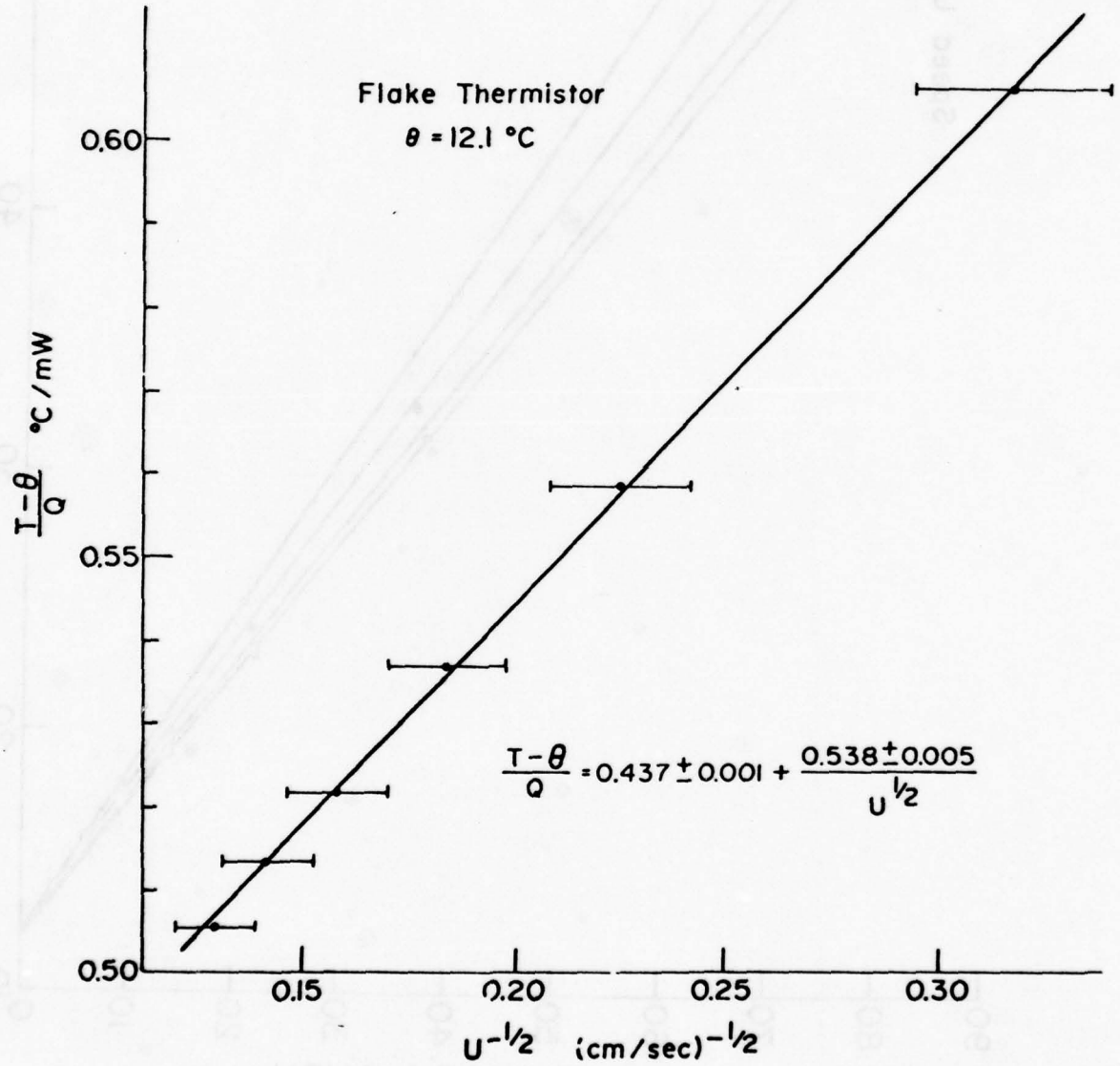

Figure 3. Thermal resistance (T-θ)/Q versus $U^{-\frac{1}{2}}$ for Lange's 0.051 x 0.051 x 0.0025 cm paralene-c coated flake thermistor.

3b. Sphere

Using the equipment specified above, Lange (personal communication) also tested an ellipsoidal microbead thermistor with a nominal semi-minor axis diameter of 0.013 cm coated with paralene-C to a thickness of 0.0018 cm. The temperature vs heat flux curves for the various tow speeds are shown in Figure 4. We have calculated the microbead's Nusselt number using equation 3 and the parameter values in Table 1. The microbead's thermal resistance is plotted against the inverse of its Nusselt number (in Figure 5). The least square fitted line in Figure 5 is

$$\frac{T - \theta}{Q} = 0.59 + \frac{2.51}{Nu} \frac{^{\circ}C}{mw} \quad .$$

In comparison, the relationship predicted by equation 2 is

$$\frac{T - \theta}{Q} = 2.85 + \frac{3.35}{Nu} \frac{^{\circ}C}{mw}$$

The agreement between the predicted and the observed coating resistance (2.85 vs 0.59 °C/mw) is poor and the agreement between the predicted and the observed Nusselt number coefficient (3.35 vs 2.51) is only fair. However, in the absence of more precise knowledge about the thermistor's diameter and its coating thickness it is not clear if the thermal model is in error or if the parameters used are erroneous.

For further tests we ordered a set of 20 microbead thermistors from one production batch. The thermistors' semi-minor axis are, nominally, 0.015 cm. Half (10) of the thermistors were coated with glass to a nominal thickness of 0.00254 cm. All 20 microbeads were

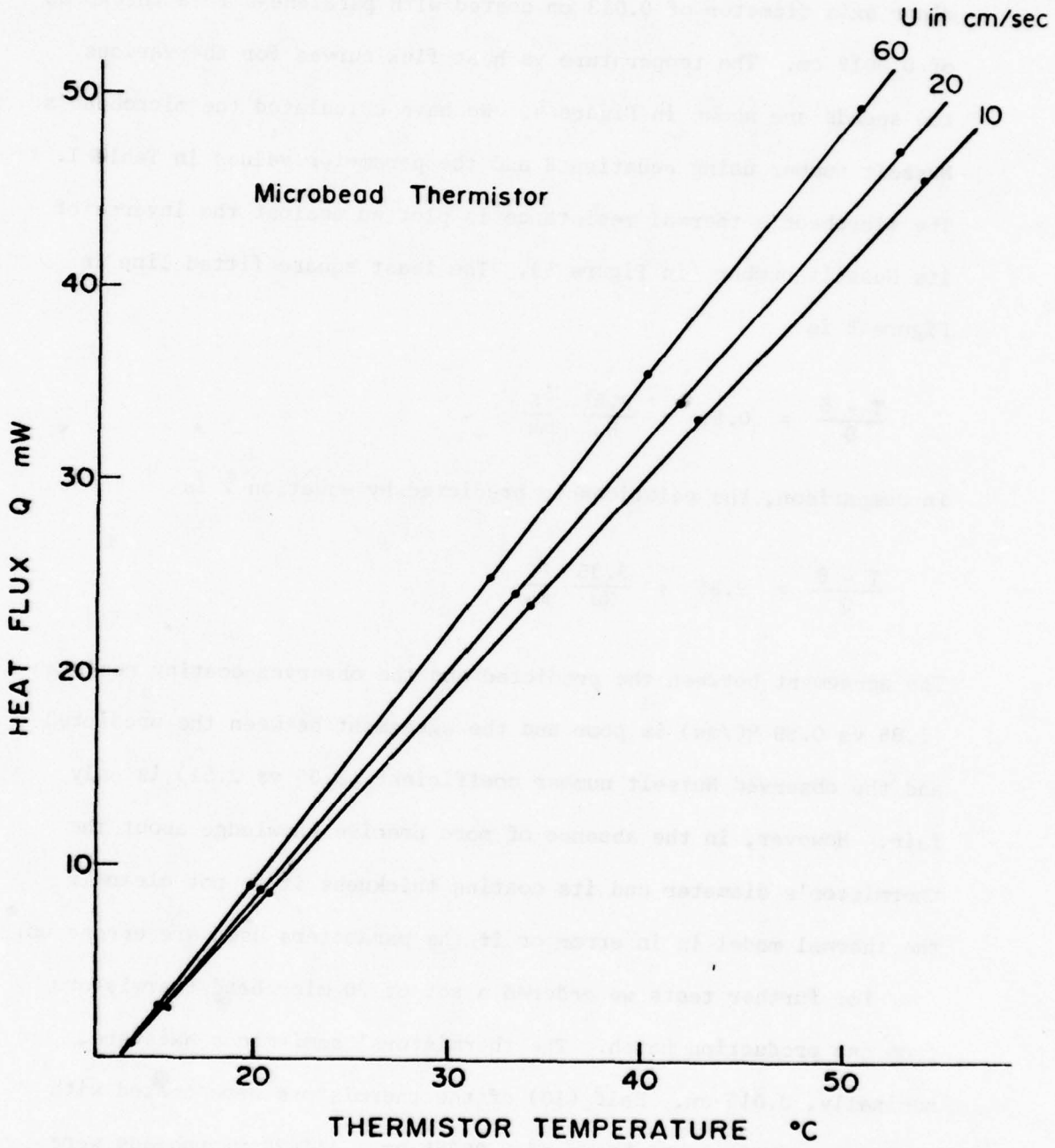

Figure 4. Heat flux versus temperature for various speeds for Lange's paralene-c coated micro-bead thermistor.

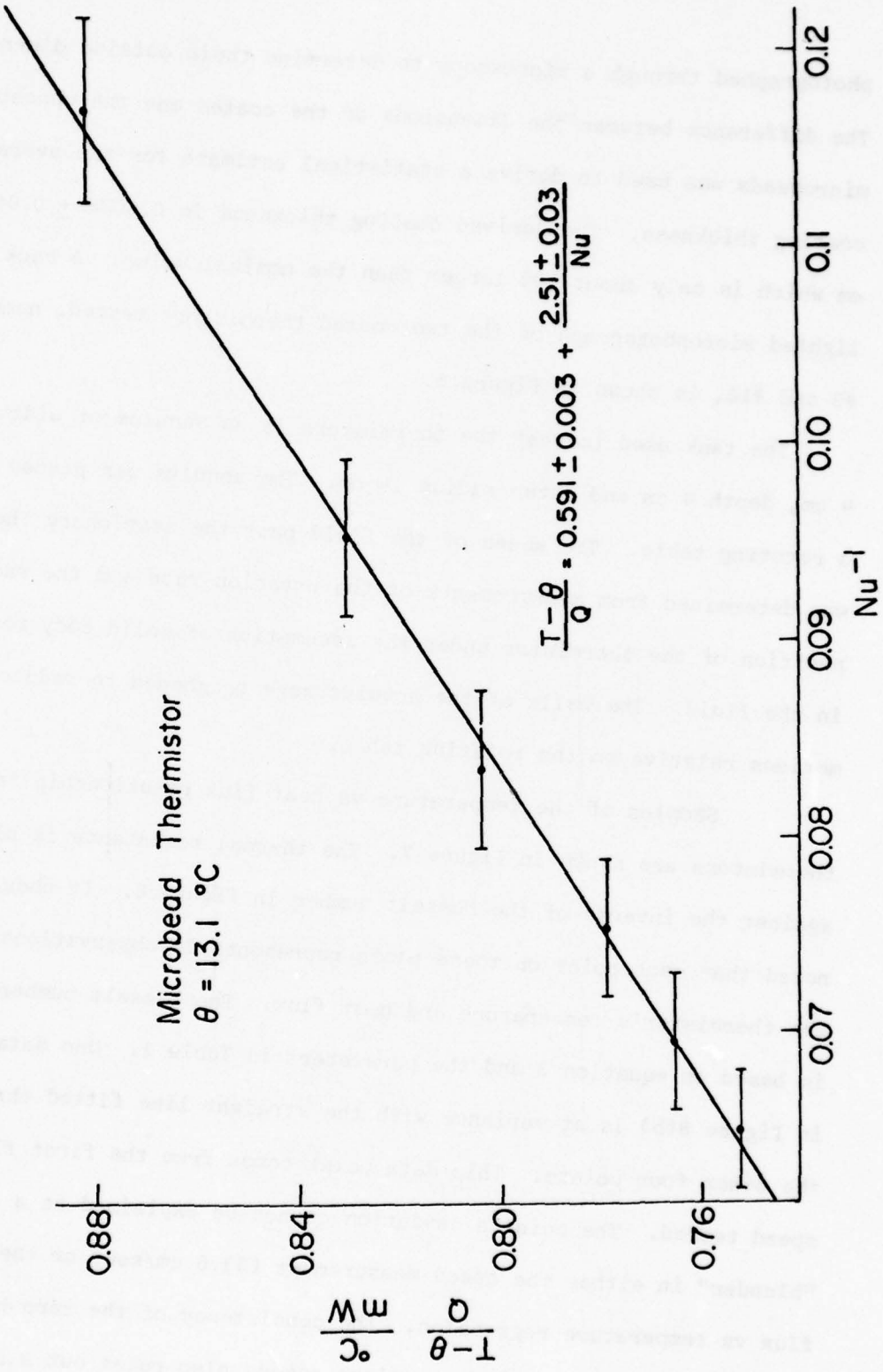

Figure 5. Thermal resistance (T-θ)/Q versus the inverse Nusselt number of Lange's paralene-c coated micro-bead thermistor. The Nusselt number is after equation 3 and the parameters in table 1.

photographed through a microscope to determine their outside dimensions. The difference between the dimensions of the coated and the uncoated microbeads was used to derive a statistical estimate for the average coating thickness. The derived coating thickness is 0.0028 $\pm$ 0.007 cm which is only about 10% larger than the nominal value. A back lighted microphotograph of the two coated thermistors tested, namely #9 and #10, is shown in Figure 6.

The tank used to test the thermistors is an annulus of width 4 cm, depth 4 cm and outer radius 14 cm. The annulus was placed on a rotating table. The speed of the fluid past the stationary thermistor was determined from measurements of the rotation rate and the radial position of the thermistor under the assumption of solid body rotation in the fluid. The walls of the annulus were roughened to reduce fluid motions relative to the rotating table.

Samples of the temperature vs heat flux relationship for the thermistors are shown in Figure 7. The thermal resistance is plotted against the inverse of the Nusselt number in Figure 8. It should be noted that each point on these plots represents 10 observations of the thermistor's temperature and heat flux. The Nusselt number used is based on equation 3 and the parameters in Table 1. One data point in Figure 8(b) is at variance with the straight line fitted through the other four points. This data point comes from the first flow speed tested. The point's deviation cannot be explained as a "blunder" in either the speed measurement (33.6 cm/sec) or the heat flux vs temperature regression. The consistency of the zero heat flux intercept (Fig. 9b) for various speeds also rules out a sporadic change in the electrical resistance temperature relation for the

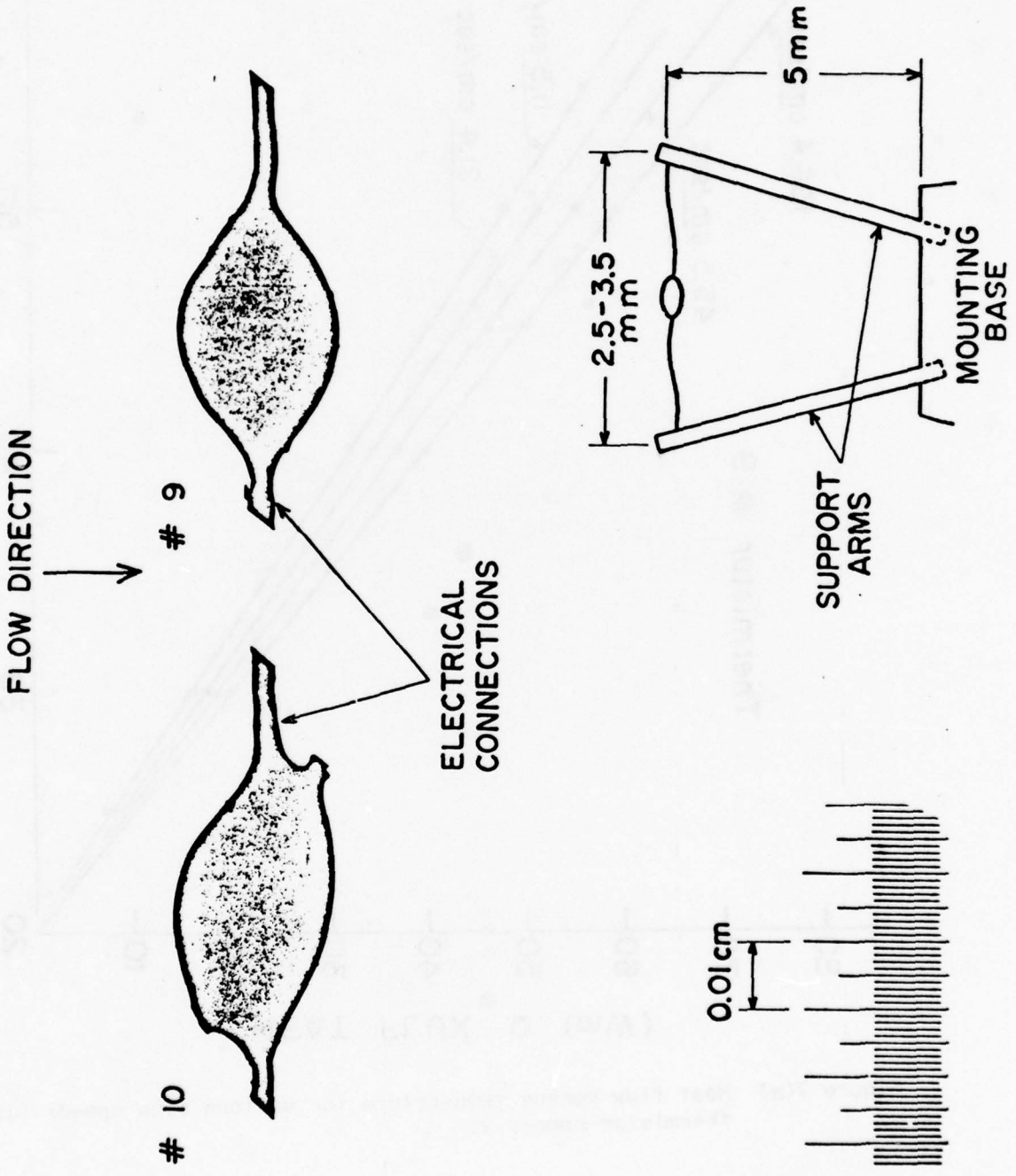

Figure 6. Back lighted micrograph of the authors' glass coated microbeads and a sketch of the thermistors mounting forks.

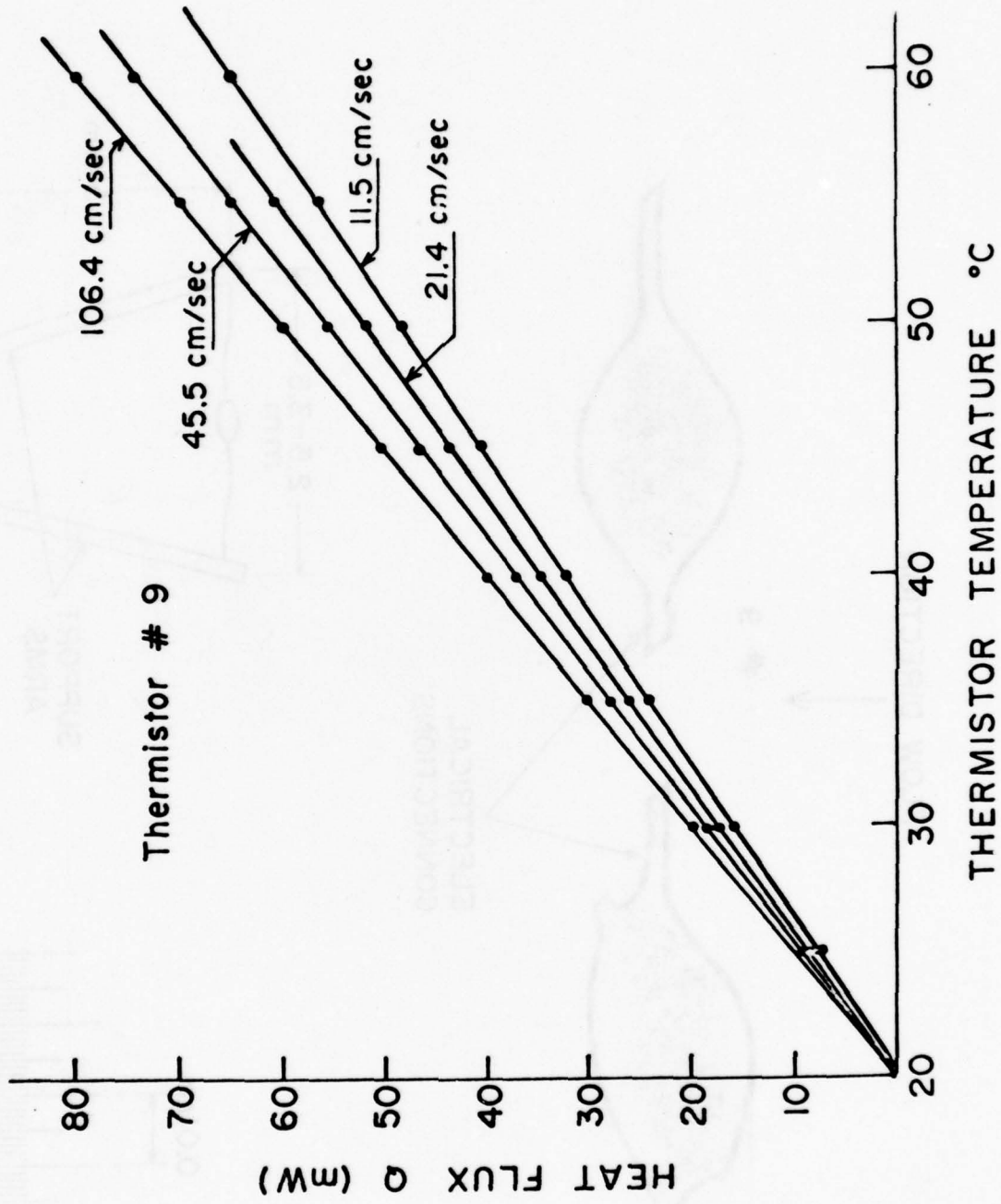

Figure 7(a) Heat flux versus temperature for various flow speeds for thermistor number 9.

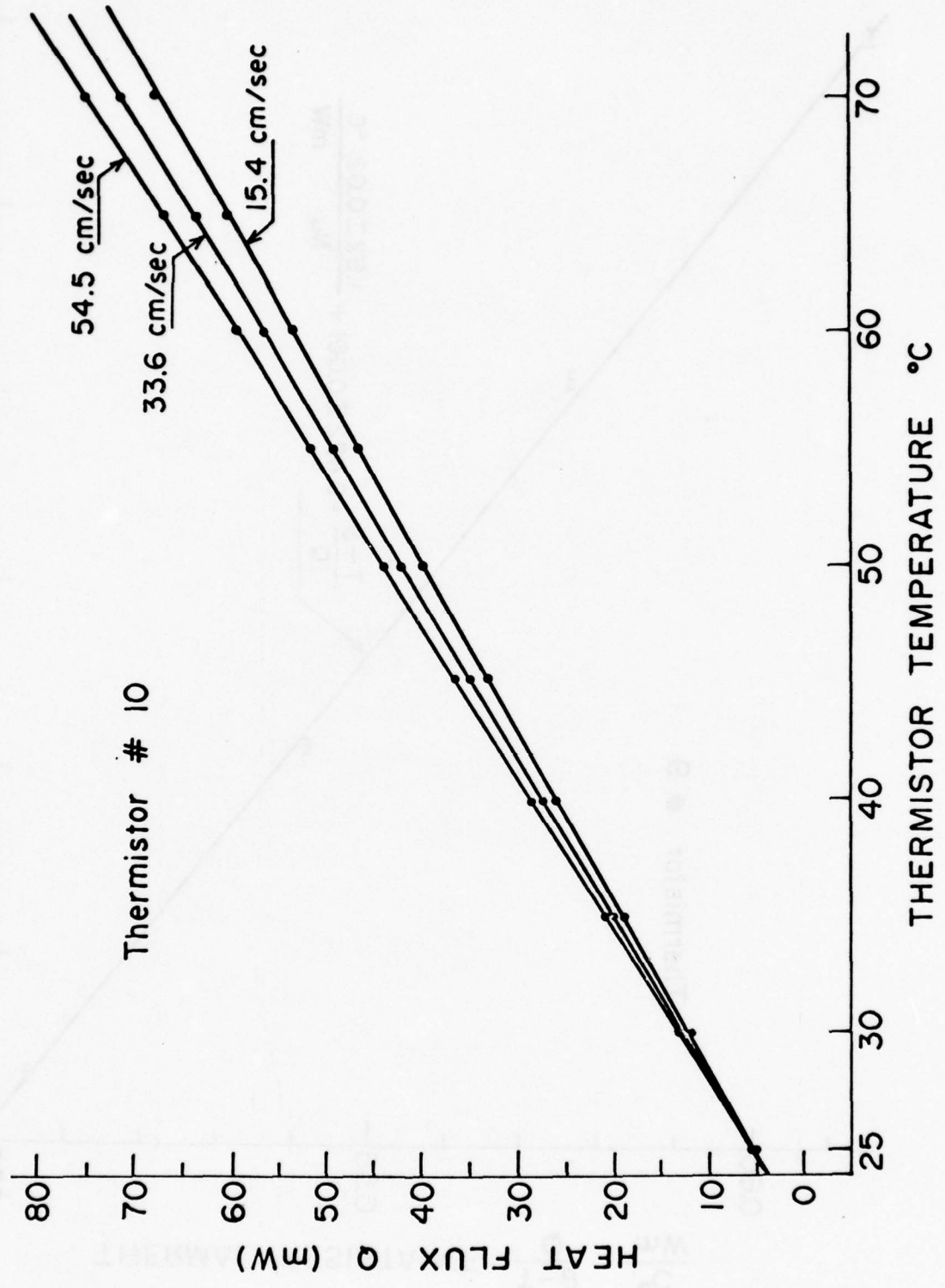

Figure 7(b) Heat flux versus temperature for various flow speeds for thermistor number 10.

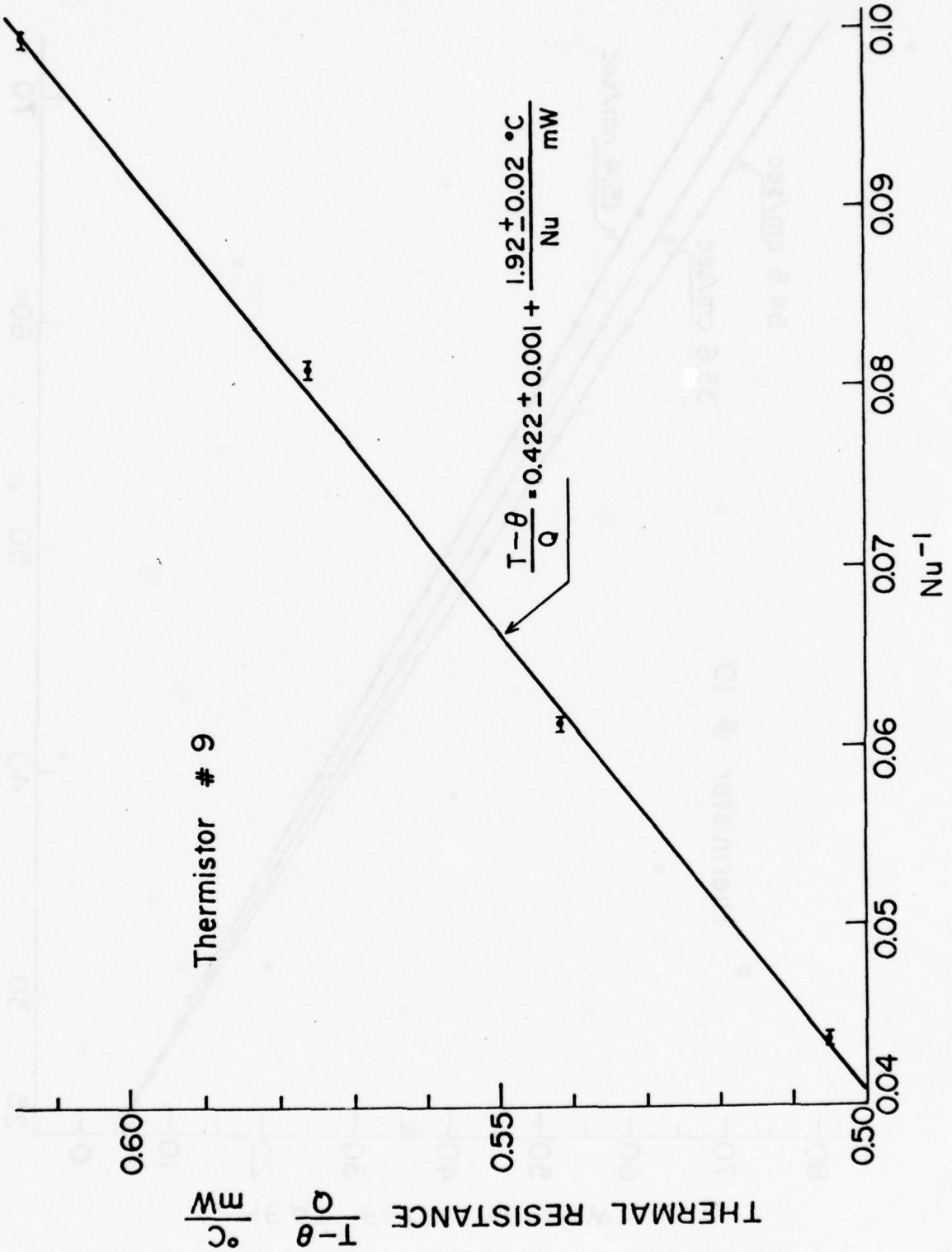

Figure 8(a) Thermal resistance (T-θ)/Q versus the inverse Nusselt number for thermistor number 9. The Nusselt number is after equation 3 and the parameters in table I.

Figure 8(b) Thermal resistance (T-θ)/Q versus the inverse Nusselt number for thermistor number 10. The Nusselt number is after equation 3 and the parameters in table I.

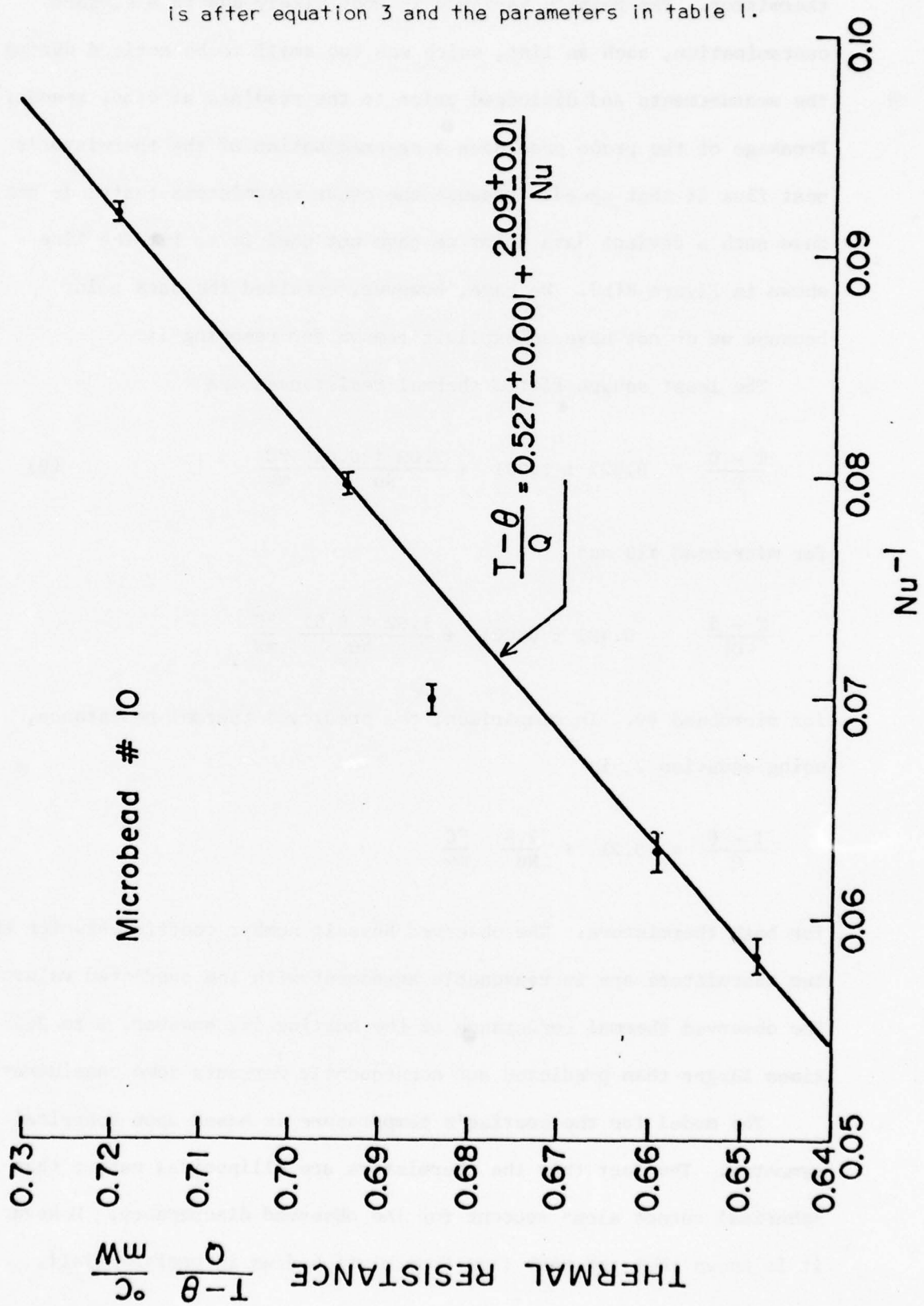

thermistor. The point's variance is most likely due to a surface contamination, such as lint, which was too small to be noticed during the measurements and dislodged prior to the readings at other speeds. Breakage of the probe precludes a re-examination of the thermistor's heat flux at that speed. Because the other thermistors tested do not have such a deviant data point we have not used it to fit the line shown in Figure 8(b). We have, however, retained the data point because we do not have an explicit reason for removing it.

The least square fitted thermal resistances are

$$\frac{T - \theta}{Q} = 0.527 \pm 0.001 + \frac{2.09 \pm 0.01}{Nu} \frac{^{\circ}C}{mw} \qquad (9)$$

for microbead #10 and

$$\frac{T - \theta}{Q} = 0.422 \pm 0.001 + \frac{1.92 \pm 0.02}{Nu} \frac{^{\circ}C}{mw}$$

for microbead #9. In comparison, the predicted thermal resistance, using equation 2, is

$$\frac{T - \theta}{Q} = 0.21 + \frac{2.4}{Nu} \frac{^{\circ}C}{mw}$$

for both thermistors. The observed Nusselt number coefficients for the two thermistors are in reasonable agreement with the predicted values. The observed thermal resistance of the coating is, however, 2 to 2.5 times larger than predicted and consequently warrants some consideration.

The model for the coating's temperature is based upon spherical symmetry. The fact that the thermistors are ellipsoidal rather than spherical cannot alone account for the observed discrepancy. However, it is known that the heat flux from bluff bodies is preferentially

biased toward their front surface where the boundary layer is thinnest. Thus the surface through which a large fraction of the heat passes is much smaller than the total surface area of the sphere. Perhaps the front hemisphere, or even less, represents the area that transmits the heat from the core to the ambient fluid. An examination of equation 2 then indicates that the term representing the coating's resistance

$$\frac{\Delta}{4\pi R(R + \Delta)\lambda_1}$$

should really be larger to account for this effective surface area reduction. Until the heat flow process is better understood, multiplying the above coating resistance by a factor of about 2 or 2.5 might maintain the usefulness of equation 2.

The Nusselt-Prandtl-Reynolds number relationship for spheres, on the other hand, is an empirical observation independent of the local heat flux distribution over the sphere's surface. The difficulty with using Kramers' (1946) Nusselt number formulation (equation 3) is that it applies only to spheres with a nearly uniform surface temperature. Because the heat flux from a sphere is not uniform over its surface, the presence of the coating leads to a non-uniform temperature over the wetted surface. Even for simple geometries such as a plate, the effect of a non-uniformity of the surface temperature on the heat flux is difficult to predict. Calculations by White (1974) suggest that the coating should make the heat flux more uniform over the wetted surface. The fact that the observed Nusselt number coefficients differ from the predicted coefficients by only 13 and 20% indicates that Kramers' relationship has some validity for the thermistors tested.

There is, however, a more general problem with predicting the response of thermistors. There is evidence for non-uniformity between nominally identical thermistors. This is particularly evident in the coating thickness which may vary considerably over the thermistor's surface and between thermistors, as noted by Gregg et al. (1978) and by us. Although we were not able to observe directly the coating thicknesses of the particular thermistors reported here, the difference between the observed response of thermistors #9 and #10, whose outside dimensions differed by less than 2%, suggest that their coatings may be quite different in thickness and in thickness distribution. Because of this non-uniformity among nominally identical thermistors it is not clear that improvements of the thermal model, although intellectually interesting, can lead to corresponding improvements in response predictability.

4. Quasi-Steady Response

The response is considered to be quasi-steady when the heat flux at any instant is that appropriate to steady conditions at the instantaneous value of the fluid's speed and temperature; i.e. the response in the limit of zero frequency.

4a. Constant Temperature T

(i) Sphere

The variation of equation 2 with respect to speed and temperature gives

$$\frac{T - \theta}{Q}\,\frac{dQ}{Q} + \frac{d\theta}{Q} = \frac{0.33\ Pr^{0.31}Re^{1/2}}{2\pi(R + \Delta)\lambda_2 Nu^2}\,\frac{dU}{U} \qquad (10)$$

The sensitivity of the heat flux to temperature is

$$\left.\frac{dQ}{d\theta}\right|_{dU=0} = \frac{-Q}{T - \theta} \qquad (11)$$

which is a constant at a given speed and readily determined from the temperature vs heat flux relationship. For thermistor #10, for example, the sensitivity to temperature is 1.39 mw/°C at 15.4 cm/sec. The sensitivity of the heat flux to speed is

$$\left.\frac{dQ}{dU}\right|_{d\theta=0} = \left(\frac{Q}{T - \theta}\right)\left(\frac{0.33\ Pr^{.31}Re^{1/2}}{2\pi(R + \Delta)\lambda_2 Nu^2}\right)\frac{T - \theta}{U} \qquad (12)$$

which at 15.4 cm/sec, using only the dimensional information in Table 1, equals 0.0111 mw/cm/sec for every centigrade degree of overheat (T - θ). Choosing, say, T - θ = 50°C results in a sensitivity of 0.553 mw/cm/sec. The relative speed-to-temperature sensitivity then is

$$\frac{(dQ/dU)d\theta=0}{(dQ/d\theta)dU=0} = -\left(\frac{Q}{T-\theta}\right)\left[\frac{0.33\ Pr^{.31}Re^{1/2}}{2\pi(R+\Delta)\lambda_2 Nu^2}\right]\ \frac{T-\theta}{U} \qquad (13)$$

and equals 0.40°C/cm/sec for thermistor #10 under the conditions specified, namely U = 15.4 cm/sec and T - θ = 50°C. The implications are that a quasi-steady fluctuation of 1 cm/sec is indistinguishable from a fluctuation of 0.4 °C. Alternate expressions for the sensitivities that clarify the effect of the coating are

$$\left.\frac{dQ}{dU}\right|_{d\theta=0} = \frac{2\ (R+\Delta)\lambda_2[0.33\ Pr^{.31}Re^{1/2}]}{(1+DF)^2}\ \frac{T-\theta}{U} \qquad (14)$$

and

$$\left.\frac{dQ}{d\theta}\right|_{dU=0} = \frac{2\pi(R+\Delta)\lambda_2 Nu}{1+DF} \qquad (15)$$

$$\frac{(dQ/dU)d\theta=0}{(dQ/d\theta)dU=0} = \frac{0.33\ Pr^{.31}Re^{1/2}}{(1+DF)Nu}\ \frac{T-\theta}{U} \qquad (16)$$

where DF represents the coating-to-boundary layer resistance ratio. For thermistor #10 the observed DF value at 15.4 cm/sec is 2.2, which implies that the speed sensitivity has been reduced by a factor of $(1 + 2.2)^2 = 10$ from its value in the absence of a coating. The temperature and the relative speed-to-temperature sensitivity, using equations 15 and 16, is reduced by a factor of (1 + 2.2) = 3.2 by the coating. Clearly the coating requires careful consideration when one chooses a thermistor for heated anemometry and heated thermometry.

We have used the observed thermal resistance of thermistor number 10 (eq. 9) to predict the speed sensitivity of that thermistor for various flow speeds. The speed sensitivity per degree of overheat is, using equation 9 and the parameters in Table 1,

		Lange		Authors	
		Plate	Microbead	Microbeads	
				# 9	# 10
R	(cm)	---	0.0064	0.0087	0.0087
L	(cm)	0.051	---	---	---
b	(cm)	0.051	---	---	---
Δ	(cm)	0.0018	0.0018	0.0028	0.0028
λ_1	(watts/cm°C)	0.0010	0.0010	0.010	0.010
λ_2	(watts/cm°C)	0.0059	0.0059	0.0059	0.0059
ν	(cm^2/sec)	0.0123	0.0120	0.0097	0.010
κ	(cm^2/sec)	0.00139	0.00139	0.0014	0.0014
Pr		8.9	8.63	7.1	6.8

Table CI

The parameter value associated with the thermistors examined. The dimensional data for Lange's thermistors are nominal values. The conductivity of paralene-C (λ_1 for Lange's thermistors) is after Alpaugh and Morrow (1974). The viscosity (ν), the diffusivity (κ), and the Prandtl number (Pr) are after Batchelor (1970, p. 597). The conductivity of glass (λ_1 for the authors' thermistors) is after Lueck, et al. (1977).

$$\frac{1}{T - \theta} \left.\frac{dQ}{dU}\right|_{d\theta=0} = \frac{0.230\sqrt{U}}{(1 + 0.235\sqrt{U})^2} \quad \frac{1}{2U} ,$$

in units of °C per cm/sec per degree centigrade, which is plotted in Figure 9. Both the speed sensitivity and the ratio of speed-to-temperature sensitivity decrease rapidly with increasing flow speed. Consequently the usefulness of heated thermistors for anemometry may be restricted to low flow speeds.

(ii) Plate

The variation of equation 7 gives the sensitivity of the plate's heat flux as

$$\left.\frac{dQ}{dU}\right|_{d\theta=0} = \frac{0.664\ b\lambda_2\ Pr^{1/3} Re^{1/2}}{(1 + \frac{\lambda_2}{\lambda_1}\frac{\Delta Nu}{L})^2} \quad \frac{T - \theta}{U} \tag{17}$$

$$\left.\frac{dQ}{d\theta}\right|_{dU=0} = -\frac{Q}{T - \theta} = \frac{-2b\lambda_2 0.664\ Pr^{1/3} Re^{1/2}}{(1 + \frac{\lambda_2}{\lambda_1}\frac{\Delta}{L} Nu)} \tag{18}$$

and

$$\frac{(dQ/dU)d\theta=0}{(dQ/d\theta)dU=0} = \frac{1}{1 + \frac{\lambda_2}{\lambda_1}\frac{\Delta}{L} Nu} \quad \frac{T - \theta}{2U} \tag{19}$$

Using the observed thermal resistance shown in equation (8) we calculate the relative sensitivity as

$$\frac{(dQ/dU)d\theta=0}{(dQ/d\theta)dU=0} = \frac{1.00}{1 + 0.825U^{1/2}} \quad \frac{T - \theta}{2U}$$

which, for comparison with the glass-coated microbead #10 equals 0.38 °C/cm/sec at T - θ = 50 °C and U = 15.4 cm/sec. The term DF equals $0.825\ U^{1/2}$ for the plate tested by Lange.

Figure 9. Speed sensitivity per degree of overheat for the authors' glass coated thermistor number 10 and Lange's paralene-c coated flake thermistor. The curves are based on the observed thermal resistances given by equations 8 and 9.

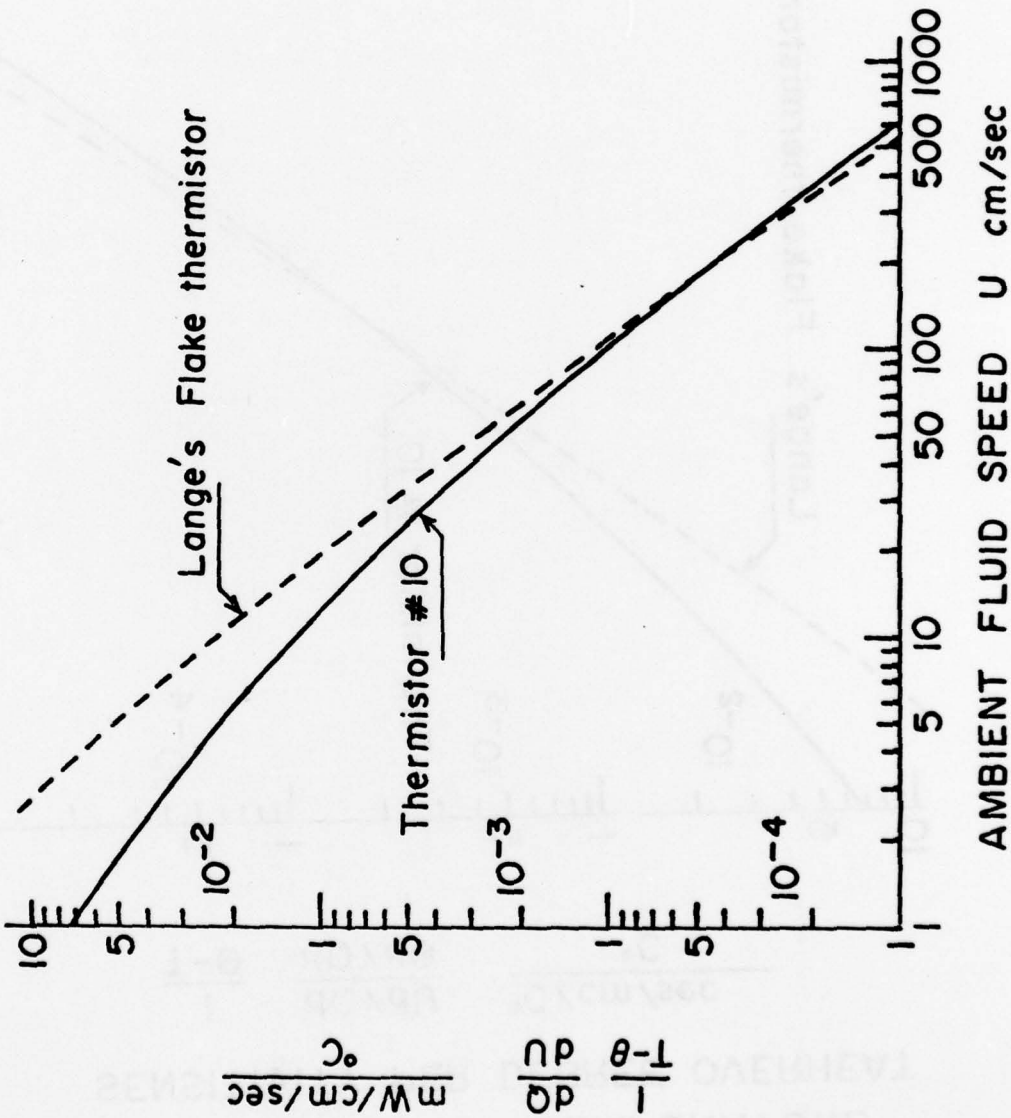

Figure 10. Relative speed-to-temperature sensitivity per degree of overheat for the authors' glass coated thermistor number 10 and Lange's paralene-c coated flake thermistor. The curves are based on the observed thermal resistances given by equations 8 and 9.

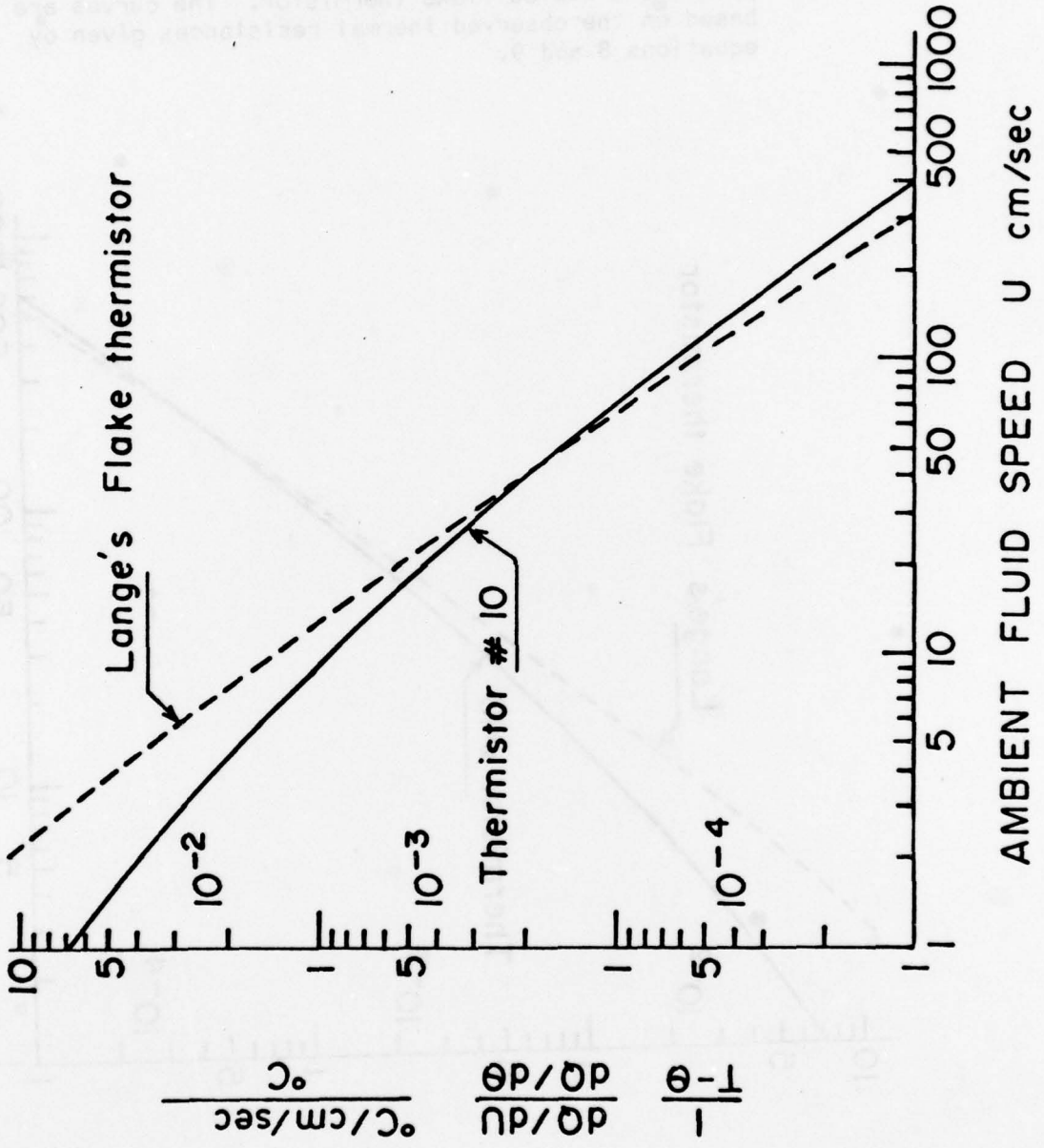

The relative speed-to-temperature sensitivity of Lange's flake thermistor is plotted in Figure 10. The speed sensitivity per degree of overheat is given by

$$\frac{1}{T - \theta} \left.\frac{dQ}{dU}\right|_{d\theta=0} = \frac{1.86}{(1 + 0.812\sqrt{U})} \frac{1}{2U}$$

which is plotted in Figure 9.

The assymptotic value of the speed sensitivity of a heated sensor at high speeds is proportional to $U^{-1/2}$ without a coating and $U^{-3/2}$ with a coating. The assymptotic value of the ratio of the speed-to-temperature sensitivity is U^{-1} without a coating and $U^{-3/2}$ with a coating.

4b. Constant Current I

(i) Sphere

In the constant current mode the temperature of the thermistor's core is variable and is, in practice, the sensed quantity. The variation of the heat flux dQ is related to the variation of the metal-oxide's temperature by

$$dQ = IdE = I^2 dR_T = Q\alpha dT \qquad (20)$$

where I is the constant current passing through the thermistor, dE is the fluctuation of the thermistor's voltage, dR_T the fluctuation in its electrical resistance, dT the fluctuation in its temperature, and α its fractional temperature coefficient of electrical resistance defined by

$$\alpha = \frac{1}{R_T} \frac{dR_T}{dT} \cong -0.04/^{\circ}C \quad .$$

The variation of equation 2 is

$$\frac{dT}{Q} - \frac{d\theta}{Q} - \frac{T - \theta}{Q}\,\frac{dQ}{Q} = \frac{0.33\ Pr^{.31}Re^{1/2}}{2\pi(R + \Delta)\lambda_2 Nu^2}\,\frac{dU}{U}$$

which, when combined with equation 20, yields for the sphere,

$$[1 - \alpha(T - \theta)]\frac{dT}{Q} - \frac{d\theta}{Q} = \frac{0.33\ Pr^{.31}Re^{1/2}}{2\pi(R + \Delta)\lambda_2 Nu^2}\,\frac{dU}{U} \qquad (21)$$

The constant current temperature sensitivity is

$$\left.\frac{dT}{d\theta}\right|_{dU=0} = \frac{1}{1 - \alpha(T - \theta)} \qquad (22)$$

According to (22) the temperature sensitivity is unity at zero overheat which is desired if the thermistor is to be used as a temperature sensor with infinitesimal internal heating. The temperature sensitivity decreases with increasing internal heating (noting that $\alpha < 0$) and vanishes at very high levels of internal heating. It is very interesting to observe that sensors with positive temperature coefficients ($\alpha > 0$) increase their temperature sensitivity with increasing internal heating in the constant current mode. The condition $T - \theta = \alpha^{-1}$ corresponds to an instability for positive temperature coefficient sensors. In contrast, the temperature sensitivity in the constant temperature mode is independent of the overheat $T - \theta$.

The speed sensitivity of the spherical thermistor's heat flux is

$$\left.\frac{dT}{dU}\right|_{d\theta=0} = \left(\frac{Q}{T - \theta}\right)\frac{0.33\ Pr^{.31}Re^{1/2}}{[1 - \alpha(T - \theta)]2\pi(R + \Delta)\lambda_2 Nu^2}\,\frac{T - \theta}{U} \qquad (23)$$

At zero overheat ($T = \theta$) the thermistor has no speed sensitivity. The speed sensitivity increases with increasing overheat to the limit

$$\left.\frac{dT}{dU}\right|_{d\theta=o} = -\frac{1}{\alpha}\frac{0.33\ Pr^{.31}Re^{1/2}}{2\pi(R+\Delta)\lambda_2 Nu^2}\ \frac{Q}{T-\theta}\ \frac{1}{U}$$

limit $Q \to \infty$

which is independent of the overheat because $Q/(T - \theta)$ is a constant at a given Nusselt number. The ratio of the quasi-steady speed-to-temperature sensitivity is

$$\frac{(dT/dU)d\theta=0}{(dT/d\theta)dU=0} = \left(\frac{Q}{T-\theta}\right)\ \frac{0.33\ Pr^{.31}Re^{1/2}}{2\pi(R+\Delta)\lambda_2 Nu^2}\ \frac{T-\theta}{U}$$

which is identical to the relative sensitivity in the constant temperature heating mode. The advantages, if any, of operating the thermistor in the constant temperature mode over operating it in the constant current mode are reflected in the unsteady response which has, so far, not been measured.

5. Discussion

Some knowledge of the relative activity of temperature and velocity in the fluid being probed (such as the ocean) is necessary to determine the suitability of heated thermistors for turbulence measurements and to assess the velocity contamination of (nearly) unheated thermistors used for thermometry. We will use as a basis for discussion some of the available observations of the kinetic energy dissipation rate ε and the temperature dissipation rate χ where, assuming isotropy

$$\varepsilon = 15\nu \left(\frac{\partial w'}{\partial z} \right)^2 \quad (24a) \quad , \quad \chi = 6\kappa \left(\frac{\partial \theta'}{\partial z} \right)^2 \quad (24b)$$

$\partial w'/\partial z$ is the vertical gradient of the vertical component of the velocity fluctuations and $\partial \theta'/\partial z$ is the vertical gradient of the temperature fluctuations. Gregg (1976) reported temperature dissipation rates of 4.3×10^{-9} to 1.1×10^{-10} $^{o}C^2$/sec averaged over several tens of metres in the mixed layer and values of 3.6×10^{-8} to 2.1×10^{-9} $^{o}C^2$/sec averaged over several tens of metres in the thermocline of the central North Pacific. Gregg (1977) also observed temperature dissipation values of 2.2×10^{-12} to 6×10^{-11} $^{o}C^2$/sec for depths below 1000 metres in several widely spaced locations in the Pacific. Gargett (1978) measured dissipation rates as large as 9.8×10^{-7} $^{o}C^2$/sec in an upper ocean frontal regime.

The rate of kinetic energy dissipation near the Azores has been measured by Osborn (1978). Averaged over 5 metres of depth the values were typically 10^{-4} cm^2/sec^3 but ranged as high as 10^{-2} cm^2/sec^3. Crawford and Osborn (1978) reported averaged kinetic energy dissipation rates of up to 7×10^{-3}, 4×10^{-5} and 2×10^{-3} cm^2/sec^3 for the regions above, in and below the core of the Atlantic Equatorial Undercurrent.

If we denote the ratio of a probe's speed-to-temperature sensitivity by β, then the velocity contamination of a temperature dissipation rate measurement is, using 24a and b,

$$\chi_{cont} = \frac{2}{5Pr} \beta^2 \varepsilon \quad . \tag{25}$$

Correspondingly, the temperature contamination of a kinetic energy dissipation rate measurement is

$$\varepsilon_{cont} = \frac{5Pr}{2} \frac{1}{\beta^2} \chi \tag{26}$$

Using Gargett's (1978) value of 9.8×10^{-7} $^{\circ}C^2$/sec as an upper limit for χ in the thermocline, and using the observed relative sensitivity of 0.29 $^{\circ}C$/cm/sec for thermistor #10 (Fig. 10) at $T - \theta = 50^{\circ}C$, U = 15.4 cm, and Pr = 8 gives a contamination of

$$\varepsilon_{cont} \cong 2.3 \times 10^{-4} \text{ cm}^2/\text{sec}^3$$

which is comparable to the values of ε reported by Osborn (1978) in the seasonal thermocline adjacent to the island of Santa Maria in the Azores. In the mixed layer, using Gregg's (1976) upper value of 4.3×10^{-9} $^{\circ}C^2$/sec,

$$\varepsilon_{cont} = 1.0 \times 10^{-6} \text{ cm}^2/\text{sec}^3$$

which may be small compared to the kinetic energy dissipation in the mixed layer. At large depth the contamination is, using $\chi = 6 \times 10^{-11}$ $^{\circ}C^2$/sec, 1.4×10^{-8} cm^2/sec^3. However, there are no values of ε available for depths of $\sim$ 1000 metres.

If thermistor #10 were to be used for temperature measurements then the level of velocity contamination in the measured temperature dissipation rate is from equation 25

$$\chi_{cont} = 1.7 \times 10^{-6} (T - \theta)^2 \varepsilon$$

where we have used, from Figure 10,

$$\beta = 5.8 \times 10^{-3} \frac{^{o}C/cm/sec^{-1}}{^{o}C} (T - \theta)$$

at U = 15.4 cm/sec. Taking, for example, an upper value of 10^{-2} cm^2/sec^3 for ε in the mixed layer, and $\chi = 10^{-10}$ $^{o}C^2/sec$ as the lowest dissipation rate to be resolved implies a 1% contamination at an overheat $(T - \theta)$ of only 7.7×10^{-3} ^{o}C. Using Figure 7b we calculate that this temperature rise results from only

$$Q = 1.39 \frac{mw}{^{o}C} \times 7.7 \times 10^{-3} \, ^{o}C = 1.1 \times 10^{-5} \text{ watts}$$

of internal heating in the thermistor. Gregg et al. (1978) reports internal heating levels of 4 to 13 x 10^{-6} watts for his thermistors which, however, have a different mounting and are 2.5 times larger than the microbeads discussed here. Several people have suggested warmed thermistors for high frequency thermometry, however, because even very small amounts of self heating may lead to velocity contamination it appears that grossly and moderately heated thermistors cannot be very useful for thermometry in the ocean.

We have used, in the above discussion, temperature dissipation rates that were averaged over several tens of metres or more and kinetic energy dissipation rates that were averaged over 5 metres or more. On a more local scale, however, the dissipation rates are

larger than cited, and consequently the amount of signal contamination may be more severe than the values given above because temperature and velocity activity are not necessarily correlated. We have also ignored the effect of the heated thermistor's frequency response. Lueck (1979) has shown that the frequency response bandwidth of a heated plate is larger for speed than for temperature. However, in the ocean the wavenumber range of the temperature gradient spectrum is typically larger than the range of the velocity gradient spectrum.

6. Conclusions

A model for the heat flux from internally heated spherical and plate-shaped thermistors to their fluid environment has been derived. The model incorporates the effects of a thermistor's coating and the effects of forced convection in its boundary layer through the use of an established Nusselt number. The model agrees favourably with the heat flux from a paralene-C coated flake thermistor as observed by Lange. Agreement between the model and our observations for the heat flux from two glass coated microbead thermistors is also favourable except that the effect of the coating is approximately two times larger than predicted. Preferential heat conduction through the frontal surface of the thermistor could account for this difference. The model agrees well with the observations if the coating's surface area is reduced to an effective surface area.

The heat flux from heated sensors, in general, depends on both the temperature and the speed of the ambient fluid. The simultaneous sensitivity of thermistors to speed and temperature has been explicitly derived. The coating reduces both the thermistor's sensitivity to speed and to temperature from its value in the absence of a coating. The reduction in sensitivity is greater for speed than for temperature, and hence, the relative speed-to-temperature sensitivity is also reduced by the coating.

Some implication of the results for anemometry and thermometry in the ocean have been discussed. The level of contamination of a measurement, due to the thermistor's simultaneous sensitivity to speed and temperature, depends on the amount of internal heating and on the

relative intensity of velocity and temperature turbulence in the fluid being probed. Consequently the contamination of a measurement depends strongly on one's particular circumstances. Using observed values for the rate of temperature and kinetic energy dissipation in the ocean we conclude that it is possible that (1) velocity measurements made by heated thermistors may be contaminated by temperature in the main thermocline, that (2) temperature measurements made by nearly unheated thermistors may be contaminated by velocity in the mixed layer and in other regions of high velocity but low temperature activity, and that (3) moderately or grossly heated thermistors are not useful for thermometry.

Bibliography

Alpaugh, W.A. and D.R. Morrow, 1974, The thermal properties of monochloro-para-xylylene. Thermochimica Acta, 9, 171-204.

Batchelor, G.K., 1970, An Introduction to Fluid Mechanics, Cambridge University Press, paperback, 615 pp.

Crawford, W.R. and T.R. Osborn, 1979, Microstructure measurements in the Atlantic Equatorial Undercurrent during GATE, submitted to Deep-Sea Research.

Gargett, A.E., 1978, Microstructure and finestructure in an upper ocean frontal regime, Journal of Geophysical Research, 83(C10), 5123-5134.

Gregg, M.C., 1976, Finestructure and microstructure observations during the passage of a mild storm, Journal of Physical Oceanography, 6, 528-555.

Gregg, M.C., 1977, Variations in the intensity of small-scale mixing in the main thermocline, Journal of Physical Oceanography, 7, 436-454.

Gregg, M.C., T. Meagher, A. Pederson and E. Aagaard, 1978, Low noise temperature microstructure measurements with thermistors, Deep-Sea Research, 25, 843-856.

Kramers, H., 1946, Heat transfer from spheres to flowing media, Physica, 12, 61-80.

Lueck, R.G., O. Hertzman, and T.R. Osborn, 1977, The spectral response of thermistors, Deep-Sea Research, 24, 951-970.

Lueck, R.G., 1979, The non-steady flux of heat and momentum from a flat plate, submitted to Journal of Fluid Mechanics.

Osborn, T.R., 1978, Measurement of energy dissipation adjacent to an island, Journal of Geophysical Research, 83(C6), 2939-2957.

Schlichting, H., 1955, Boundary Layer Theory, Pergamon Press, 535 pp.

White, F., 1974, Viscous Fluid Flow, McGraw-Hill, 725 pages.